Title
Oxysterol control of macrophage-dependent inflammation

Author
Dang, Eric Van

Publication Date
2018

Peer reviewed|Thesis/dissertation

Oxysterol control of macrophage-dependent inflammation

by

Eric Van Dang

DISSERTATION

Submitted in partial satisfaction of the requirements for the degree of

DOCTOR OF PHILOSOPHY

in

Biomedical Sciences

in the

GRADUATE DIVISION

To my parents, Mary and Chi Dang

For encouraging me to value education and giving me freedom to discover my passion

Acknowledgements

UCSF has been a truly special place to conduct my graduate studies. First and foremost, I must thank my advisor Jason Cyster. He has been a constant source of motivation, ideas, and constructive criticism. Jason sets a tremendous example of what it means to be a true scientist. I have always admired his commitment to improve, and to never be satisfied with data or accomplishments. Jason has a reputation of being quite hands on, but he gave me a lot of implicit trust in terms of dictating the directions of my project. I will consider myself lucky if a fraction of his rigor and attention to detail rubs off on me.

I thank my thesis committee members, Richard Locksley and Jeff Cox, for their encouragement and bottomless train of ideas. In particular, I am grateful to Jeff, who volunteered to continue serving on my committee even after leaving UCSF for Berkeley. Mark Ansel and Hiten Madhani were my first two rotation advisors and set me off to a fantastic start at UCSF. Special thanks go to Anita Sil and Kevin Shannon who set aside time to meet and informally advise me on various career decisions.

I would like to acknowledge those who started me off in science and enforced my decision to go to graduate school. Drew Pardoll at Johns Hopkins was my undergraduate PI and gave me more freedom and trust than a college student deserved. In Drew's lab I worked closely with Fan Pan, who taught me everything I know about molecular biology. Anne O'Garra at the NIMR in Mill Hill let me join her laboratory for a year after college. It was at the NIMR that I was immersed into immunology, which has been my passion ever since.

I thank the UCSF BMS and MSTP programs for always making things run smoothly. In particular, Demian Sainz and Geri Ehle have been amazong sources of support.

I am indebted to the original members of the Cyster lab who showed me the ropes as a rotation and early graduate student. In particular, Andrea Reboldi was a tremendous mentor and friend to me. The first year I spent in the lab working on the first Ch25h story with him was the most fun I've ever had in science. Tangsheng Yi, my rotation mentor, set an example of tremendous productivity. Oliver Bannard was always appreciated for his British sense of humor and insightful caveats brought up during lab meeting. Jagan Muppidi was impressive for his saint-like patience in the face of constant abuse from Andrea. Francisco Ramirez-Valle was a fantastic baymate and provided many laughs, often in the form of Britney Spears music. Brenda Han was a senior graduate student who was often my partner in crime in many lab pranks. Last but not least, I thank Michael Barnes for being the most entertaining and enigmatic member of the Cyster lab.

I also thank the current members of the Cyster lab for providing a fantastic working environment. Shelly Mintz has been a fantastic baymate and friend who gave me lots of advice on B cell immunology, along with many drinks and board games at her apartment. Lauren Rodda is my contemporary graduate student in the lab, and is always the most fun person to talk science with, as she always questions conventional thinking and tends to push ideas into very interesting places. Erick Lu was my first rotation student, and is the hardest working graduate student I've ever come across. Antonia Gallman is the most recent MSTP to join the lab, and she always brings a

positive attitude and impressive attention to detail to all of her endeavors. Lastly I'd like to pay special thanks to Elise Wolf for making the bay an incredibly fun place to work every day. Elise trained under me during her first year in the lab, during which time we became close friends.

I've made some lifelong friends during my time in San Francisco. Max Horlbeck, Jason Chung, and Andrew Lechner were my former roommates and like a second family to me. My MSTP class has been lucky in that we are incredibly close, and I'd like to acknowledge Dana Neel, Krister Barkovich, Jinwoo Lee, Misty Montoya, John Liu, Anna Hauswirth, and Geoff Smith for many good times. Phil Dumesic was a senior MSTP student in Hiten Madhani's lab when I rotated, and he has always set the bar for what I aspire to be as a scientist.

None of this would have been possible without the love and support of my wife Lauren, who has put up with a lot of late nights and weekends spent in the laboratory. Lauren's parents Nancy and Steve have also been wonderful sources of support and it has been great having them live nearby. I have always strived to be a good role model for my younger sister Vanessa, and I've watched with great pride as she has progressed through medical school and married a fantastic partner in her husband Donald. My mother Mary has there for support and advice when things have gone poorly. She also always keeps my ego in check at the times when it needs checking. Finally, I would like to acknowledge my father Chi, who sets the example of what it means to have a love for science and service to others. Any success I've had in science I owe to him.

Chapter 1 was work done in collaboration with Andrea Reboldi and is reprinted largely as it appears in:

Reboldi A., Dang E.V., McDonald J.G., Liang G., Russell D.W., Cyster J.G. 25-hydroxycholesterol suppresses interleukin-1-driven inflammation downstream of type I interferon. Science *6197*, 679-684.

Chapter 2 is reprinted largely as it appears in:

Cyster J.G., Dang E.V., Reboldi A., Yi T. 25-hydroxycholesterols in innate and adaptive immunity. Nature Reviews Immunology *11*, 731-743.

Chapter 3 is reprinted largely as it appears in:

Dang E.V.*, McDonald J.G., Russell D.W., Cyster J.G*. Oxysterol restraint of cholesterol synthesis prevents AIM2 inflammasome activation. Cell 2017, 5: 1057-1071. *Co-corresponding author

Oxysterol control of macrophage-dependent inflammation

Eric V. Dang

Abstract

Cholesterol is a key structural component of mammalian cell membranes. Unlike other lipids such as fatty acids, cholesterol cannot be catabolized for energy production, necessitating feedback mechanisms to prevent pathological cholesterol accumulation. Feedback inhibition of cholesterol metabolism involves regulation of SREBP2, the master transcriptional regulator of cholesterol synthesis, and its chaperone protein SCAP. In states of high cholesterol content, cholesterol causes SCAP/SREBP2 to be retained in the ER. Interestingly, biochemical studies have shown that the oxysterol 25-hydroxycholesterol (25-HC) is also capable of blocking SREBP2 activation by trapping it in the ER. This has raised the question of whether endogenous oxysterols have a physiologic function in controlling cholesterol metabolism.

Ch25h is an ER transmembrane enzyme that catalyzes the conversion of cholesterol to 25-hydroxycholesterol. The knockout mouse for this enzyme was reported to have no baseline defects in cholesterol homeostasis, calling into question whether 25-HC is required for inhibition of SREBP2 in vivo. In this thesis, I find that Ch25h upregulation is required in macrophages to shut down their endogenous cholesterol biosynthesis in response to bacterial pathogen sensing. Deletion of Ch25h in activated macrophages results in increased expression of cholesterol biosynthesis genes, as well as a hyper-inflammatory phenotype characterized by overproduction of the cytokine IL-1β. These findings identify a new role for regulation of the SREBP2 pathway in controlling set-points for inflammation.

IL-1β normally exists in the cytosol in a pro-form and must be cleaved by an oligomeric protein complex known as the 'inflammasome' to become active. Here, I find that Ch25h provides a check on IL-1β overproduction by preventing cholesterol-dependent activation of the AIM2 inflammasome, which is triggered by the presence of cytosolic DNA. I find that Ch25h-deficient activated macrophages have impaired mitochondrial function, signs of mitochondrial membrane damage, and cytosolic accumulation of mitochondrial DNA. Thus, Ch25h is induced in macrophages by type I IFN to protect mitochondria from cholesterol-dependent damage upon bacterial sensing. Since AIM2 is a sequence non-specific DNA binding protein, I suggest that this circuit exists to prevent macrophages from spuriously engaging inflammation in response to host-derived nucleic acids.

The work described in this thesis identifies a metabolic circuit that sheds light on how cellular cholesterol accumulation can trigger inflammasomes. This has implications for metabolic inflammation, and provides a framework for future explorations into the role of cholesterol as an inflammatory driver in diseases such as atherosclerosis and metabolic syndrome.

Table of contents

List of tables

Chapter 1

List of figures

Chapter 1

Chapter 2

Chapter 3

Chapter 1

25-hydroxycholesterol blocks interleukin 1-driven inflammation downstream of type I interferon

Summary

Type-I interferon (IFN) protects against viruses yet it also has a poorly understood suppressive influence on inflammation. Here we report that activated mouse macrophages lacking the IFN-stimulated gene, cholesterol 25-hydroxylase (*Ch25h*), and that are unable to produce the oxysterol 25-hydroxycholesterol (25-HC), overproduce inflammatory interleukin 1 (IL1)-family cytokines. 25-HC acts by antagonizing sterol response element binding protein (SREBP) processing to reduce *Il1b* transcription and to broadly repress IL1-activating inflammasomes. In accord with these dual actions of 25-HC, Ch25h-deficient mice exhibit increased sensitivity to septic shock, exacerbated experimental autoimmune encephalomyelitis and a stronger ability to repress bacterial growth. These findings identify an oxysterol, 25-HC, as a critical mediator in the negative feedback pathway of IFN signaling on IL1-family cytokine production and inflammasome activity.

Introduction

As well as having potent anti-viral activity, type I IFN has a suppressive influence on immunity, an action that helps prevent uncontrolled inflammation and that underlies its utility in treatment of certain autoimmune diseases such as multiple sclerosis (*1-4*). This suppressive action also contributes to the increased propensity for bacterial infection following viral infection (*1, 2*). A central facet of the IFN-mediated suppressive effect is down-regulation of inflammasome activity and IL1β production (*3, 5*). However, which of the several hundred IFN-stimulated genes are responsible for these effects are poorly defined. The IFN-stimulated gene *Ch25h* (*6*) was recently shown to have broad anti-viral activity (*7, 8*), but whether this gene has an anti-inflammatory role is unknown.

Results

Ch25h is an enzyme that hydroxylates cholesterol at the 25 position to generate 25-hydroxycholesterol (25-HC) (*9*). Ch25h is strongly induced in myeloid cells by Toll-like receptor (TLR) ligands in a type I IFN–dependent manner (*10*). Recently, we and others identified a role for a downstream product of Ch25h, 7α,25-dihydroxycholesterol (7α,25-HC), as a ligand for EBI2 (GPR183) (*11*, *12*). During studies comparing Ch25h- and EBI2-deficient mice, we found that *Ch25h*$^{-/-}$ mice had increased frequencies of IL-17A^{+} T cells in spleen and lymph nodes (Fig. 1A). The frequencies of IFN-γ–producing and regulatory T cells were unaffected (fig. S1A). Ch25h-deficient mice also had increased neutrophil counts (Fig. 1B), a phenotype seen in other strains with elevated IL-17A^{+} cells (*13*, *14*). *Gpr183*$^{-/-}$ mice were not affected in these parameters (fig. S1B). These data indicated that Ch25h was acting via an EBI2-independent pathway to regulate IL-17A^{+} T cell and neutrophil numbers, two cell populations that often promote inflammation.

Because Ch25h can be expressed at high levels in activated macrophages (*7*, *8*, *15*–*17*), we asked whether the IL-17A–polarizing activity of lipopolysaccharide (LPS)–stimulated macrophage cultures was altered by Ch25h deficiency. Culture supernatants from Ch25h-deficient macrophages induced more IL-17A^{+} T cells than supernatants from control macrophages (Fig. 1Cand fig. S1, C and D). T helper 1 (T_H1) and T_H2 cell differentiation were unaffected (Fig. 1C and fig. S1C). As expected, LPS stimulation of bone marrow–derived macrophages (BMDMs) caused *Ch25h* induction in an IFN-α receptor (IFNαR)–dependent manner (fig. S1E), and this was associated with increased 25-HC in culture supernatants (fig. S1F). However, when 25-HC was added

to T cell cultures at this concentration (100 nM), it was without effect (fig. S1G). These data suggested that the *Ch25h*$^{-/-}$ and control macrophage culture supernatants were differing in some other constituent that affected T_H17 cell differentiation.

Cytokines that synergize with transforming growth factor–β (TGFβ) to induce T_H17 cells include IL-1β, IL-23, and IL-6 (*18*). Analysis after LPS stimulation revealed that *Il1b* was transiently overproduced in Ch25h-deficient macrophages, whereas *Il6* and *Il23* were unaltered (Fig. 2A). LPS stimulated EBI2-deficient BMDMs had wild-type amounts of *Il1b* (fig. S2A). Activated BMDMs lacking *Cyp7b1*, the enzyme that converts 25-HC to 7α,25-HC, also produced normal *Il1b* levels (fig. S2A), and their culture supernatants contained unaltered amounts of 25-HC (fig. S2B), consistent with minimal *Cyp7b1* expression in BMDMs (fig. S2C). Flow cytometric analysis showed elevated pro–IL-1β in Ch25h-deficient compared with wild-type macrophages (Fig. 2B). Confirming the presence of secreted IL-1β, IL-17A induction by Ch25h-deficient macrophage supernatants required T cell IL-1 receptor (IL-1R) expression (fig. S2D). The *Il1b* elevation in *Ch25h*$^{-/-}$ BMDMs occurred without a change in transcript stability and was preceded by induction of precursor mRNA, which indicated that it was due to increased transcription (Fig. 2C).

IL-1β secretion occurs after cleavage of pro–IL-1β by the inflammasome-activated protease caspase-1 (*19*). LPS treatment causes inflammasome priming by up-regulating expression of *Casp-1*, *Nlrp3*, and *Asc* (*19*), and induction of these transcripts occurred normally in Ch25-deficient BMDMs (fig. S2E). Full inflammasome activation depends on exposure to an activating agent, such as adenosine triphosphate (ATP) (*19*). IL-1β was elevated in the supernatant of LPS-stimulated *Ch25h*$^{-/-}$ BMDMs

exposed to ATP (Fig. 2D), whereas IL-6 was unaffected (Fig. 2D), and IL-23 was too low for measurement by enzyme-linked immunosorbent assay. LPS-stimulated Ch25h-deficient BMDMs also overproduced IL-18, another caspase-1–dependent IL-1 family member (*19*) (Fig. 2D). The increased secretion of IL-18 occurred in the absence of any transcript level differences (fig. S2F), which suggested that Ch25h-deficient BMDMs had elevated inflammasome activity.

Type I IFN inhibits NLRP3-containing inflammasomes by an undefined mechanism (*2*, *4*, *5*). LPS-primed Ch25h-deficient BMDMs exposed to ATP showed exaggerated caspase-1 activity, compared with equivalently treated control macrophages (Fig. 2), F and G, and generated more processed IL-1β (Fig. 2H). A slight elevation in caspase-1 activity was evident in *Ch25h*$^{-/-}$macrophages not exposed to ATP (Fig. 2, F and G), consistent with the elevated IL-1β bioactivity in these supernatants (Fig. 1C). Increased caspase-1 activity in Ch25h-deficient BMDMs was also observed after treatment with the additional NRLP3-inflammasome activators nigericin and alum, the NLRC4-inflammasome activator flagellin, and the AIM2-inflammasome activator poly(deoxyadenylic-deoxythymidylic) acid [poly(dA:dT)] (Fig. 2I). This broad inflammasome-repressive action of Ch25h suggests that it acts across nucleotide-binding oligomerization domain–like receptors (NLRs) or at a site downstream of the NLRs.

To test whether the Ch25h product was sufficient to regulate *Il1b* expression and caspase-1 activation, LPS-treated BMDMs were incubated with 25-HC. 25-HC suppressed *Il1b* mRNA, protein expression, and inflammasome activity in Ch25h-deficient cells, such that the amounts induced were similar to endogenously 25-HC–

producing control cells (Fig. 3A and fig. S3A). 25-HC had no significant effect on *Il6* expression (fig. S3A). Mass spectrometry of *Ch25h*$^{-/-}$ BMDMs incubated with 25-HC confirmed their ability to take up the oxysterol (fig. S3B). Incubation with similar concentrations of cholesterol or 7α,25-HC did not cause any change in *Il1b* levels or protein expression (Fig. 3A). Moreover, although transduction of both control and Ch25h-deficient BMDMs with wild-type Ch25h repressed *Il1b* expression and inflammasome activity, transduction with a point mutant that lacks enzymatic function (*20*) did not (Fig. 3B and fig. S3C).

25-HC is one of several oxysterol ligands for the nuclear hormone receptors, liver X receptor–α (LXRα, encoded by *Nr1h3*) and LXRβ (*Nr1h2*) (*21*, *22*), which can negatively regulate *Il1b* expression (*23*–*26*). However, whether 25-HC has a physiological role as an LXR ligand remains unclear (*27*, *28*). We did not observe any overinduction of *Il1b* transcripts, intracellular pro–IL-1β, or secreted IL-1β after LPS exposure of macrophages generated from LXR-deficient (*Nr1h2*$^{-/-}$*3*$^{-/-}$) mice compared with those from control bone marrow (BM) (fig. S3D). Moreover, transduction of LXR-deficient cells with Ch25h led to a similar repression in IL-1β production to that observed with control BMDMs (fig. S3E). These observations suggest that 25-HC acts via an LXR-independent mechanism to regulate *Il1b* transcription.

In vitro, 25-HC can repress sterol response element–binding protein (SREBP) processing into active transcription factors, which are required for cholesterol biosynthesis (*29*, *30*) (fig. S3F). However, Ch25h-deficient mice have intact cholesterol metabolism, which makes it unclear whether 25-HC has a physiological role as a negative regulator of SREBP processing and, therefore, sterol biosynthesis (*9*, *28*). To

further explore how Ch25h might regulate *Il1b* expression and inflammasome activity, we performed RNA sequencing (RNAseq) on LPS-treated BMDMs. This analysis revealed a striking elevation in transcripts for SREBP target genes in *Ch25h*$^{-/-}$ macrophages (Fig. 3C and fig. S3G). It also confirmed the elevation in *Il1b* and showed that *Il18*, *Il6*, and tumor necrosis factor (*Tnf)* were not greatly changed (fig. S3H). A panel of IFN-stimulated genes was induced in both wild-type and Ch25h-deficient cells compared with *Ifnar1*$^{-/-}$ BMDMs (fig. S3I). *Nr1h2*$^{-/-}$*3*$^{-/-}$ macrophages showed little alteration in the expression of SREBP target genes (Fig. 3C and fig. S3H). Western blotting confirmed that Ch25h deficiency was sufficient to deregulate SREBP processing in activated BMDMs (fig. S3J). These data implicate repression of SREBPs as a major pathway of gene regulation by 25-HC in activated macrophages. Sterol biosynthesis is down-regulated in IFN-exposed cells (*7*, *31*), and our findings suggest that Ch25h is a key IFN-induced gene responsible for this repression.

25-HC antagonizes processing of SREBP-1 and -2 by promoting their insulin-induced gene (INSIG)–mediated retention in the endoplasmic reticulum (ER), out of reach of activator proteases in the Golgi (*32*) (fig. S3F). To test whether 25-HC–mediated suppression of *Il1b* could be explained by activation of INSIG, we took advantage of the observation that INSIG overexpression is sufficient to inhibit SREBP processing even without addition of a ligand (*32*). Indeed, INSIG1 overexpression in Ch25h-deficient BMDMs led to reductions in LPS-stimulated *Il1b* transcripts and pro–IL-1β levels, whereas expression of *Il6* was unaffected (Fig. 3D). In a second approach, we examined macrophages lacking the SREBP-cleavage–activating protein (SCAP) that is required for transport of SREBPs from the ER to the Golgi for processing (*32*)

(fig. S3F). SCAP-deficient BMDMs expressed reduced amounts of *Il1b* and underwent reduced caspase-1 activation (Fig. 3E). These data indicate that repression of SREBP processing contributes to the mechanism of 25-HC–mediated down-regulation of *Il1b* and inflammasome activity.

To test whether IL-1 family cytokine production was regulated by Ch25h in vivo, mice were treated with LPS. After a sublethal LPS dose, Ch25h-deficient mice had more IL-1β and IL-18 in serum compared with controls (Fig. 4A and fig. S4A). IL-1α, a cytokine that is often coreleased with IL-1β (*33*), was also increased (fig. S4A). Serum IL-6 levels were unaffected (fig. S4B), and TNF was too low to measure. Splenic macrophages from the knockout mice showed deregulated expression of several SREBP-target genes (fig. S4C). BM chimera analysis established that Ch25h was required in hematopoietic cells for regulation of IL-1β and IL-1α and that both hematopoietic and stromal cell Ch25h regulated IL-18 (fig. S4, D and E). Overexpression of Ch25h in hematopoietic cells led to elevated baseline 25-HC in serum (fig. S4F) and to reduced IL-1β production after LPS treatment (fig. S4G). After exposure to a lethal LPS dose, Ch25h-deficient mice succumbed ~12 hours sooner than controls (Fig. 4B). Although it is recognized that LPS-induced death is influenced by factors besides IL-1 family cytokines, these data establish the important role of this single enzyme in resisting the lethal impact of septic shock (fig. S4H).

We also tested the effect of Ch25 deficiency on the course of myelin oligodendrocytes glycoprotein (MOG)–induced EAE, an IL-17–driven inflammatory disease (*2*). In accord with increased IL-17A$^+$ cell generation and with evidence that IL-

1β contributes to central nervous system pathology in this model (*4*), Ch25h-deficient mice suffered from exacerbated disease compared with controls (Fig. 4C).

Macrophage infection by the bacterium *Listeria monocytogenes* induces type I IFN and Ch25h expression, and bacterial replication in liver and spleen is promoted by type I IFN signaling (*1*, *2*). Ch25h-deficient mice were more resistant to *Listeria* growth than littermate controls (Fig. 4D); IL-1β, IL-1α, and IL-18 were elevated in the serum of infected mice (fig. S5A) and in BMDMs (fig. S5B); and the macrophage supernatants induced greater IL-17A$^+$ T cell differentiation (fig. S5C). Bacterial growth in BMDMs initially occurred at the same rate and then became more strongly repressed in Ch25h-deficient cells (fig. S5D). Although there is not yet a consensus on the mechanism of IFNαR-mediated augmentation of *Listeria* growth (*1*, *2*), our data indicate that type I IFN–mediated Ch25h induction contributes to host susceptibility to bacterial infection (fig. S5E).

Neutrophil recruitment to the peritoneum in response to the inflammasome activator, alum, is IL-1β–dependent (*5*). After treatment with alum alone, Ch25h-deficient and wild-type mice showed similar amounts of neutrophil recruitment (Fig. 4E). However, Ch25h-deficient mice suffered an inability to suppress neutrophil recruitment after type I IFN induction by poly(I:C) treatment (Fig. 4E). Similar findings were made in Ch25h-deficient BM chimeras (fig. S5F). Six hours after poly(I:C) treatment, wild-type mice showed a 20-fold increase in 25-HC serum concentrations (Fig. 4F). These data indicate that 25-HC functions downstream of type I IFN to repress IL-1β–mediated peritoneal inflammation (fig. S5E).

Discussion

We identify Ch25h as an essential part of the negative-feedback mechanism regulating IL-1 family cytokine production during inflammatory conditions involving type I IFN. 25-HC functions as a repressor of *Il1b* expression and as a broad inhibitor of inflammasome activity. Our findings support a model where 25-HC engagement of INSIG and antagonism of SCAP-dependent SREBP processing reduces *Il1b* expression and inflammasome activity. We speculate that repression of SREBP decreases *Il1b* expression and inflammasome activity by reducing cellular content of key sterols, possibly including cholesterol itself. 25-HC–mediated feedback regulation of inflammation requires multiple steps (fig. S3F), and we suggest that this serves as a built-in delay to allow adequate IL-1 family cytokine production and inflammasome activation before repression occurs. The anti-inflammatory actions of 25-HC defined in this study reveal a pathway that may contribute to the therapeutic activity of type I IFN in treatment of inflammasome-dependent autoimmune disease (***4***), the successful use of type I IFN in treatment of some types of cancer (***1***), and the widespread occurrence of uncontrolled bacterial infection after viral infection (***1***, ***2***) (fig. S5E).

Experimental procedures

Mice. Wild-type and Ly5.2 (CD45.1) congenic C57BL/6 (B6) mice, 6–12 weeks old, were from National Cancer Institute. Ebi2-/- mice(*42*) were backcrossed to C57BL/6J for 11 generations. These mice carry an eGFP gene inserted in place of the Ebi2 open reading frame. Ch25h-/- mice(*15*) were backcrossed to C57BL/6J for 10 generations. Lxra+/- and Lxrb+/- mice were from Jackson laboratories. Animals were housed in a specific pathogen–free environment in the Laboratory Animal Research Center at UCSF and all experiments conformed to the ethical principles and guidelines approved by the UCSF Institutional and Animal Care and Use Committee.

Cells. Bone marrow (BM) cells were differentiated in DMEM with 10% FBS and 10% M-CSF-conditioned medium for 6–7 days, then plated at 1 x 10^6 cells/ml and cultured overnight. BMDMs were primed with 100 ng/ml LPS (E. coli 0111:B4; Sigma) for the indicated time. For ELISA detection of IL1β, IL1α and IL18 and Caspase-1, ATP (Sigma) was added at the concentration of 5 mM for the final 45 min of culture. In one set of experiments nigericin (0.4 mM; Sigma-Aldrich), alum (300 mg/ml; Pierce Biochemicals), poly(dA:dT) (1 mg/10^6 cells; Sigma-Aldrich) and flagellin (1 mg/10^6 cells; a gift from Anthony DeFranco) were added to LPS-stimulated BMDMs for 12 hours in order to activate inflammasomes.

Bone marrow chimeras. Ly5.2 congenic or Ch25h-/- mice were lethally irradiated with either 1,100 or 1,300 rad in split doses and reconstituted with 1–3 x 10^6 BM cells from wild-type and Ch25h–/– donors. Mice were analyzed 8–12 weeks later.

BMDM transduction. BM cells were differentiated in DMEM with 10% FBS and 10% M-CSF-conditioned medium for 2 days then spin-infected with a retroviral construct expressing Ch25h, Ch25h mut(*20*), Insig1 or control and an IRES–Thy1.1 cassette as a reporter. In some experiments a retroviral construct expressing ER-Cre and an IRES-hCD4 was used. Two days after the spin infection, Thy1.1 positive cells were FACS sorted and cultured for a further 3 days before performing any experiment. Cells were always cultured in presence of 10% M-CSF-conditioned medium. ER-Cre transduced BMDMs were cultured in the presence of 4-hydroxytamoxifen (1 μM) for 2 days before performing any experiment.

Flow Cytometry. Cells were stained with Abs to TCRγδ (GL3), TCRβ (H57-597), IL17A (17B7), IFNγ (XMG1.2), CD11b (M1/70), Ly6G (1A8), Ly6C (HK1.4), CD115 (AFS98), F4/80 (CI:A3-1), pro-IL1β (NJTEN3), CD4 (RM4-5), CD44 (IM7) and CD25 (PC61) (from Biolegend, BD Biosciences, or eBioscience). Biotin conjugates were detected with streptavidin Qdot605 (Invitrogen). To detect IL17A and IFNγ, cells were stimulated for 4 h with 50 ng/ml PMA (Sigma-Aldrich) and 1 mg/ml ionomycin (EMD Biosciences) in brefeldin A (BD Biosciences). Cells were stained with fixable viability dye (eFluor780; eBioscience) to exclude dead cells then stained for surface antigens, treated with BD Cytofix Buffer and Perm/Wash reagent (BD Biosciences), and stained with anti–IL17A and anti-IFNγ . To detect pro-IL1β cells were treated with BD Cytofix Buffer and Perm/Wash reagent (BD Biosciences), and stained with anti-pro-IL1β. Intracellular caspase-1 activity was analyzed with CaspaLux1 E1D2 kit (OncoImmunin, Inc.) following the manufacturer's protocol.

Cytokine enzyme-linked immunosorbent assays. Supernatants from cultured BMDMs were collected at the times indicated. Enzyme-linked immunosorbent assay (ELISA) antibody pairs used for IL6, IL1β, IL1α and IL18 were as listed below. All ELISA antibodies were used at 2 mg/ml for capture and 1 mg/ml for detection. Detection antibodies were biotinylated and labelled by streptavidin-conjugated horseradish peroxidase (HRP), and visualized by the addition of Substrate Reagent Pack (R&D). Color development was stopped with 3 M H2SO4. Recombinant cytokines served as standards and were purchased from Peprotech or R&D. Absorbances at 450 nm were measured on a tunable microplate reader (VersaMax, Molecular Devices). Cytokine supernatant concentrations were calculated by extrapolating absorbance values from standard curves where known concentrations were plotted against absorbance using SoftMax Pro 5 software. Capture/detection antibody pairs were as follows: anti-IL1α unconjugated (364/3B3-14) and biotinylated (Polyclonal) from eBioscience; anti-IL1β, unconjugated (B122) and biotinylated (polyclonal); anti-IL18 biotinylated (74) and biotinylated (93-10C) from MBL international; anti-IL6 unconjugated (MP5-20F3) and biotinylated (MP5-32C11).

Sterols. 25-hydroxycholesterol, 7a25 hydroxycholesterol and cholesterol (Avanti Polar Lipids) were prepared in ethanol as 10 mM stock solutions.

Endotoxic shock model. Mice (8–10 weeks old) were injected i.v. with 50 mg/kg LPS (E. coli 0111:B4; Sigma) and monitored 8 times daily for a total of 6 days. For serum

cytokine measurements, a separate cohort of mice received 20 mg/kg LPS and blood was collected 12 h later.

In vivo peritonitis. For neutrophil recruitment in the peritoneum, mice were injected i.v. with 200 ug poly(I:C) followed by a second i.p. injection of 350 mg alum (Pierce) 5 hr later. 12–14 hr after alum injection, mice were sacrificed, peritoneal cavities were lavaged with 6 ml of medium and peritoneal cells were analyzed by FACS.

EAE model. Groups of female mice 8–10 weeks of age were immunized subcutaneously on day 0 with 100 mg MOG(35–55) (Genemed) emulsified in CFA (Chondrex). Pertussis toxin (List Biological Labs) in 100 ul saline was injected intravenously twice, on days 0 and 2, and disease severity was assigned scores.

Th17 priming. Naive CD4+ T cells were first enriched from spleen and peripheral lymph nodes with anti-CD4-coated magnetic beads (Miltenyi Biotec) and then sorted with a FACSAria (BD Biosciences) as CD4+ CD8– CD25- CD44lo CD62Lhi. Naive CD4+ T cells were stimulated with plate-bound anti-CD3 (2 μg/ml) and soluble anti-CD28 (2 μg/ml) for 4 days. For experiments with BMDM supernatants, the T cells were incubated in a 1 in 2 dilution of 12 hr LPS stimulated BMDM culture supernatant that had been centrifuged and 0.2μm filtered and in the presence or absence of TGFβ (1 ng/ml). For conventional Th17 priming, the T cells were cultured in medium containing IL6 (20 ng/ml, Peprotech), TGFβ (1 ng/ml), IL1β (10 ng/ml, R&D Systems), anti-IFNγ (10 μg/ml) and anti-IL4 (10 μg/ml, BD Biosciences).

Listeria infection. For *in vivo* infection, mice aged 8-10 weeks were infected intravenously with 5 x 10^5 *L. monocytogenes* i.v. for 2 days. For in vitro infection, BMDMs were seeded onto TC-treated dishes, incubated overnight, and infected with *L. monocytogenes* at a multiplicity of infection (MOI) of 10. After 30 min the infected cells were washed, gentamicin (50 ug/ml) treated and the cells and the supernatant were analyzed after 24 or 48 hours.

Quantification of 25-Hydroxycholesterol. BMDM were treated as above, medium was extracted with organic solvents and 25-HC quantified on a 4000 QTRAP liquid chromatography mass spectrometer (Applied Biosystems) as described(*15*).

RNA Isolation and Real-Time RT-PCR. Total RNA was isolated from ~5.0x10^5 BMDMs with the Trizol reagent (Life technology) following the manufacturer's protocol. Real-time PCR was performed using SYBR Green PCR Mix (Roche) and an ABI prism 7300 sequence detection system (Applied Biosystems, Foster city, CA). Hprt mRNA levels were used as internal controls. Primer sequences are shown in Table S1.

RNA-seq and analysis. Bone marrow-derived macrophages (1x10^7) were stimulated with 100ng/ml LPS for 8hrs. Cells were then washed 2x with PBS and the cell pellets were snap frozen in liquid nitrogen and stored at -80°C. RNA was extracted using the Qiagen RNeasy Kit. RNA quality was checked using the Agilent 2100 Bioanalyzer (RIN > 9 for all samples). Barcoded sequencing libraries were then generated using 100ng of RNA with the Ovation RNA-seq System V2 and Encore Rapid Library System. The UCSF Human Genetics Core performed next-generation sequencing (Illumina HiSeq

2500) with 100bp paired end reads. Sequences were reported as FASTQ files, which were aligned to the mm9 mouse genome using STAR (Spliced Transcript Alignment to a Reference) (*43*). Generation of Log2FC values and further analyses were performed using a Bioconductor package on RStudio.

Acknowledgements

We thank Judith Hellman for help with the sepsis model, Jeffrey Bluestone for help with the EAE model, and Ying Xu and Jinping An for expert technical assistance. A.R. was an Irvington Institute Postdoctoral Fellow at the Cancer Research Institute, E.V.D is supported by the UCSF Medical Scientist Training Program (MSTP) and the Biomedical Sciences (BMS) Graduate program, D.V.R. by the Clatyon Foundation for Research, and J.G.C. is an Investigator at the Howard Hughes Medical Institute and recipient of an Award from the American Asthma Foundation. This work was supported by NIH grants AI40098, HL20948 and 2P01HL20948.

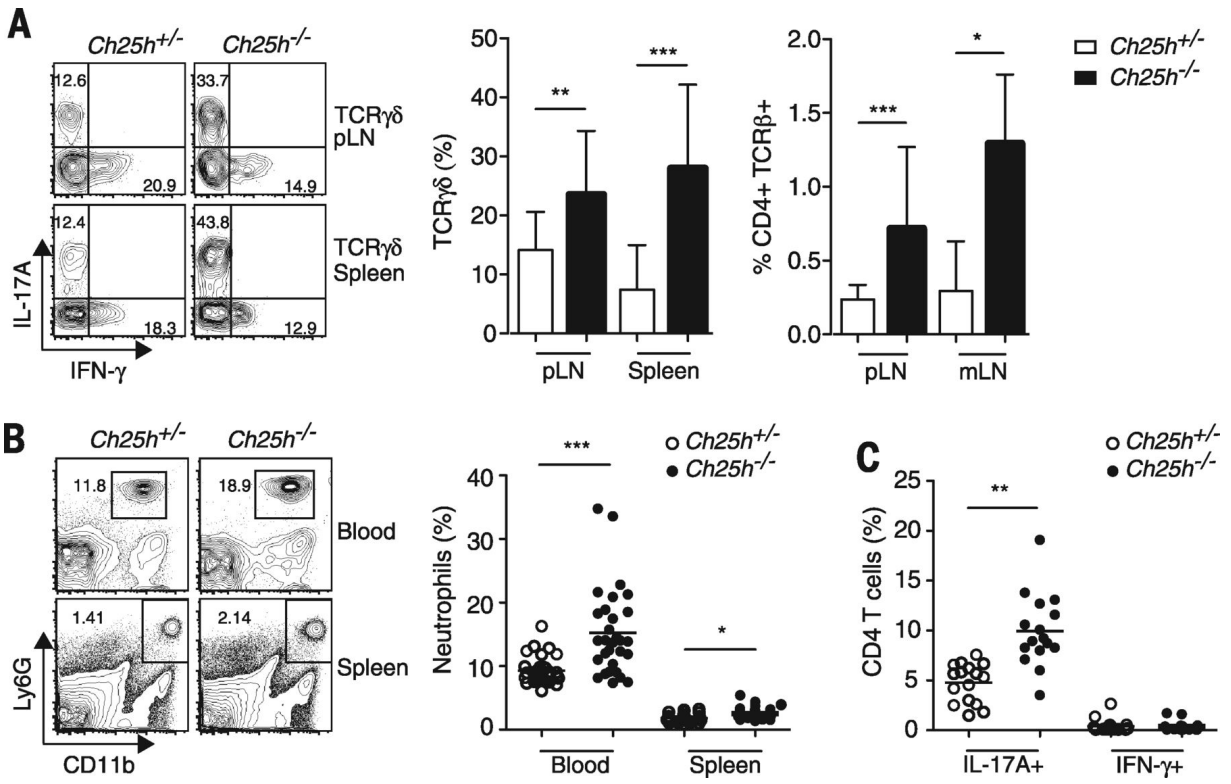

Figure 1. Elevated frequency of IL-17A–producing T cells in *Ch25h*$^{-/-}$ mice and increased IL-17A^{+} T cell induction by activated *Ch25h*$^{-/-}$ macrophages

(A) (Left) Representative fluorescence-activated cell sorted (FACS) plots of intracellular staining for IL-17A and IFN-γ in T cell receptor (TCR) γδ+ cells. (Right) Percentage of IL-17A^{+} γδ T cells and IL-17A^{+} CD4^{+} T cells in the indicated organs in *Ch25h*$^{+/-}$ and *Ch25h*$^{-/-}$ mice (n = 22 per genotype, means ± SD).

(B) (Left) Representative FACS plot showing frequency of neutrophils, detected by staining for Ly6G and CD11b, in blood and spleen of *Ch25h*$^{+/-}$ and *Ch25h*$^{-/-}$ mice. (Right) Percentage of neutrophils in blood and spleen for 25 mice of each genotype (means ± SD).

(C) Percentage of IL-17A^{+} CD4 T cells primed in vitro with supernatant of 8-hour LPS-stimulated *Ch25h*$^{+/-}$ or *Ch25h*$^{-/-}$ BMDMs, in the presence of 1 ng/ml of TGFβ, for 4 days. Each point represents cells from an individual mouse, and data are pooled from more than 10 experiments. *P < 0.05; **P < 0.01, ***P < 0.005 (unpaired Student's t test).

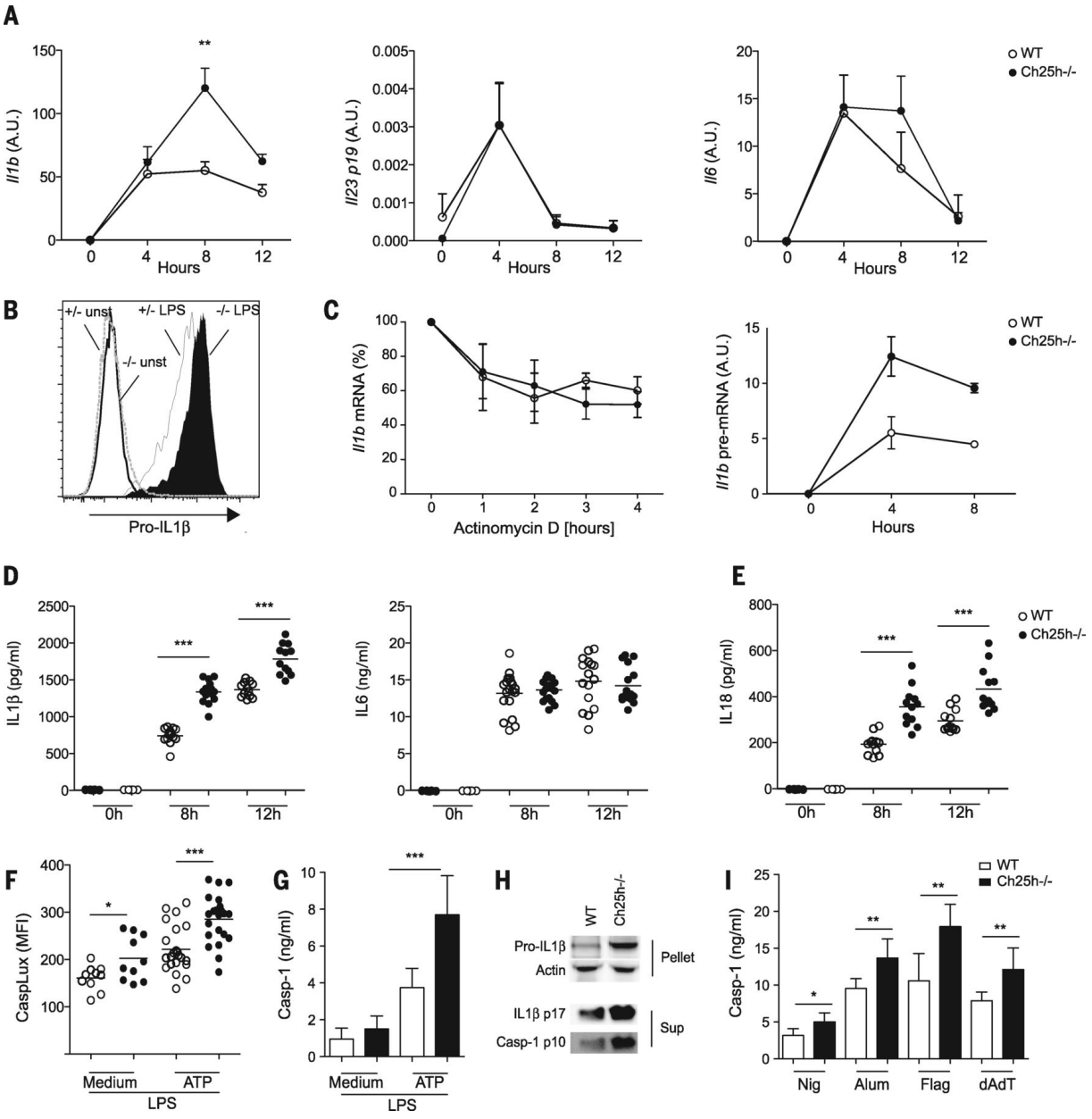

.

Figure 2. LPS-activated *Ch25h*$^{-/-}$ macrophages overproduce IL-1β and show increased inflammasome activity.

(A) Time course quantitative real-time fluorescence polymerase chain reaction (qPCR) analysis of *Il1b*, *Il23*, and *Il6* expression in BMDMs stimulated with LPS. Data are standardized by comparison to *Hprt*, and A.U. indicates arbitrary unit (means ± SD from six independent experiments).

(B) Pro–IL-1β intracellular level (arbitrary units) in BMDMs stimulated with LPS for 8 hours. Histogram plot is representative of data from more than 20 mice of each type.

(C) (Left) Time course qPCR analysis of *Il1b* mRNA expression after treatment with actinomycin D for the indicated time, starting 4 hours after LPS stimulation. (Right) Time course qPCR analysis of intron-containing (newly transcribed) pre-*Il1b* mRNA expression in BMDMs after stimulation with LPS. Both panels show means ± SD from three independent experiments.
(D) (Left) IL-1β secretion by BMDMs stimulated with LPS for 8 or 12 hours and incubated with 5 mM ATP for 45 min. (Right) IL-6 secretion by BMDMs stimulated with LPS for 8 or 12 hours.
(E) IL-18 secretion by BMDMs stimulated with LPS for 8 or 12 hours and with ATP for 45 min. (F) Intracellular level of activated caspase-1 in BMDMs stimulated with LPS for 8 hours and ATP for 45 min. Each point in (D), (E), and (F) represents data for an independent BMDM culture, and data are pooled from five experiments.
(G) Caspase-1 secretion by BMDMs stimulated with LPS for 8 hours and with ATP for 45 min. MFI, mean fluorescence intensity.
(H) Immunoblotting on cell pellet (pellet) and supernatant (sup) for pro–IL-1β and mature IL-1β (p17) and for activated caspase-1 (p10) in BMDMs stimulated with LPS for 8 hours and with ATP for 45 min. (I) Caspase-1 secretion by BMDMs stimulated with LPS for 8 hours, after culture with nigericin, alum, flagellin, or poly(dA:dT). Bars in (G) and (I) show means (±SD) of three experiments.

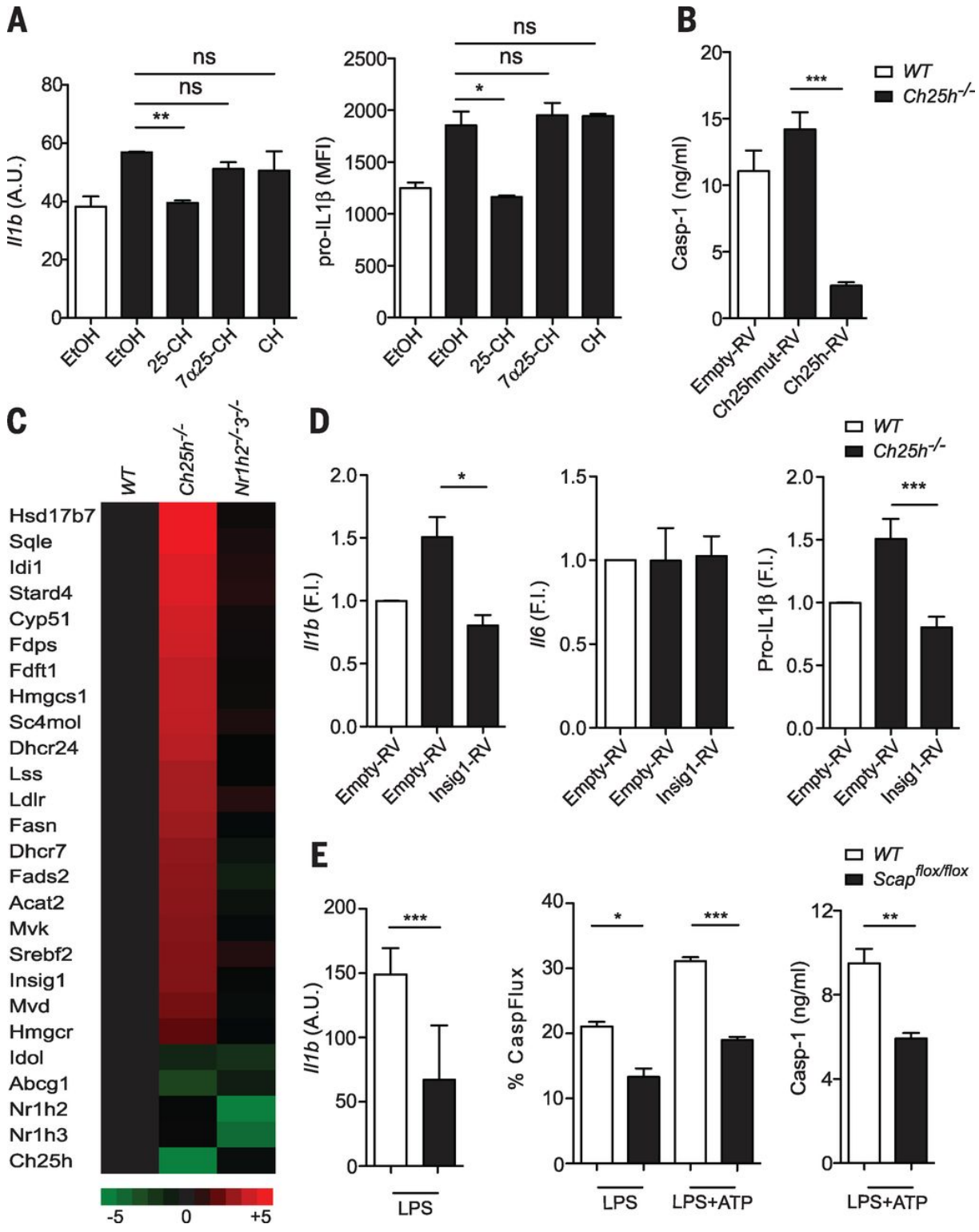

Figure 3. 25-HC represses IL-1β expression and inflammasome activation, and Ch25h-deficient macrophages show overexpression of SREBP-target genes.

(A) *Il1b* expression and pro–IL-1β intracellular level in wild-type and *Ch25*$^{-/-}$ BMDMs stimulated with LPS for 8 hours in the presence of 100 nM 25-HC; 7α,25-HC; or cholesterol (CH) or with carrier (means ± SD from three independent experiments). EtOH, ethanol.
(B) Secreted caspase-1 in BMDMs retrovirally (RV) transduced with empty vector, vector encoding Ch25h, or mutated Ch25h and then stimulated with LPS for 8 hours and ATP for 45 min (means ± SD from three independent experiments).
(C) Heat map of differentially expressed genes after RNAseq of wild-type, *Ch25h*$^{-/-}$, and *Nr1h2*$^{-/-}$*3*$^{-/-}$ BMDMs stimulated with LPS for 8 hours (determined based on log2 fold change).
(D) Effect of *Insig1* overexpression on *Il1b*, *Il6*, and pro–IL-1β levels in 8-hour LPS-stimulated BMDMs (means ± SD from three independent experiments). F.I., fold induced.
(E) *Il1b* expression, intracellular level of activated caspase-1 and secreted caspase-1 in wild-type and *Scap*$^{flox/flox}$ BMDMs retrovirally transduced with ER-Cre, treated for 2 days with 4-hydroxytamoxifen, and then stimulated with LPS for 8 hours (means ± SD from three independent experiments). **P* < 0.05; ***P* < 0.01, ****P* < 0.005 (unpaired Student's *t* test).

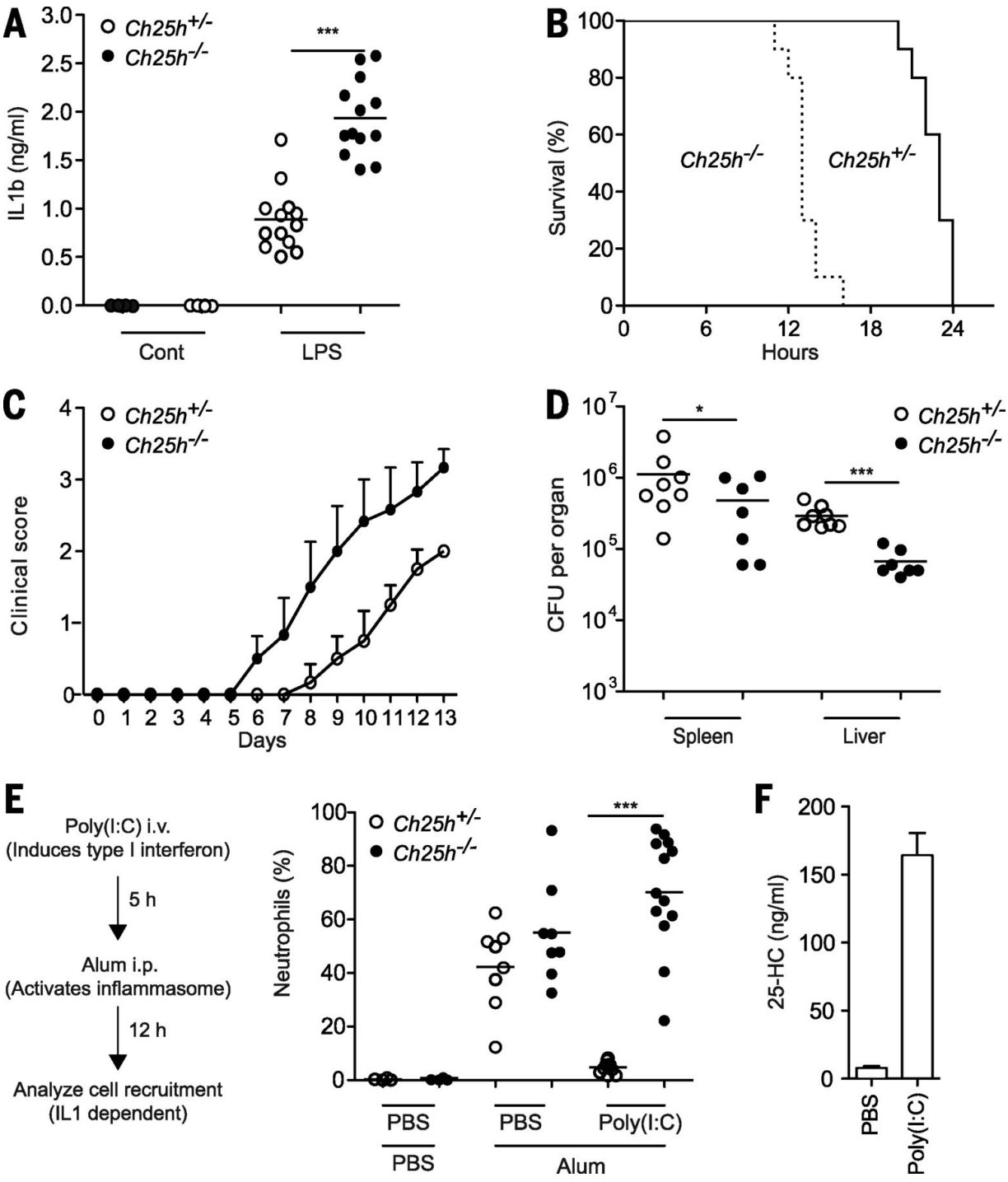

Figure 4. Exaggerated IL-1 family cytokine production, septic shock, and EAE and improved antibacterial response in Ch25h-deficient mice.
(A) Serum IL-1β in *Ch25h*$^{+/-}$ and *Ch25h*$^{-/-}$ mice 12 hours after injection of 20 mg/kg LPS. Each point represents an individual mouse, and data are pooled from three experiments.

(B) Survival of mice (n = 10 per genotype) injected with 50 mg/kg LPS ($P < 0.0001$ by Gehan-Breslow-Wilcoxon test).
(C) EAE severity in *Ch25h*$^{+/-}$ and *Ch25h*$^{-/-}$ mice immunized with MOG_{35-55} in CFA plus PTX (n = 12 per genotype, means ± SD).
(D) Bacterial growth in spleen and liver of mice infected with 5×10^5 *L. monocytogenes* for 3 days.
(E) Frequency of neutrophils in the peritoneal cavity of mice challenged with PBS or poly(I:C) intravenously followed by alum intraperitoneally. Treatments were as indicated in diagram on left. Each point represents cells from an individual mouse, and data are pooled from at least three experiments.
(F) 25-HC concentration in serum of PBS or poly(I:C)-injected mice (means ± SD from three independent experiments). *$P < 0.05$; **$P < 0.01$, ***$P < 0.005$ (unpaired Student's t test).

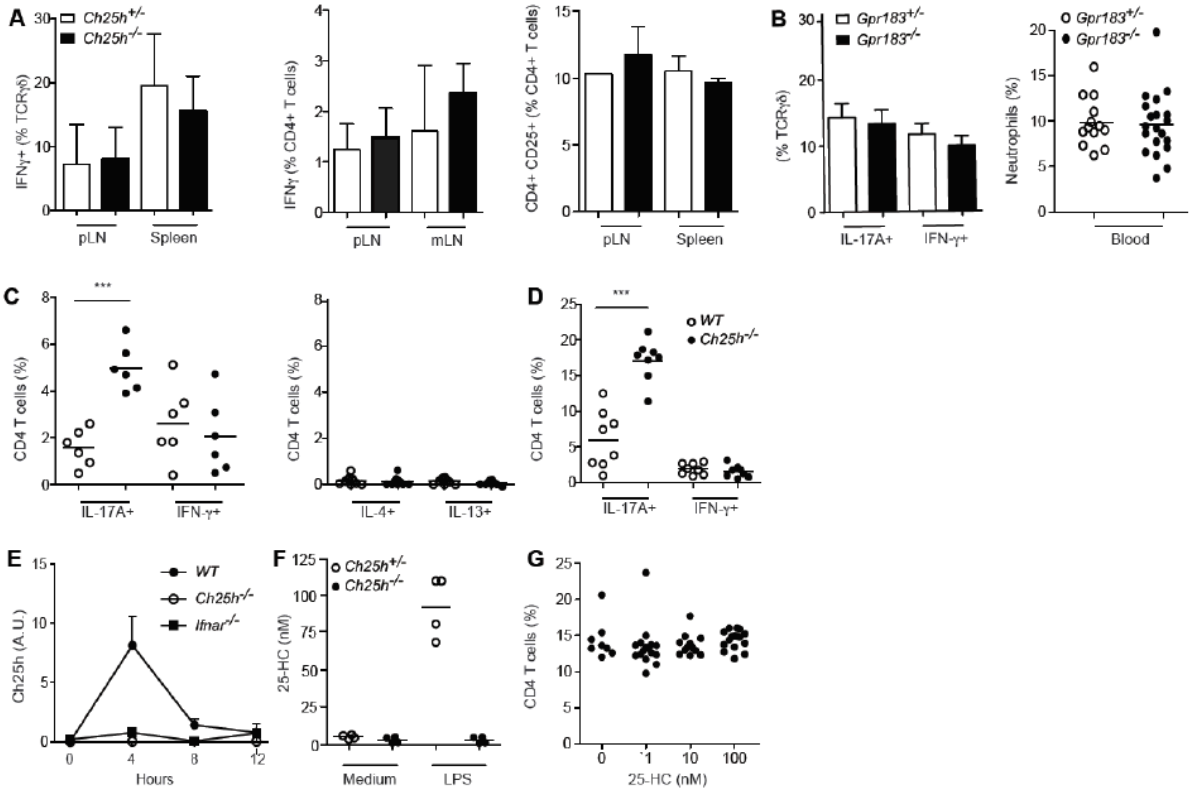

Supplemental Figure 1. Cytokine production by lymphocytes in Ch25h-/- mice.
(A) Percent of IFNγ^+ $\gamma\delta$ T cells, IFNγ^+ CD4$^+$ T and CD4$^+$ CD25$^+$ T cells in the indicated organs in Ch25h$^{+/-}$ and Ch25h$^{-/-}$ mice (n=22 per genotype, mean ± s.d.).
(B) (Left) percent of IL17A$^+$ and IFNγ^+ $\gamma\delta$ T cells in pLN in EBI2$^{+/-}$ and EBI2$^{-/-}$ mice (n=13 per genotype, mean ± s.d.). (Right) percent of neutrophils in blood of EBI2$^{+/-}$ and EBI2$^{-/-}$ mice (n=13 per genotype, mean ± s.d.).
(C) (Left) percent of IL17A$^+$ and IFNγ^+ CD4 T cells primed *in vitro* with supernatant of LPS-stimulated Ch25h$^{+/-}$ or Ch25h$^{-/-}$ BMDMs in the absence of TGFβ for 4 days. (Right) percent of IL4$^+$ and IL13$^+$ CD4 T cells primed *in vitro* with supernatant of LPS-stimulated Ch25h$^{+/-}$ or Ch25h$^{-/-}$ BMDMs in the presence of 1 ng/ml TGFβ for 4 days.
(D) Percent of IL17A$^+$ CD4 T cells primed in vitro with supernatant of LPS-stimulated Ch25h$^{+/-}$ or Ch25h$^{-/-}$ peritoneal macrophages in the presence of 1 ng/ml of TGFβ for 4 days. Each point indicates an individual culture and data are pooled from 3 experiments
(E) Time course of *Ch25h* mRNA expression in BMDMs generated from the indicated mice and stimulated with LPS (mean +/- SD from 6 independent experiments).
(F) 25-HC concentration in supernatants of control and LPS-stimulated *Ch25h*$^{+/-}$ or *Ch25h*$^{-/-}$ BMDMs.
(G) Percent of CD4 T cells expressing IL-17A following in vitro priming under Th17 polarizing conditions and treatment with 25-HC at the indicated concentrations for 5 days. Each point indicates an individual culture and data are pooled from 3 experiments
*, p<0.05; **, p<0.01, ***, p<0.005 (unpaired Student's T-test).

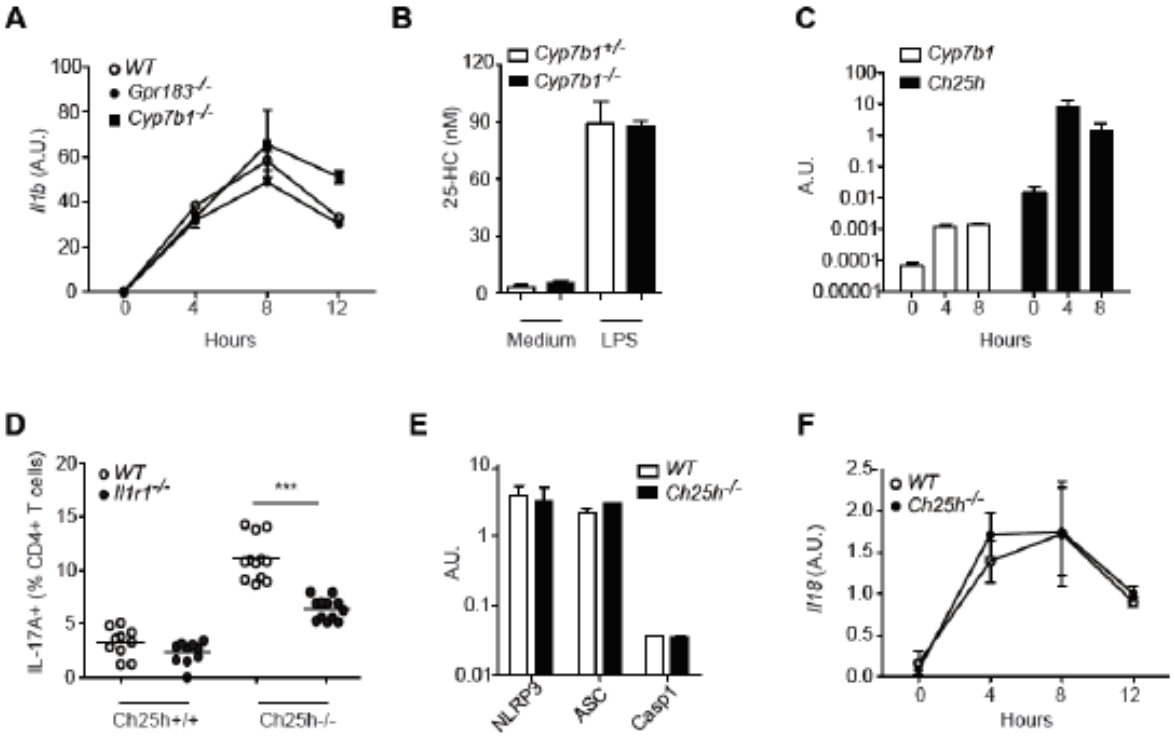

Supplemental Figure 2. EBI2 is not responsible for the Ch25h phenotype.
(A) Time course of *Ch25h* mRNA expression in BMDMs from wild-type, EBI2$^{-/-}$ and Cyp7b1$^{-/-}$ mice stimulated with LPS (mean ± s.d**.** from 6 independent experiments**).**
(B) 25-HC concentration in supernatant of LPS-stimulated Cyp7b1$^{+/-}$ or Cyp7b1$^{-/-}$ BMDMs**.**
(C) Time course of *Ch25h* and *Cyp7b1* mRNA expression in BMDMs stimulated with LPS.
(D) Percent of IL17A^{+} CD4 T cells from wild-type or IL1R1$^{-/-}$ mice primed *in vitro* with supernatant of LPS-stimulated Ch25h$^{+/+}$ or Ch25h$^{-/-}$ BMDMs in the presence of 1 ng/ml of TGFβ for 4 days.
(E) *Nlrp3, Asc* and *Casp-1* expression in wild-type and Ch25h$^{-/-}$ BMDMs stimulated with LPS for 8 hours.
(F) Time course of *Il18* expression in wild-type and Ch25h$^{-/-}$ BMDMs stimulated with LPS for 8 hours.
*, p<0.05; **, p<0.01, ***, p<0.005 (unpaired Student's T-test).

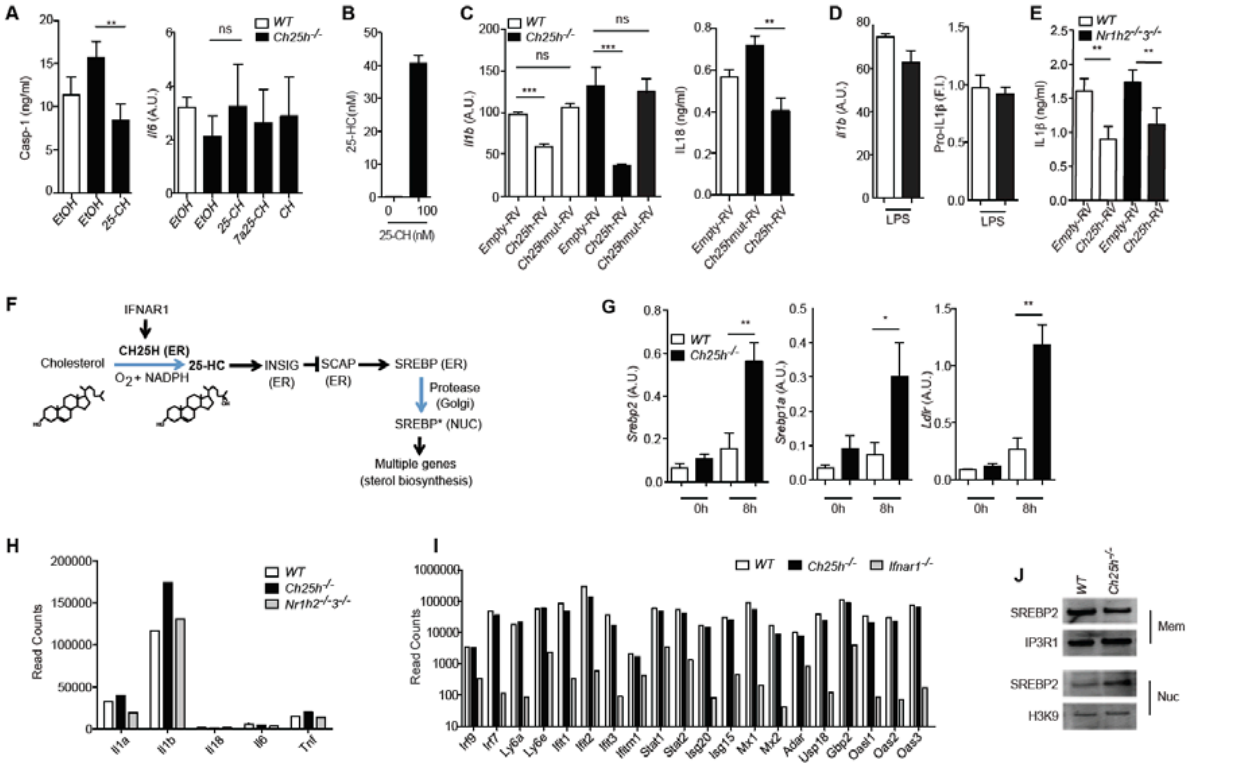

Supplemental Figure 3. SREBP pathway overactivation in Ch25h-/- BMDMs

(A) (Left) Secreted caspase-1 in wild-type and *Ch25h*$^{-/-}$ BMDMs stimulated with LPS for 8hrs in the presence of 100nM 25-HC or carrier. Secreted caspase-1 was measured after incubation with ATP. (Right) *Il6* expression in wild-type and *Ch25h*$^{-/-}$ BMDMs stimulated with LPS for 8hrs in the presence of 100nM 25-HC, 7α,25-HC, or cholesterol (CH) or with carrier (mean +/- SD from 3 independent experiments).

(B) 25-HC concentration in cell pellet of LPS-stimulated *Ch25h*$^{-/-}$ BMDMs incubated with 100nM 25-HC for 8 hours**.** Right panel, 25-HC concentration in supernatant from 293T cells transduced with empty vector or Ch25h-encoding retroviral vector (mean ± s.d**.** from 3 independent experiments).

(C) (Left) *Il1b* in BMDMs transduced with empty vector, vector encoding Ch25h or mutated Ch25h and stimulated with LPS for 8hrs. (Right) IL-18 in BMDMs transduced with empty vector, vector encoding Ch25h or mutated Ch25h and stimulated with LPS for 8hrs and ATP for 45min (mean +/- SD from 3 independent experiments).

(D) *Il1b* and pro-IL1β intracellular level in wild-type and LXRα/β double-deficient BMDMs stimulated with LPS for 8 hours (mean ± s.d**.** from 3 independent experiments**)**.

(E) IL1β secretion by wild-type and LXRα/β double-deficient BMDMs retrovirally transduced with empty vector or vector encoding Ch25h and stimulated with LPS for 8 hours and ATP for 45 min (mean +/- SD from 3 independent experiments)

(F) Pathway of 25-HC induction and repressive action on sterol biosynthesis. CH25H, INSIG, SCAP, and SREBP are each transmembrane proteins situated in the endoplasmic reticulum (ER). IFNAR1 signaling upregulates CH25H, generating 25-HC that binds INSIG and causes it to inhibit SCAP and prevent SREBP from leaving the

ER. When 25-HC is low, INSIG releases SCAP and allows it to chaperone SREBP to the Golgi where it undergoes proteolytic processing, leading to release of the active form (SREBP*) for movement to the nucleus (NUC) to act as a transcription factor
(G) *Srebp1a*, *Srebp2*, and *Ldlr* transcript expression determined by qPCR in wild type and *Ch25h*$^{-/-}$ BMDMs stimulated with LPS for 8 hours (mean +/- SD from 3 independent experiments)
(H) RNAseq data for inflammatory cytokines from 8 hour LPS-stimulated wild-type, Ch25h$^{-/-}$ or LXRα/β$^{-/-}$ BMDMs**.** Bars indicate means (±s.d., n=2).
(I) RNAseq data for IFN-stimulated genes from 8hr LPS-stimulated wild-type, *Ch25h*$^{-/-}$, or *Ifnar1*$^{-/-}$ BMDMs. Bars indicate means (n=2)
(J) Immunoblotting for membrane resident and nuclear SREBP2 and loading controls (IP3R1 and H3K9) on membrane and nuclear fractions from wild-type and *Ch25h*$^{-/-}$ BMDMs stimulated with LPS for 8hrs.

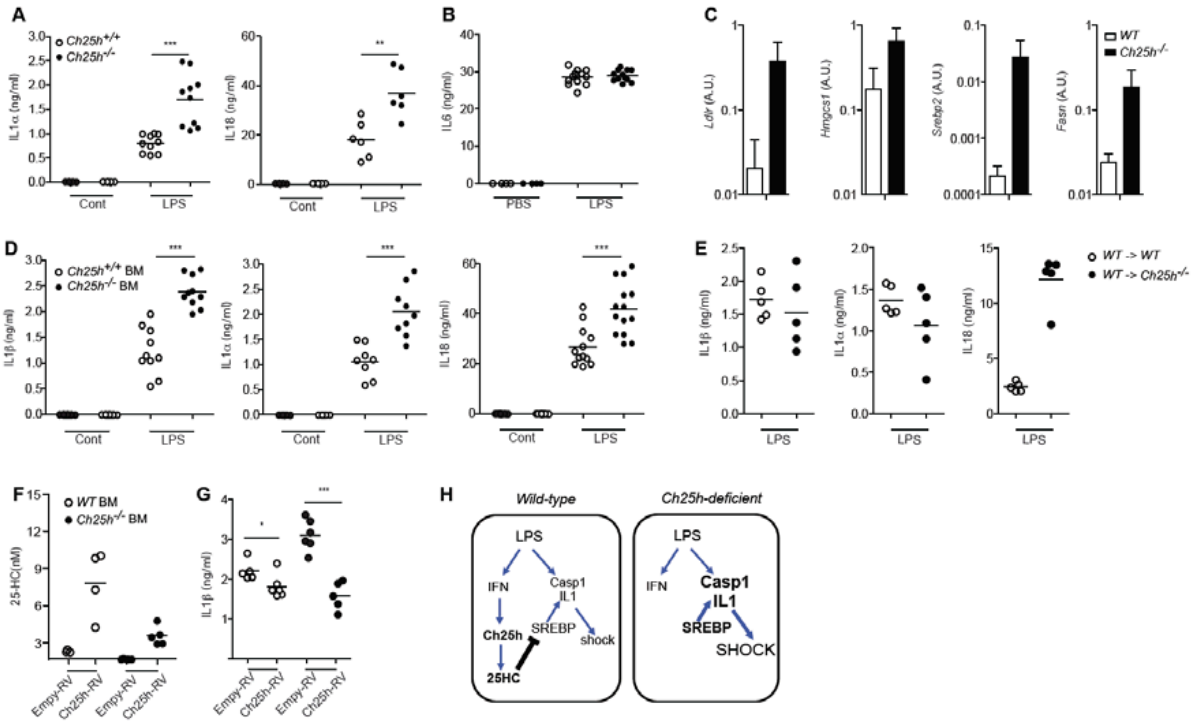

Supplemental Figure 4. Hematopoietic expression of Ch25h blocks LPS-induced IL-1 family cytokine production in vivo

(A) Serum IL-1α and IL-18 in *Ch25h*$^{+/-}$ and *Ch25h*$^{-/-}$ 12 hours after injection of 20mg/kg LPS. Each point in A and B represents an individual mouse and data are pooled from 3 experiments

(B) Serum IL6 in wild-type and *Ch25h*$^{-/-}$ mice 12 hours after injection of 20 mg/kg LPS.

(C) *Ldlr*, *Hmgcs1*, *Srebp2*, and *Fasn* transcript expression determined by qPCR in splenic macrophages from wild-type and *Ch25h*$^{-/-}$ mice injected 6 hours earlier with 20mg/kg LPS (mean +/- SD, n=3)

(D) Serum IL1β, IL1α and IL18 12 hours after injection of 20 mg/kg LPS in wild-type mice irradiated and transplanted with wild type or *Ch25h*$^{-/-}$ BM for 8 weeks. Cont indicates uninjected control chimeras. Each point represents an individual mouse and date are pooled from 3 experiments.

(E) Serum IL1β, IL1α and IL18 12 hours after injection of 20 mg/kg LPS in wild-type or Ch25h$^{-/-}$ mice irradiated and transplanted with wild-type BM for 8 weeks. Each point represents an individual mouse and date are pooled from 2 experiments.

(F) 25-HC concentration in serum of mice irradiated and transplanted with wild-type or Ch25h-/- BM retrovirally transduced with either empty vector or vector encoding Ch25h.

(G) Serum IL1β 12 hours after injection of 20 mg/kg LPS in mice of the type in F. Each point in F and G represents an individual mouse and data are pooled from 2 experiments

(H) Model for 25-HC induction and repressive action during LPS-induced septic shock

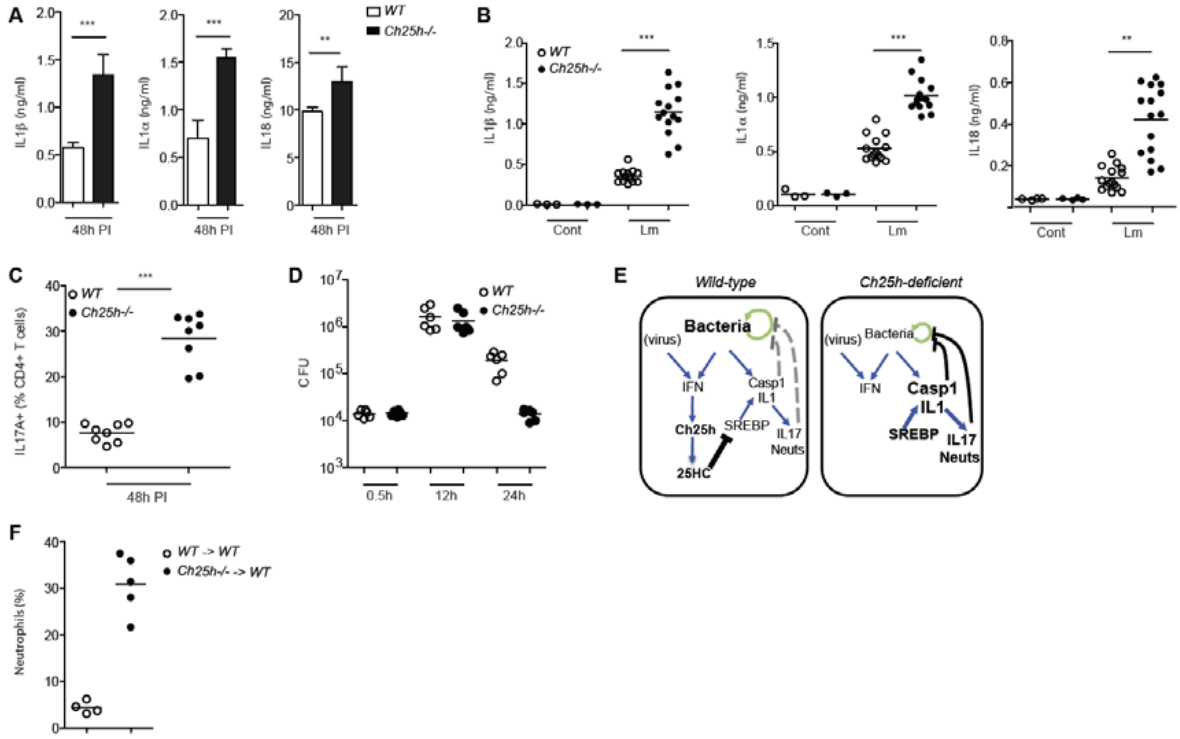

Figure S5. Ch25h-/- mice have exaggerated inflammatory responses to Listeria
(A) Serum IL1β, IL1α and IL18 from mice infected with $5x10^5$ *L. monocytogenes* for 3 days. (mean +/- SD from 3 independent experiments)
(B) IL1β, IL1α and IL-18 secreted by BMDMs cultured with *L. monocytogenes* for 48 hours (MOI=10). Each point represents an individual mouse and data are pooled from 3 experiments
(C) Percent of $IL17A^+$ CD4 T cells primed for 4 days *in vitro* with supernatant of BMDMs cultured with *L. monocytogenes* for 48 hours (MOI=10). Each point represents an independent BMDM culture and data are pooled from 3 experiments
(D) Intracellular growth of *L. monocytogenes* in wild type or *Ch25h*$^{-/-}$ BMDMs. Each point represents an independent BMDM culture and data are pooled from 2 experiments
(E) Model for 25-HC induction and repressive actions during a type I IFN-inducing bacterial infection or bacterial and viral co-infection. Neuts, neutrophils
(F) Frequency of neutrophils in the peritoneal cavity of BM chimeric mice challenged with Poly(I:C) followed by alum as in Fig. 4E. Each point represents an individual mouse and data are pooled from 2 experiments
*, $p<0.05$; **, $p<0.01$, ***, $p<0.005$ (unpaired Student's T-test).

Supplemental Table 1. Primers used in this study

	Forward primer	Reverse primer
Hprt	AGGTTGCAAGCTTGCTGGT	TGAAGTACTCATTATAGTCAAGGGCA
Il1b	AGCTTCCTTGTGCAAGTGTCT	GACAGCCCAGGTCAAAGGTT
Il6	TGGCTAAGGACCAAGACCATCCAA	AACGCACTAGGTTTGCCGAGTAGA
Il18	TCAAAGTGCCAGTGAACCCC	GGTCACAGCCAGTCCTCTTAC
Il23p19	TATCCAGTGTGAAGATGGTTGTG	CACTAAGGGCTCAGTCAGAGTTG
Ch25h	GCGACGCTACAAGATCCA	CACGAACACCAGGTGCTG
Cyp7b1	TTCCTCCACTCATACACAATG	CGTGCTTTTCTTCTTACCATC
Abcg1	TTCCCCTGGAGATGAGTGT	CAGTAGGCCACAGGGAACAT
Nlrp1a	AGGCTCTTTACCCTCTTCTA	ATGTGCTTCTTCTTCTGGTA
Nlrp3	TCCTGCAGAGCCTACAGTTG	ACGCCTACCAGGAAATCTCG
Nlrc4	TCACCACGGATGACGAACAG	GTCAATCAGACCACCTGGCA
Aim2	ACAAAGGCAGTGGGAACAAGA	GAAAACTTCCTGACGCCACC
Asc	GCCAGAACAGGACACTTTGTG	ACACTGCCATGCAAAGCATC
Caspase1	CGCCCTGTTGGAAAGGAACT	CCCTCAGGATCTTGTCAGCC
Caspase11	ACAATGCTGAACGCAGTGAC	CTGGTTCCTCCATTTCCAGA
Srebp1a	TTGGCACCTGGGCTGCT	GCGCCATGGACGAGCTG
Srebp2	CTTGACTTCCTTGCTGCA	GCGTGAGTGTGGGCGAATC
Ldlr	GAAGTCGACACTGTACTGACCACC	CTCCTCATTCCCTCTGCCAGCCAT
pre-Il1b	GGGCCTCAAAGGAAAGAATC	AAAGGCAGAGTCTTCGGTGA
Fasn	ACCCGAGGGATCTGGTGAA	CTGTCGTGTCAGTAGCCGAG
Hmgcs1	GGAAGCCTTTGGGGACGTTA	ACACTCCAACCCTCTTCCCT

References

1. G. Trinchieri, Type I interferon: friend or foe?, *J. Exp. Med.* **207**, 2053 (2010).
2. J. M. Gonzalez-Navajas, J. Lee, M. David, E. Raz, Immunomodulatory functions of type I interferons, *Nat. Rev. Immunol.* **12**, 125 (2012).
3. K. Ludigs, V. Parfenov, R. A. Du Pasquier, G. Guarda, Type I IFN-mediated regulation of IL-1 production in inflammatory disorders, *Cell. Mol. Life Sci.* **69**, 3395 (2012).
4. M. Inoue, M. L. Shinohara, The role of interferon-beta in the treatment of multiple sclerosis and experimental autoimmune encephalomyelitis - in the perspective of inflammasomes, *Immunology* **139**, 11 (2013).
5. G. Guarda *et al.*, Type I interferon inhibits interleukin-1 production and inflammasome activation, *Immunity* **34**, 213 (2011).
6. S. Y. Liu, D. J. Sanchez, R. Aliyari, S. Lu, G. Cheng, Systematic identification of type I and type II interferon-induced antiviral factors, *Proc. Natl. Acad. Sci. U. S. A.* **109**, 4239 (2012).
7. M. Blanc *et al.*, The transcription factor STAT-1 couples macrophage synthesis of 25-hydroxycholesterol to the interferon antiviral response, *Immunity* **38**, 106 (2013).
8. S. Y. Liu *et al.*, Interferon-inducible cholesterol-25-hydroxylase broadly inhibits viral entry by production of 25-hydroxycholesterol, *Immunity* **38**, 92 (2013).
9. D. W. Russell, The enzymes, regulation, and genetics of bile acid synthesis, *Annu. Rev. Biochem.* **72**, 137 (2003).
10. J. G. McDonald, D. W. Russell, 25-Hydroxycholesterol: a new life in immunology, *J. Leukoc. Biol.* **88**, 1071 (2010).

11. S. Hannedouche *et al.*, Oxysterols direct immune cell migration via EBI2, *Nature* **475**, 524 (2011).

12. C. Liu *et al.*, Oxysterols direct B-cell migration through EBI2, *Nature* **475**, 519 (2011).

13. C. Hong *et al.*, Coordinate regulation of neutrophil homeostasis by liver X receptors in mice, *J. Clin. Invest.*, (2011).

14. M. A. Stark *et al.*, Phagocytosis of apoptotic neutrophils regulates granulopoiesis via IL-23 and IL-17, *Immunity* **22**, 285 (2005).

15. D. R. Bauman *et al.*, 25-Hydroxycholesterol secreted by macrophages in response to Toll-like receptor activation suppresses immunoglobulin A production, *Proc. Natl. Acad. Sci. U. S. A.* **106**, 16764 (2009).

16. K. Park, A. L. Scott, Cholesterol 25-hydroxylase production by dendritic cells and macrophages is regulated by type I interferons, *J. Leukoc. Biol.* **88**, 1081 (2010).

17. T. Zou, O. Garifulin, R. Berland, V. L. Boyartchuk, Listeria monocytogenes infection induces prosurvival metabolic signaling in macrophages, *Infect. Immun.* **79**, 1526 (2011).

18. D. R. Littman, A. Y. Rudensky, Th17 and regulatory T cells in mediating and restraining inflammation, *Cell* **140**, 845 (2010).

19. L. Franchi, R. Munoz-Planillo, G. Nunez, Sensing and reacting to microbes through the inflammasomes, *Nat. Immunol.* **13**, 325 (2012).

20. E. G. Lund, T. A. Kerr, J. Sakai, W. P. Li, D. W. Russell, cDNA cloning of mouse and human cholesterol 25-hydroxylases, polytopic membrane proteins that synthesize a potent oxysterol regulator of lipid metabolism, *J. Biol. Chem.* **273**, 34316 (1998).

21. B. A. Janowski, P. J. Willy, T. R. Devi, J. R. Falck, D. J. Mangelsdorf, An oxysterol signalling pathway mediated by the nuclear receptor LXR alpha, *Nature* **383**, 728 (1996).

22. W. Chen, G. Chen, D. L. Head, D. J. Mangelsdorf, D. W. Russell, Enzymatic reduction of oxysterols impairs LXR signaling in cultured cells and the livers of mice, *Cell Metab.* **5**, 73 (2007).

23. S. B. Joseph, A. Castrillo, B. A. Laffitte, D. J. Mangelsdorf, P. Tontonoz, Reciprocal regulation of inflammation and lipid metabolism by liver X receptors, *Nat. Med.* **9**, 213 (2003).

24. S. Ghisletti *et al.*, Cooperative NCoR/SMRT interactions establish a corepressor-based strategy for integration of inflammatory and anti-inflammatory signaling pathways, *Genes Dev.* **23**, 681 (2009).

25. B. E. Bernstein *et al.*, An integrated encyclopedia of DNA elements in the human genome, *Nature* **489**, 57 (2012).

26. N. J. Spann *et al.*, Regulated accumulation of desmosterol integrates macrophage lipid metabolism and inflammatory responses, *Cell* **151**, 138 (2012).

27. I. Bjorkhem, Are side-chain oxidized oxysterols regulators also in vivo?, *J. Lipid Res.* **50 Suppl**, S213 (2009).

28. U. Diczfalusy, On the formation and possible biological role of 25-hydroxycholesterol, *Biochimie* **95**, 455 (2013).

29. G. Cui *et al.*, Liver X receptor (LXR) mediates negative regulation of mouse and human Th17 differentiation, *J. Clin. Invest.* **121**, 658 (2011).

30. C. Hong *et al.*, Constitutive activation of LXR in macrophages regulates metabolic and inflammatory gene expression: identification of ARL7 as a direct target, *J. Lipid Res.* **52**, 531 (2011).

31. M. S. Brown, J. L. Goldstein, Cholesterol feedback: from Schoenheimer's bottle to Scap's MELADL, *J. Lipid Res.* **50 Suppl**, S15 (2009).

32. T. I. Jeon, T. F. Osborne, SREBPs: metabolic integrators in physiology and metabolism, *Trends Endocrinol Metab* **23**, 65 (2012).

33. M. Blanc *et al.*, Host defense against viral infection involves interferon mediated down-regulation of sterol biosynthesis, *PLoS Biol.* **9**, e1000598 (2011).

34. J. L. Goldstein, R. A. DeBose-Boyd, M. S. Brown, Protein sensors for membrane sterols, *Cell* **124**, 35 (2006).

35. O. Gross *et al.*, Inflammasome activators induce interleukin-1alpha secretion via distinct pathways with differential requirement for the protease function of caspase-1, *Immunity* **36**, 388 (2012).

36. M. A. Williams, R. L. Schmidt, L. L. Lenz, Early events regulating immunity and pathogenesis during Listeria monocytogenes infection, *Trends Immunol.* **33**, 488 (2012).

37. N. Robinson *et al.*, Type I interferon induces necroptosis in macrophages during infection with Salmonella enterica serovar Typhimurium, *Nat. Immunol.* **13**, 954 (2012).

38. S. S. Im *et al.*, Linking lipid metabolism to the innate immune response in macrophages through sterol regulatory element binding protein-1a, *Cell Metab.* **13**, 540 (2011).

39. M. Gerlic *et al.*, NLRP1a Expression in Srebp-1a-Deficient Mice, *Cell Metab.* **19**, 345 (2014).

40. T. Yi *et al.*, Oxysterol gradient generation by lymphoid stromal cells guides activated B cell movement during humoral responses, *Immunity* **37**, 535 (2012).

41. D. Gatto, R. Brink, B cell localization: regulation by EBI2 and its oxysterol ligand, *Trends Immunol.*, (2013).

42. J. P. Pereira, L. M. Kelly, Y. Xu, J. G. Cyster, EBI2 mediates B cell segregation between the outer and centre follicle, *Nature* **460**, 1122 (2009).

43. A. Dobin *et al.*, STAR: ultrafast universal RNA-seq aligner, *Bioinformatics* **29**, 15 (2013).

Chapter 2

25-Hydroxycholesterols in innate and adaptive immunity

Summary

Cholesterol and components of the cholesterol biosynthetic pathway have fundamental roles in all mammalian cells. Hydroxylated forms of cholesterol are now emerging as important regulators of immune function. This involves effects on the cholesterol biosynthetic pathway and cell membrane properties, actions that can have anti-viral and anti-inflammatory influences. In addition, a dihydroxylated form of cholesterol functions as an immune cell guidance cue by engaging the G-protein coupled receptor EBI2, and it is required for mounting adaptive immune responses. Here we review current understanding of the closely related oxysterols, 25-hydroxycholesterol and 7a,25-dihydroxycholesterol, and the growing evidence that they have wide-ranging influences on innate and adaptive immunity.

Introduction

Cholesterol is one of the most abundant lipids in mammalian cells, constituting up to 25% of plasma membrane lipid[1]. Due to its rigid, hydrophobic structure, cholesterol increases membrane packing and different membranes within the cell have dissimilarities in fluidity as a result of differing cholesterol concentrations. Cholesterol-rich microdomains (rafts) in the plasma membrane are important for signaling by transmembrane receptors[2] and cholesterol distribution in membranes affects the entrance, replication and budding of viruses[3, 4]. The pathway of sterol biosynthesis from acetyl-CoA is active in all nucleated cells and in addition to the production of cholesterol it generates isoprenoids, lipids that are required for attaching signaling proteins to membranes[5] (Fig 1). Downstream metabolites of cholesterol include oxysterols, bile acids and steroid hormones[6, 7].

Forty years ago, 25-hydroxycholesterol (25-HC) was shown to have a potent ability to mediate feedback regulation of cholesterol biosynthesis[8, 9]; however, the physiological significance of this oxysterol came into question when mice deficient in the lipid were found to have normal whole body cholesterol metabolism[7,10, 11]. Indications that 25-HC might have immune-related functions were hinted at by the finding that the enzyme required for 25-HC synthesis was upregulated in macrophages and dendritic cells (DCs) exposed to various inflammatory mediators[12-15]. Stronger evidence that 25-HC has wide ranging roles in the immune system came from further studies of innate and adaptive immunity. One line of investigation focused on defining the requirements for anti-viral immunity and this led to the recognition that 25-HC is induced in macrophages by type I interferon (IFN) and has a broad ability to neutralize the

replication of viruses[16, 17]. A distinct set of investigations aimed at defining the guidance cue requirements for B cells during the antibody response led to the identification of a role for the G-protein coupled receptor EBI2 (GPR183) in positioning activated B cells to supportive niches[18, 19]; separate work de-orphanized EBI2 and revealed its ligand to be 7a,25-HC[20, 21]. 25-HC has also been found to regulate IgA production[13], to promote macrophage foam cell formation[22], to augment the production of some inflammatory cytokines[23, 24], and to mediate feedback inhibition of IL1-family cytokine production[25]. 7a,25-HC has been found to function as a guidance cue also for EBI2-expressing dendritic cells[26, 27]. Here, we review the requirements for 25-HC and 7a,25-HC biosynthesis and function and discuss what is known about how these 25-hydroxylated forms of cholesterol regulate innate and adaptive immune cell behavior.

Production of 25-HC and 7α,25-HC

Cholesterol has 4 rings and an 8-carbon side chain, and it carries a 3β-OH group at ring A that confers polarity on this otherwise hydrophobic molecule (Fig. 2). 25-HC is synthesized from cholesterol by the addition of a second hydroxyl group at the 25-position, located almost at the opposite end of the structure to the 3β-OH, which makes 25-HC considerably more hydrophilic than cholesterol[6]. The 25-hydroxylation reaction is carried out by cholesterol 25-hydroxylase (CH25H) a multi-transmembrane endoplasmic reticulum (ER) protein. CH25H is a member of a family of lipid desaturases and hydroxylases that contain a tripartite histidine box motif active site and use diiron-oxygen as a cofactor[7, 13, 28]. There may be other enzymes capable of producing 25-HC *in vitro*, although whether they have a role in generating this lipid *in vivo* remains to be determined[11].

Conversion of 25-HC to 7a,25-HC involves hydroxycholesterol 7α-hydroxylase (CYP7B1)-mediated hydroxylation at the 7α position[29]. CYP7B1 is a cytochrome P450 family enzyme and is also situated in the ER[29]. The enzymatic pathway generating 25-HC and 7a,25-HC was characterized as part of a series of studies that identified 17 enzymes functioning in the liver to convert cholesterol into bile acids[7]. CYP7B1 is abundant in the liver and has a role in bile acid synthesis due to its 7a hydroxylation of 27-HC[7]. By contrast, CH25H is poorly expressed in healthy liver, but is more abundant in several other tissues, leading to an early suggestion that it might function in generating 25-HC for biological processes other than bile acid production[7]. CYP7B1 is also expressed at low levels in a range of tissues in agreement with it too having roles beyond bile acid synthesis[29].

7a-hydroxylated sterols, including 7α-HC and 7α,25-HC, are metabolized by 3β-hydroxy-Δ5-C27 steroid oxidoreductase (HSD3B7) through oxidation of the 3β hydroxyl into a ketone group and isomerization of the $\Delta^{5,6}$ double bond. Like CH25H and CYP7B1, HSD3B7 is situated in the ER[7]. HSD3B7 functions at an essential step in bile acid synthesis and is very abundant in liver[30]. This enzyme is also detectable in other tissues, including lymphoid tissues[31], and recent work that is discussed further below has shown that it has an extra-hepatic role in metabolizing 7a,25-HC.

Feedback suppression of sterol biosynthesis

The existence of a negative feedback loop in which cholesterol suppresses its own biosynthesis emerged from classic studies on whole animal cholesterol homeostasis carried out in the 1930s (reviewed in[32]). Experiments exploring the mechanism of cholesterol feedback regulation led to the discovery that several oxidized forms of cholesterol, including 25-HC, were more effective at inhibiting sterol biosynthesis *in vitro* than cholesterol itself[8, 9]. A remarkable series of biochemical and cell biological studies led to the molecular definition of the cholesterol negative feedback circuit (Fig. 3)[32].

Sterol biosynthesis is promoted by sterol response element binding proteins (SREBPs; in particular SREBP2), transcription factors that derive from inactive membrane-spanning proteins in the ER[5, 32]. In its active state, SREBP2 promotes expression of 3-hydroxy-3-methyl-glutaryl-CoA reductase (HMGCR), a rate limiting enzyme in the cholesterol biosynthetic pathway, and many other enzymes in the pathway, as well as molecules involved in cholesterol uptake such as the low density lipoprotein (LDL) receptor[33]. To become active transcription factors, SREBPs must move from the ER to the Golgi to be processed by site-1 and site-2 proteases (Fig. 3). SREBPs are escorted from the ER to Golgi by the multi-transmembrane SREBP-cleavage activating protein (SCAP)[32]. SCAP is not just an escort protein, but also a cholesterol sensor, that contains a sterol-sensing domain (SSD); when cholesterol levels in the ER build up, SCAP conformation is modified, causing it to bind ER-resident INSIG proteins (insulin induced genes-1 and -2). The interaction with INSIG proteins retains SREBPs in the ER in their inactive form, accounting for the mechanism of

cholesterol-mediated feedback inhibition of sterol biosynthesis. It was predicted that 25-HC might function in the same way, but it turned out that 25-HC instead binds the multi-transmembrane INSIG proteins and modifies their conformation to cause association with SCAP. Through this alternate pathway 25-HC achieves the same outcome of preventing SREBP processing (Fig. 3)[32].

As well as repressing the expression of sterol biosynthetic enzymes such as HMGCR by inhibiting SREBP processing, sterols, including 25-HC, promote the post-translational downregulation of HMGCR[32]. 25-HC promotes INSIG association with HMGCR, and this leads to ubiquitylation and proteasomal degradation of this multi-transmembrane ER enzyme[34].

Although this work deciphered many aspects of cholesterol- and 25-HC-mediated inhibition of sterol biosynthesis, it did not elucidate the *in vivo* significance of this activity. Indeed, when *Ch25h*$^{-/-}$ mice were generated they were found to be 25-HC-deficient as expected, but they suffered no defects in whole animal cholesterol metabolism[7] leaving an important question mark over the understanding of 25-HC function[10, 11]. New findings about the actions of 25-HC in the immune system are now beginning to show that this oxysterol does have a physiological role as a regulator of sterol synthesis. Rather than functioning to control cholesterol homeostasis at the organismal level, 25-HC may provide a mechanism to enable selective control of the sterol biosynthetic pathway in restricted populations of cells responding to infectious agents and inflammatory mediators, as discussed further below.

Antiviral effects of 25-HC

Viruses often alter cellular lipid metabolism to support their replication[3, 4]. Over the past two decades several studies have found that inhibition of the cholesterol biosynthetic pathway or reducing cellular cholesterol content can decrease virus entry and replication[4, 35-42]. This in turn led to the discovery that type I IFNs, a family of cytokines that are strongly induced by most viral infections, cause down-regulation of sterol biosynthesis in a mechanism that contributes to protection of the cell[43].

It was therefore speculated that oxysterols might have a role in the negative regulation of sterol synthesis during viral infection. Mass spectrometry analysis of murine cytomegalovirus (MCMV)-infected macrophage cultures for ~20 different oxysterols revealed, remarkably, that the only one to increase substantially after viral infection was 25-HC[16, 44]. Similar observations were made for type I IFN– and IFNγ–stimulated cells. In complementary work, CH25H was found to be one of the more strongly induced interferon stimulated genes (ISGs) out of several hundred such genes[14, 15, 45]. In a screen of almost 300 ISGs for suppression of vesicular stomatitis virus (VSV) replication in HEK293T cells, CH25H was amongst the most efficacious[45]. 25-HC had anti-viral activity in cell culture assays against more than 10 enveloped viruses (including MCMV, vesicular stomatitis virus (VSV), West Nile virus, HIV, influenza virus, murid herpesvirus 68 (MHV68), and Ebola virus)[16, 17 35, 44, 46, 47] and one non-enveloped virus (polio virus)[48], but was inactive against another non-enveloped virus (adenovirus)[16, 17]. Reciprocally, CH25H-deficient macrophages and B cells were more sensitive to infection by VSV[17]. Although the number of *in vivo* experiments has so

far been limited, treatment of mice with high doses of 25-HC decreased MHV68 lytic infection and HIV replication, and *Ch25h*-deficient mice had increased MHV68 growth[17]. Although they agreed about the importance of 25-HC as an anti-viral mediator, these studies differed in their conclusions about the mechanism of action. One study found that 25-HC blocked entry of VSV and HIV and suggested that the effect of 25-HC might be through direct modification of cell membranes[17] (Fig. 4). In accord with this model, 25-HC causes cholesterol to become more readily extracted from the plasma membrane and it (together with other side chain oxysterols) has direct membrane-disordering effects[49, 50]. At high concentrations 25-HC increases cholesterol ester formation in cells and this may contribute to its mechanism of altering membrane properties[44, 51]. Cholesterol esters are forms of cholesterol with a fatty acid (typically oleic acid) attached via the 3β-hydroxyl; cholesterol esters do not partition effectively into bilayers, but intercalate into lipid droplets. In contrast with this direct membrane modification model, another study suggested that 25-HC blocks viral replication after entry into the cell by impeding viral gene expression[16] (Fig. 4). Evidence was provided that 25-HC-mediated antagonism of SREBPs might be involved, although this pathway was not thought to account for all of the observed anti-viral effect[16]. SREBP pathway inhibition would fit with the finding that addition of isoprenoids partially rescues viral replication in IFN-treated cells[16]. Several viruses require prenylation of either viral or host proteins for productive infection[4]. Inhibition of SREBPs also antagonized WNV, hepatitis C virus (HCV) and Andes virus infection, possibly by reducing plasma membrane cholesterol or by decreasing fatty acid synthesis[35, 38, 47]. A further possible mechanism for the anti-viral action of 25-HC has been suggested by the finding that

exposure of cells to micromolar amounts of this oxysterol activates the integrated stress response by an undefined pathway[44]. This response causes suppression of protein synthesis and can thereby inhibit viral replication[44]. Finally, 25HC-mediated repression of polio virus replication was suggested to occur through interaction with oxysterol binding protein (OSBP)[48] and hence a reduction in cholesterol accumulation in membranes that function as platforms for viral replication[52]. By interacting with OSBP, 25-HC can repress OSBP-mediated delivery of cholesterol from the ER to the Golgi[53]. Inhibition of OSBP function might also contribute to the mechanism of 25-HC-mediated inhibition of influenza virus and VSV replication[54]. Taken together, these observations indicate that the lipid synthesis and compartmentalization-altering activities of 25-HC enable it to inhibit viral replication at multiple steps along the pathway of entry, replication and budding.

Inflammation-regulatory effects of 25-HC

As well as having anti-viral and pro-inflammatory actions, type I IFNs have a suppressive effect on the immune response, an action that helps to prevent uncontrolled inflammation and that underlies their use for the treatment of certain autoimmune diseases such as multiple sclerosis[55-58]. This suppressive action also contributes to an increased propensity for bacterial infection following IFN induction by viral infection and to the detrimental effect of type I IFN induction during various primary bacterial infections[55, 56]. A central facet of the IFN-mediated suppressive effect is down-regulation of inflammasome activity and the production of IL-1 family (IL-1a, IL-1β and IL-18) cytokines[57, 59]. Recent work has provided evidence that 25-HC has a role downstream of type I IFN in mediating this anti-inflammatory effect (Fig. 5). *Ch25h*-deficient macrophages over-produce *Il1b* transcripts and have deregulated caspase-1-activating inflammasome activity[25]. Both of these effects are due to a loss of 25-HC-mediated repression of SREBP processing[25]. The mechanism by which SREBPs promote *Il1b* transcription is not yet clear although no direct interaction between SREBPs and the *Il1b* promoter has been reported, which indicates that the effect is probably indirect.

Inflammasome activation is a complex process that involves an activator engaging a triggering protein that catalyzes high order oligomerization of ASC (apoptosis-associated speck-like protein containing a CARD), which in turn leads to recruitment and activation of the caspase-1 protease[60, 61]. Active caspase-1 then cleaves the pro-forms of IL-1β and IL-18 for release from the cell while also promoting a form of cell death known as pyroptosis[61]. The ability of 25-HC to antagonize

inflammasome activation by NLRP3-, NLRC4- and AIM2-containing inflammasomes indicates that SREBP activity influences a step downstream of the activator, perhaps the ASC oligomerization or caspase-1 activation step[61]. Consistent with such antagonism, overexpression of *Ch25h* represses caspase-1 processing and cell death induced in response to *Listeria monocytogenes* infection[15]. As the suppressive effect of 25-HC depends on repression of SREBP processing[25], it seems reasonable to speculate that altered cellular lipid content downstream of altered SREBP activity influences the oligomerization of inflammasome components. Changes to cellular lipid content may not be due to repression of HMGCR expression by decreased SREBP activity, however, as treatment of cells with statins can promote IL-1β release[62, 63]. Instead it may reflect an influence of SREBP on lipid uptake and distribution in the cell. The loss of 25-HC-mediated repression of IL-1-family cytokine production and inflammasome activity in mice was evident in a number of ways. *Ch25h*-deficient mice over-produced IL-1β, IL-1a and IL-18 following LPS injection and died more rapidly from septic shock[25]. When immunized under conditions that promote an IL-1-dependent form of experimental autoimmune encephalomyelitis[58], *Ch25h*-deficient mice had more severe disease than littermate controls[25]. *Ch25h*-deficient mice also had a stronger ability to repress the growth of *Listeria monocytogenes*[25] whereas mice with overexpression of *Ch25h* were less able to control infection[15], which is consistent with type I IFN induction by this organism favoring growth by causing the repression of IL-1β production[55, 56]. Type I IFN induction by a range of bacteria, including *Mycobacterium tuberculosis*[64, 65], is associated with decreased IL-1β levels and enhanced bacterial

growth[55, 56]. It will be important to determine whether 25-HC contributes to the repression of IL-1 family cytokine production in these infections also.

IL-1β over-production is seen in several human genetic disorders that lead to increased inflammasome activity[66]. One such disease, hyperimmunoglobulinemia D with periodic fever syndrome (HIDS) is caused by hypomorphic mutations in mevalonate kinase (MVK), an enzyme catalyzing the second step in isoprenoid and sterol synthesis (Fig. 1)[66]. It is not clear why MVK-deficient patients have increased levels of IL-1β although some work has suggested that it reflects a role for geranylgeraniol pyrophosphate in suppressing IL-1β secretion, probably through its role in protein prenylation[67-69]. Fibroblasts from MVK-deficient patients compensate for the decreased MVK activity by upregulating HMGCR expression to increase levels of mevalonate (Fig. 1) and enable normal sterol synthesis[70]. However, given that fever in MVK-deficient patients is triggered periodically, possibly by type I IFN-provoking stimuli[66], the MVK deficiency may cause cholesterol availability in the ER of activated macrophages to be scarce under conditions where CH25H is normally highly active. This could limit 25-HC production and lead to the type of exaggerated SREBP activation that is observed in IFN-exposed CH25H-deficient cells[25]. These observations also raise the question of whether mutations in other enzymes or components of the isoprene and sterol biosynthetic pathways occur in autoinflammatory diseases.

In contrast to the repressive action of 25-HC on IL-1-family cytokine production, other work found that 25-HC can augment macrophage and epithelial cell secretion of some inflammatory cytokines, such as IL-6, IL-8 and MCSF[23, 24]. These CH25H-dependent effects were observed most clearly in the context of cells stimulated with the

dsRNA mimetic poly(I:C), which engages Toll-like receptor 3 (TLR3) and the intracellular dsRNA-sensing pathway. Infection of *Ch25h*-deficient mice with influenza virus, a dsRNA virus, led to decreased production of IL-6, MCSF and type I IFN in the lung, less lung pathology and enhanced survival[23]. The authors conclude that 25-HC-mediated amplification of inflammation during viral infection can contribute to tissue pathology. The mechanism by which 25-HC augmented IL-6, IL-8 and MCSF production was not defined although it was suggested to involve increased promoter binding by AP1 and NF-κB transcription factors[23, 24]. The related oxysterol 27-HC may augment inflammatory cytokine production by binding oestrogen receptor-a (ERa) and stimulating NF-kB activation[71]. Whether the ERa-binding ability of 25-HC[72] has relevance in this context is not known.

More studies are needed to determine the full range of conditions under which 25-HC represses versus augments inflammatory cytokine production. In particular it will be important to determine whether these effects occur under the same inducing conditions and at the same time, or whether the effects are temporally separated. It will also be important to compare the dose-sensitivity of the effects. 25-HC-mediated suppression of IL-1β production and of caspase-1 activation was observable with 100nM concentrations, whereas some of the pro-inflammatory effects of 25-HC occurred during exposure to several uM or higher concentrations. Whether such high concentrations are physiologically relevant is unknown, although high levels of 25-HC have been reported in the sputum of patients with chronic obstructive pulmonary disease[24]. Perhaps the amount of 25-HC induced during a response determines whether an anti- or pro-inflammatory output of this pathway dominates. The importance

of achieving the correct balance of anti- and pro-inflammatory effects may be particularly significant during viral and bacterial co-infection. 25-HC may help to achieve control of both the viral infection (through direct anti-viral effects) and the bacterial infection (for example, through IL-6-mediated augmentation of adaptive immunity and 7a,25-HC-mediated immune cell recruitment) while limiting the extent of inflammasome- and IL-1-mediated tissue damage.

25-HC and macrophage foam cell formation

An important function of macrophages is the phagocytic clearance of dying cells. Such engulfment loads the macrophage with a large amount of cholesterol and other lipids. Engulfment of cholesterol-rich substances stimulates acyl-coenzyme A:cholesterol acyltransferase 1 (ACAT1), the enzyme that forms cholesterol esters, and these bud off from the ER for storage in lipid droplets within the cytoplasm[51]. Mice or humans on a high cholesterol diet can develop atherosclerosis and a signature feature of this inflammatory disease is the appearance of lipid-laden macrophages (foam cells) in vascular lesions[73]. As well as being rich in cholesterol, atherosclerotic plaques contain a range of oxysterols including 25-HC[74]. Using systems biology approaches in a model macrophage system, it was found that the transcription factor ATF3 mediates protection against lipid body formation in macrophages[22]. The gene that is most strongly regulated by ATF3 is CH25H. Given that 25-HC at high concentrations promotes cholesterol esterification and lipid body formation[75-77], the authors provided support for a model whereby ATF3-mediated suppression of CH25H expression and hence 25-HC production functioned to antagonize foam cell formation[22]. Atherosclerosis-prone apoe$^{-/-}$ mice that additionally lacked Cyp7b1 suffered more severe disease[71]. This was attributed to the increased levels of 27-HC in these animals[71] (Fig. 2), but it seems possible that it was also a consequence of increased 25-HC[78]. The importance of Ch25h in vivo during foam cell formation and atherosclerotic disease progression needs to be investigated.

As well as being induced within atherosclerotic plaques, ATF3 is induced in macrophages by LPS and functions as a negative regulator of a range of inflammatory

genes including those encoding IL-6, IL-12b and iNOS[79]. ATF3-mediated repression of Ch25h might contribute to this regulatory effect[22]; however, as LPS strongly induces CH25H under a variety of conditions[80], more work needs to be done to understand how the negative influence of ATF3 on the CH25H promoter[23] is overcome in some settings. Under conditions in which both ATF3 and CH25H are upregulated, combined repression of IL-6, IL-12 and IL-1 family cytokine production may occur, perhaps achieving a more global anti-inflammatory feedback effect.

7a,25-HC as an EBI2 ligand

Whereas the evidence that 25-HC is biologically active has existed since at least the 1970s, a biological activity for 7a,25-HC was discovered only in 2011. Due to an interest in identifying ligands for orphan G protein-coupled receptors (GPCRs) that are abundant in the immune system, two groups carried out large-scale biochemical fractionation of porcine and ovine liver extracts that activated the orphan receptor EBI2 (GPR183)[20, 21]. Both groups identified 7a,25-HC as the most active ligand for EBI2, with the related oxysterol 7a,27-HC having about 10-fold less potency. Despite differing by only a single hydroxyl group, 25-HC was almost inactive as a ligand for EBI2[20, 21]. EBI2 was identified as an Epstein-Barr virus (EBV)-induced gene in B cells[81]. EBI2 is coupled with $G\alpha_i$ and ligand engagement leads to the activation of Rho family GTPases and mitogen-activated protein kinases including ERK and p38, and to intracellular calcium flux[20, 82-84]. Binding of EBI2 by 7α,25-HC also induces β-arrestin recruitment to the receptor and receptor internalization[20, 21, 31]. Structural models of oxysterol–EBI2 docking and mutation analysis have identified many key residues of EBI2 for ligand binding[85-87]. These include a glutamate in extracellular loop 2 (ECL2) that is suggested to be held in place by disulphide bonds and to contact the 3 hydroxyl of 7a,25-HC[87]. The 7a and 25 hydroxyl groups of 7α,25-HC are predicted to contact essential residues within the transmembrane domains of EBI2[87]. If, as suggested, ECL2 occupies a pre-folded position over the binding pocket of EBI2, this orientation may indicate that 7a,25-HC accesses EBI2 laterally from the lipid bilayer, as has been proposed for sphingosine-1-phosphate access to S1PR1[88]. Tool compounds with EBI2 antagonistic

activity have recently been identified and may prove useful in interrogation of the oxysterol-EBI2 pathway[89].

For B cell guidance

EBI2 is widely expressed in the immune system and is rapidly upregulated in B cells following B cell receptor engagement[90]. Activated B cells migrate strongly in response to nanomolar concentrations of 7a,25-HC[20, 21, 31]. Within a few hours of antigen encounter, EBI2 promotes B cell positioning in the outer follicles of lymphoid tissue, close to sites where antigen enters these structures[91] (Fig. 6). After 6 hours to 1 day of antigen encounter, EBI2 functions together with the chemokine receptor CCR7 to distribute activated B cells along the interface between the B cell follicle and T cell zone, a location that facilitates encounters between B cells and cognate T helper (T_H) cells[18, 19, 91, 92]. CD40 signals derived from T_H cells sustain EBI2 expression on activated B cells while promoting CCR7 downregulation, which leads to EBI2-dependent B cell positioning again in the outer follicle but now with a preference for interfollicular regions[91, 93]. The purpose of B cell positioning in interfollicular regions needs further investigation, but the enriched presence of DCs in these areas and the ability of DCs to augment plasmablast responses[94, 95] points to a possible role for EBI2 in favouring B cell-DC contacts. Alternatively, macrophages or specialized stromal cells of this region[96] may provide supportive or mitogenic signals for B cells[97] or the position may enhance exposure to newly arriving antigen[98]. During differentiation into GC B cells, EBI2 down-regulation is important for precursor cell movement to the follicle centre[18, 19]. Downregulation of EBI2 probably occurs due to BCL6-mediated repression and may

involve signaling through STAT6-dependent cytokine receptors[99, 100]; however, low levels of EBI2 expression can be maintained in some GC B cells such that the receptor could potentially influence cells even in this compartment[92].

EBI2 deficiency in mice leads to reduced early IgM and IgG antibody responses against several types of T cell-dependent antigen, and when EBI2 deficiency is restricted to B cells, antibody responses remain defective[18, 19]. Each B cell migration step that is influenced by EBI2 seems likely to have some effect on the efficiency with which B cells acquire antigen and receive signals from T_H cells, and possibly from DCs and other accessory cells. The extent to which each of these EBI2-dependent steps is required for mounting a plasma cell response can be expected to differ depending on the properties and amount of the inducing antigen. Although EBI2 was suggested to have direct signaling influences on B cell responses *in vitro*[21] this effect was not found in all studies[18]. It remains to be seen whether the receptor will have influences on B cell responses beyond those on positioning.

In contrast to their compromised IgM and IgG responses, *Ch25h*$^{-/-}$ mice have increased IgA production[13]. However, this effect does not reflect a role for CH25H in generating 7a,25-HC as *Cyp7b1*$^{-/-}$ mice have the opposite phenotype, having a slight reduction in serum IgA[13], and EBI2-deficient mice have not been reported to have altered IgA production. The mechanism at work is not yet clear although it was suggested that 25-HC could antagonize IgA isotype switching *in vitro*[13]. Beyond direct effects on B cells, it might be speculated that altered inflammatory cytokine production in intestinal tissues due to the lack of 25-HC leads directly, or perhaps indirectly through alterations in the commensal flora[101], to effects on IgA production.

Although it is strongly upregulated after B cell activation, EBI2 also influences the distribution of naïve B cells, favoring their migration to the outer edge versus center of the follicle, and one real-time imaging study provided evidence that *Ebi2*$^{-/-}$ B cells migrate faster than wildtype B cells inside follicles[102]. The dominant chemoattractant receptor on naïve B cells, CXCR5, guides the cells into follicles in response to the chemokine CXCL13[98]. An *in vitro* study suggested that EBI2 can heterodimerize with CXCR5, but the functional relevance of this putative interaction for *in vivo* B cell migration remains untested[103]. $CD4^+$ T cells and a subset of $CD8^+$ T cells also express EBI2 and these cells migrate in response to 7a,25-HC[21]. In addition, the receptor is upregulated in some effector T cells[20, 104]. BCL6-mediated repression of EBI2 expression in T_{FH} cells may be important for their ability to support GC responses[105]. The impact of EBI2 deficiency in T cells on immune responses remains to be investigated.

For dendritic cell homeostasis

DCs in mice and humans highly express EBI2 and mouse DCs migrate *in vitro* in response to 7a,25-HC[20, 21, 26, 27]. When the DC compartment in EBI2-deficient mice was closely examined it was found that the frequency of $CD4^+$ DCs in the spleen and lymph nodes was significantly reduced; this is also the DC subset that expresses the highest levels of EBI2 and that migrates most vigorously in response to ligand[26, 27]. Within the spleen, $CD4^+$ DCs that express the lectin DCIR2 are enriched in marginal zone bridging channels, a specialized type of interfollicular region, and in situ staining revealed that EBI2 is necessary for DC positioning in this location[26, 27]. The marginal zone bridging

channels are located adjacent to the marginal zone, a site where blood is released by open-ended terminal arterioles[106], and EBI2-mediated positioning in the bridging channels was shown to facilitate DC encounter with particulate antigens[27]. This work provided an explanation for the decreased number of $CD4^+$ DCs in EBI2-deficient mice as these cells are dependent on lymphotoxin (LT)-a□□□cytokine signals for survival and positioning in the bridging channels provides exposure to this B cell-derived trophic factor[27, 107]. Thus, EBI2 and 7a,25-HC have an important homeostatic role in $CD4^+$ DCs by promoting their positioning in a location where they encounter both a trophic factor and blood-borne particulate antigens. EBI2 deficiency in DCs is associated with a reduced ability to support $CD4^+$ T cell and B cell responses to particulate blood-borne antigens[26, 27]. EBI2-mediated positioning of B cells and DCs (and possibly $CD4^+$ T cells) in interfollicular regions may foster interactions between these cell types that directly augment the antibody response.

In inflammatory and autoimmune diseases

A genetic study in spontaneous hypertensive rats linked a single nucleotide polymorphism (SNP) in the *Ebi2* promoter to inflammation of the heart, pancreas and several other organs[108]. *EBI2*-linked SNPs have also been associated with cardiac inflammation, type I diabetes and inflammatory bowel disease in humans[108–110]. Some of the macrophages present in mouse heart, pancreas, kidney and liver express EBI2 and *in vitro* studies with rat macrophages suggested that the inflammation-associated SNP causes decreased EBI2 expression[108]. Lower EBI2 expression was argued to lead to less inhibition of an IRF7-driven inflammatory gene network[108]. This may occur due to

EBI2 signaling negatively regulating IRF7 activity, and such an EBI2-dependent effect was recently suggested to occur in plasmacytoid DCs[111]. Alternatively, and perhaps more likely, decreased EBI2 expression may have migration-dependent effects that shift the balance of myeloid cells in the tissue in favor of more inflammatory cells. Human blood-derived macrophages upregulate EBI2 after activation and migrate in response to 7a,25-HC[112, 113]. Consistent with EBI2 influencing cell recruitment in a range of tissues, EBI2 ligand, detected using a sensitive bioassay, was present in all tissues examined including liver, lung, heart and brain[91]. However, studies in EBI2-deficient mice have not reported spontaneous tissue inflammation and therefore more work is needed to establish that the causative rat and human SNPs are acting through effects on EBI2 expression.

Given the function of EBI2 in B cells and DCs in augmenting responses to T cell-dependent antigens, it is perhaps not surprising that the *EBI2* gene is within a chromosomal interval linked with susceptibility to systemic lupus erythematosus (SLE)[114, 115]. Further work will be needed to determine whether this linkage involves an *EBI2* allele that is over- or under- expressed. One study did find *EBI2* downregulation in total white blood cells from patients with SLE, although this may have been an indirect effect of increased type I IFN levels causing alterations in circulating cell types[116]. The association between increased type I IFN levels and SLE[117] and the development of autoantibody-mediated diseases in type I IFN-treated patients with hepatitis C[118] does, however, raise the question of whether CH25H induction and increased production of 25-HC and 7a,25-HC contribute to autoantibody production or end organ inflammation. In addition to inflammatory and autoimmune disease, dysregulated EBI2 expression has

been observed in some lymphoid and myeloid malignancies[90]. EBI2 was cloned as an EBV-induced gene and it is notable that EBV^+ B cells concentrate in interfollicular regions of tonsil, which is perhaps consistent with EBI2 having a dominant influence on their positional behavior[119, 120]. EBI2 induction may also contribute to the mechanism by which EBV predisposes to the development of SLE[121].

Enzyme distribution and 7a,25-HC gradients

Although studies on the anti-viral and inflammation-regulatory functions of 25-HC have highlighted its strong inducibility in myeloid cells by inflammatory signals, the main *Ch25h* and *Cyp7b1*-expressing cell types required for B cell and DC positioning are radiation-resistant stromal cells[31]. *Ch25h* and *Cyp7b1* are abundantly expressed in inter- and outer-follicular regions of lymphoid tissues whereas their expression is repressed in the central region of follicles[31]. Both enzymes are also abundant in the T-cell zone, but in this region there is also a high level of expression of HSD3B7, the enzyme that converts 7a,25-HC to a metabolite that is no longer active as a ligand for EBI2[31] (Fig. 2). These observations begin to provide an explanation for how the pattern of 7a,25-HC in lymphoid tissues is established in the steady state; however, it remains unknown how the upregulation of CH25H that occurs after exposure to inflammatory agents re-shapes the 7a,25-HC gradient(s).

Ch25h- and *Cyp7b1*-deficient mice phenocopy *Ebi2*-deficient mice in terms of showing defective B cell positioning in interfollicular regions and reduced T cell-dependent antibody responses[20, 31]. They also show an equivalent reduction in $CD4^+$ DC numbers[26, 31]. These data provide strong support for the conclusion that the major

EBI2 ligand guiding B cell and DC movements in steady-state lymphoid tissues and early following immunization is 7a,25-HC. The involvement of the related oxysterol, 7a,27-HC (Fig. 2) as a migratory cue under some *in vivo* conditions or in locations that have not yet been examined remains likely, particularly considering that 27-HC is the most abundant oxysterol detected in circulation[7]. It also remains possible that enzymes in addition to CH25H may contribute measurably to the generation of 25-HC and 7a,25-HC in some circumstances[6, 11, 102]. Interestingly, *Hsd3b7*-deficient mice show similar B cell and DC defects to *Ebi2*-deficient mice despite having markedly raised concentrations of 7a,25-HC in lymphoid tissues[31]. These data provide support for a model where the distribution of 7a,25-HC rather than merely its presence is crucial for EBI2 function, which is consistent with this oxysterol functioning in a compartmentalized manner, possibly in gradients, to guide cell positioning.

Are 25-HC and 7a,25-HC functions integrated?

Given that 7a,25-HC can only be made in regions where 25-HC is generated, an important question arises regarding how the abundance and distribution of these closely related lipids is coordinated. Both are able to readily travel out of cells, although it is unknown whether specific transporters contribute to this flux. How they move through the interstitial space between cells is only partially understood[122], but it can be anticipated that the greater hydrophilicity of 7a,25-HC enables it to spread more efficiently through aqueous environments. 25-HC can travel between cells and this was shown to occur during *in vitro* studies where supernatants from virally infected cells could protect other cells in a 25-HC-dependent manner[16, 17]. Similarly, 25-HC from the supernatants of CH25H-expressing cells can enter CYP7B1-expressing cells and become converted into 7a,25-HC[31]. This serves both to generate the EBI2 ligand and to inactivate 25-HC as a regulator of SREBP and HMGCR, as well as probably also to loss of its membrane-modulating influences. Whether CYP7B1 is the only enzyme involved in metabolizing 25-HC in tissues is not yet clear, but it is known that *Cyp7b1*$^{-/-}$ mice have increased 25-HC levels[13, 78]. 25-HC may also be cleared from tissues by movement into the circulation and uptake by the liver for conversion into bile acids[6] or by esterification and association with lipoproteins[122]. Understanding the factors that control the relative expression levels of CH25H and CYP7B1 in cells will be crucial for elucidating how the two sets of functions are integrated. It is tempting to speculate that the 25-HC and 7a,25-HC systems operate hand-in-hand. We propose that when inflammatory signaling leads to marked upregulation of CH25H (while having less effect on CYP7B1 expression) this probably causes an increase in the level of 25-HC that is

layered on top of an existing gradient of 7a,25-HC (see model in Fig. 7). Both 25-HC and 7a,25-HC levels increase at the whole organ level following exposure to TLR agonists[20] and 25-HC levels increase in the serum of LPS-treated mice and humans[12, 13]. EBI2-expressing cells that are recruited by low nanomolar 7a,25-HC concentrations might be expected to move into a region of high nanomolar 25-HC concentrations (Fig. 7). This migration may enable the newly arriving cells exposed to 25-HC to establish an anti-viral state, thereby protecting them from infection. In the case of B cells that often capture antigens in an intact form, this effect may help to ensure that they are not immediately infected by their cargo[123]. The 25-HC may also dampen inflammasome activity in arriving cells, perhaps helping to limit the rate of caspase-induced pyroptosis and thereby allowing them to make a more prolonged contribution to the response.

Summary and future directions

It is remarkable how a chemical difference as small as a single hydroxyl group can convert a molecule from a structural part of the cell (cholesterol) to an anti-viral mediator and inflammation regulator (25-HC), and with one further hydroxyl to a GPCR-binding guidance cue (7α,25-HC). As highlighted in this review, the last few years have seen important advances in understanding the functions of 25-HC and 7α,25-HC as regulators of immune cell function. Of course, with new findings come new questions. Beyond the topics for investigation highlighted above, there are many other questions that arise. The nuclear hormone receptors LXRα and LXRβ are established targets of 25-HC based on a range of *in vitro* studies[33, 124], yet at this time there is only limited *in vivo* evidence that 25-HC functions via these receptors. To the contrary, several reports have excluded LXRs as having a role in the 25-HC-mediated effects that were studied[13, 16, 17, 25, 44]. Given the wide-ranging influences of LXR-mediated gene regulation on immune cell behavior[33, 125], it remains important to ask whether some *in vivo* actions of 25-HC occur via LXRs. Similarly, more work is needed to understand whether the ability of 25-HC to bind RORγt has physiological relevance[126–128]. SREBP contributes to the metabolic reprogramming of effector T cells[129] raising the question of whether 25-HC from activated macrophages or other tissue cells modulates this reprogramming, perhaps in a manner coordinated by 7α,25-HC-mediated chemoattraction.

The inflammation-regulatory effects of 25-HC — repressing the inflammasome and IL-1 production while augmenting expression of other inflammatory cytokines such as IL-6 — indicate that it should not be thought of as a simple negative or positive regulator of immunity, but as a mediator acting at the 'knifes edge' to balance infection-

controlling responses with tissue-damaging inflammation. The logic of this circuit and how it is integrated with the numerous other inflammation-induced genes will require a lot of *in vivo* work to decipher. As this work proceeds it will be important to bear in mind that we don't yet know how the activities of 25-HC made intrinsically versus encountered from outside the cell compare in their effects on cell behaviour. Similarly, we don't know the range of relevant *in vivo* concentrations for these lipids, although the effects that have been observed in the nM range seem more likely to be physiologically relevant than those effects requiring exposure to μM concentrations of lipid. It is also not known over what *in vivo* distances 25-HC and 7α,25-HC typically function. This in turn raises the question of how guidance by an oxysterol chemoattractant compares with guidance by protein chemoattractants, and how the ability of 7α,25-HC to pass in and out of cells affects the speed with which gradients can be formed and shaped, and how sharp their 'edges' can be. Finally, given that 25-HC and 7α,25-HC are made from cholesterol, are there connections between their function and the levels of cholesterol in a tissue? Do widely used cholesterol-lowering drugs, such as statins, affect 25-HC or 7α,25-HC levels sufficiently to alter their immune activities? We can expect that many areas of immunology, microbial pathogenesis and metabolic research will converge in illuminating these and other questions about the effects of 25-HC and 7α,25-HC on innate and adaptive immunity in the years ahead. We can also anticipate creative efforts to develop 25-HC- and 7α,25-HC-related molecules that tap the anti-viral and immune-modulatory activities of the parent molecules for therapeutic purposes.

Acknowledgements

We thank R. Locksley and D. Russell for comments on the manuscript. Work from the Cyster laboratory discussed in this review was supported in part by NIH grant AI40098 and a grant from the American Asthma Foundation.

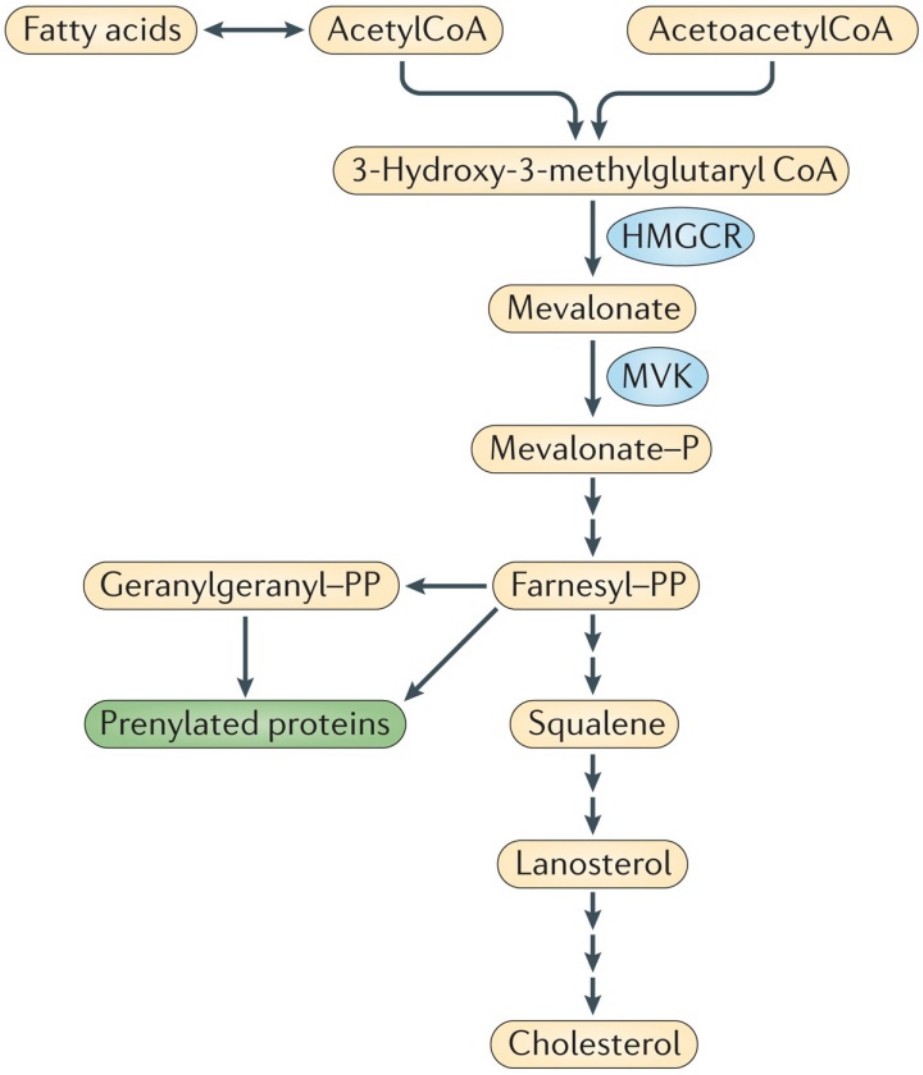

Figure 1. Pathway of cholesterol and nonsterol isoprene biosynthesis.
Mevalonate is the first committed intermediate of the pathway and lanosterol is the first sterol in the pathway. Not all steps are shown and the only enzymes labelled are the two referred to in the text: HMGCR (3-hydroxy-3-methylglutaryl-CoA reductase) and MVK (mevalonate kinase). Additional products of the isoprene pathway include ubiquinone, dolichol and heme A (not shown). P, phosphate; PP, pyrophosphate.

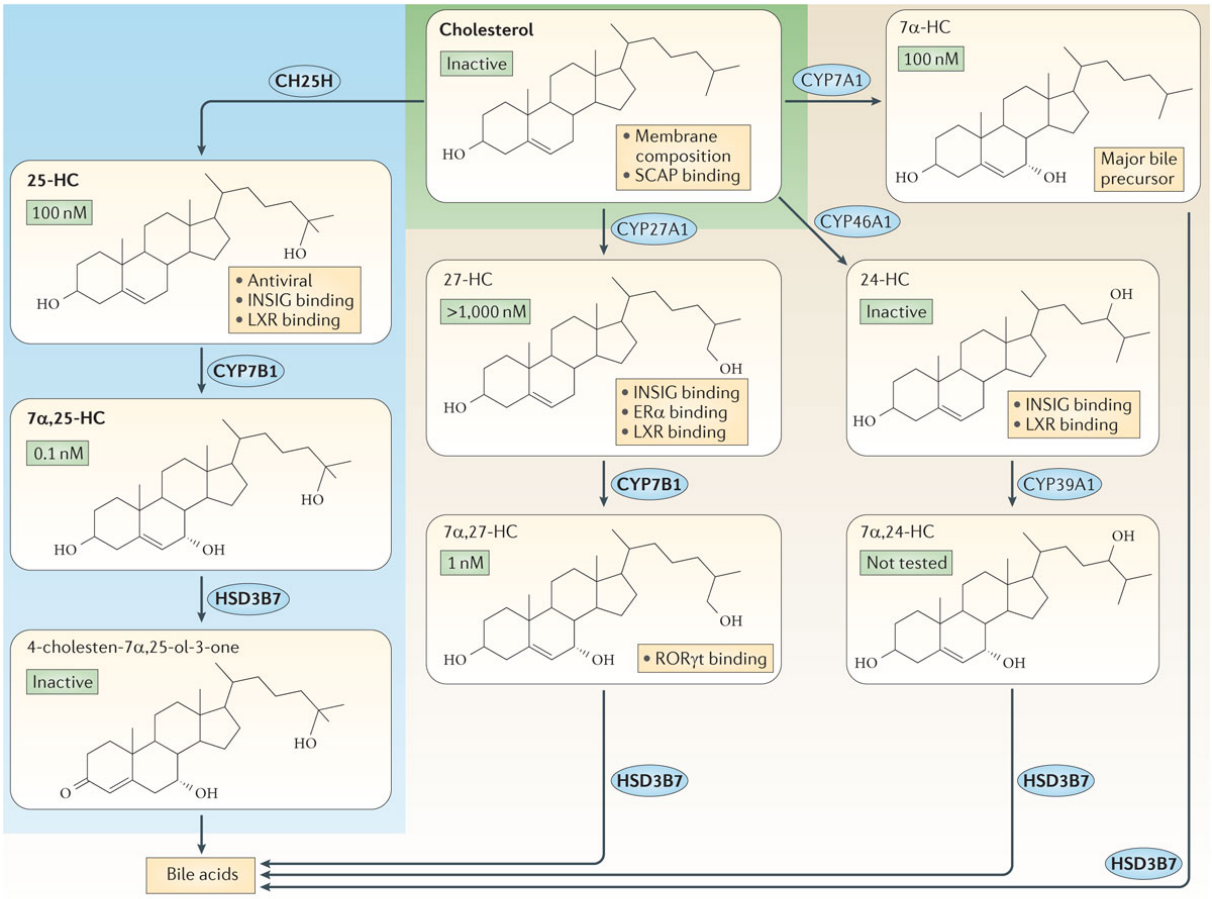

Figure. 2. Enzymatic steps involved in the generation of oxysterols from cholesterol.

The hydroxyl groups are highlighted in red. Numbers in top left of boxes indicate approximate minimum concentrations that give an EBI2-dependent response in various *in vitro* assays. Some of the other reported activities of the oxysterols are indicated in the lower right of each box. 'Antiviral' indicates the ability to inhibit replication of many viruses; Insulin-induced genes 1 and 2 (INSIG) proteins and SREBP-cleavage activating protein (SCAP) are part of the feedback pathway that negatively regulates activation of sterol response element binding proteins (SREBPs); ligand binding to INSIG proteins also represses HMGCR; LXR, ERα and RORγt binding indicates activity *in vitro* on the respective nuclear hormone receptors, although the *in vivo* relevance is not clear. Not all of the 25-HC activities discussed in the main text are listed. Blue shading highlights the pathway of focus in this review and enzymes required for this pathway are in bold. The major pathway of bile acid synthesis is via CYP7A1 and HSD3B7.

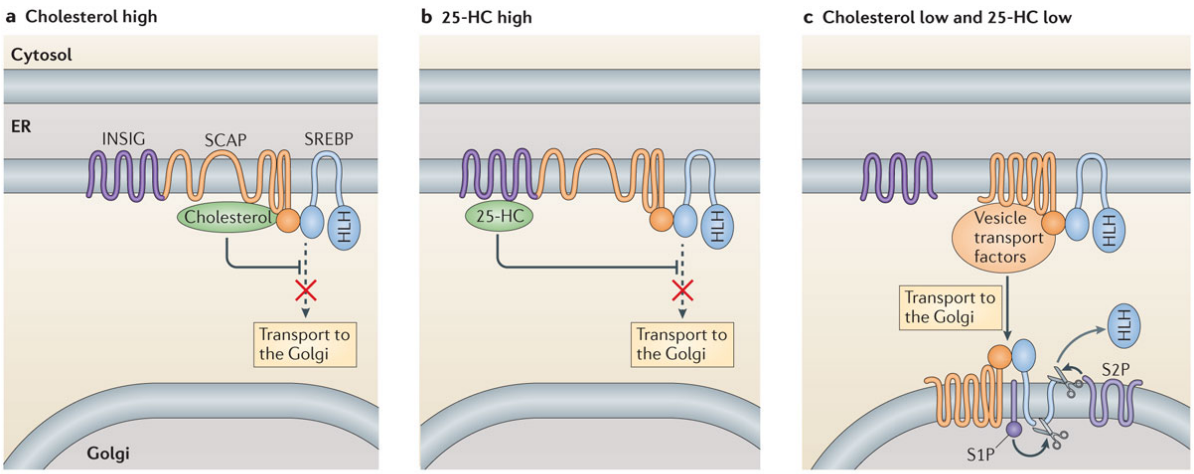

Figure 3. Pathway of SREBP regulation by cholesterol and 25-HC.
Insulin-induced genes 1 and 2 (INSIG) proteins, SREBP-cleavage activating protein (SCAP) and sterol response element binding proteins (SREBPs) are membrane-spanning ER proteins. Cholesterol binding to the sterol-sensing domain of SCAP (a), or 25-HC binding to INSIG proteins (b), promotes complex formation between INSIG proteins and SCAP–SREBP and blocks transport of SCAP–SREBP to the Golgi. When levels of cholesterol and 25-HC are low (c), the SCAP-SREBP complex dissociates from INSIG protein, which enables binding of transport proteins to SCAP and movement to the Golgi. Here SREBP is cleaved sequentially by site-1-protease (S1P) and site-2-protease (S2P) to cytosolically release the helix-loop-helix (HLH) domain of SREBP. This transcription factor then travels to the nucleus to promote the expression of genes involved in cholesterol uptake and biosynthesis, such as HMGCR.

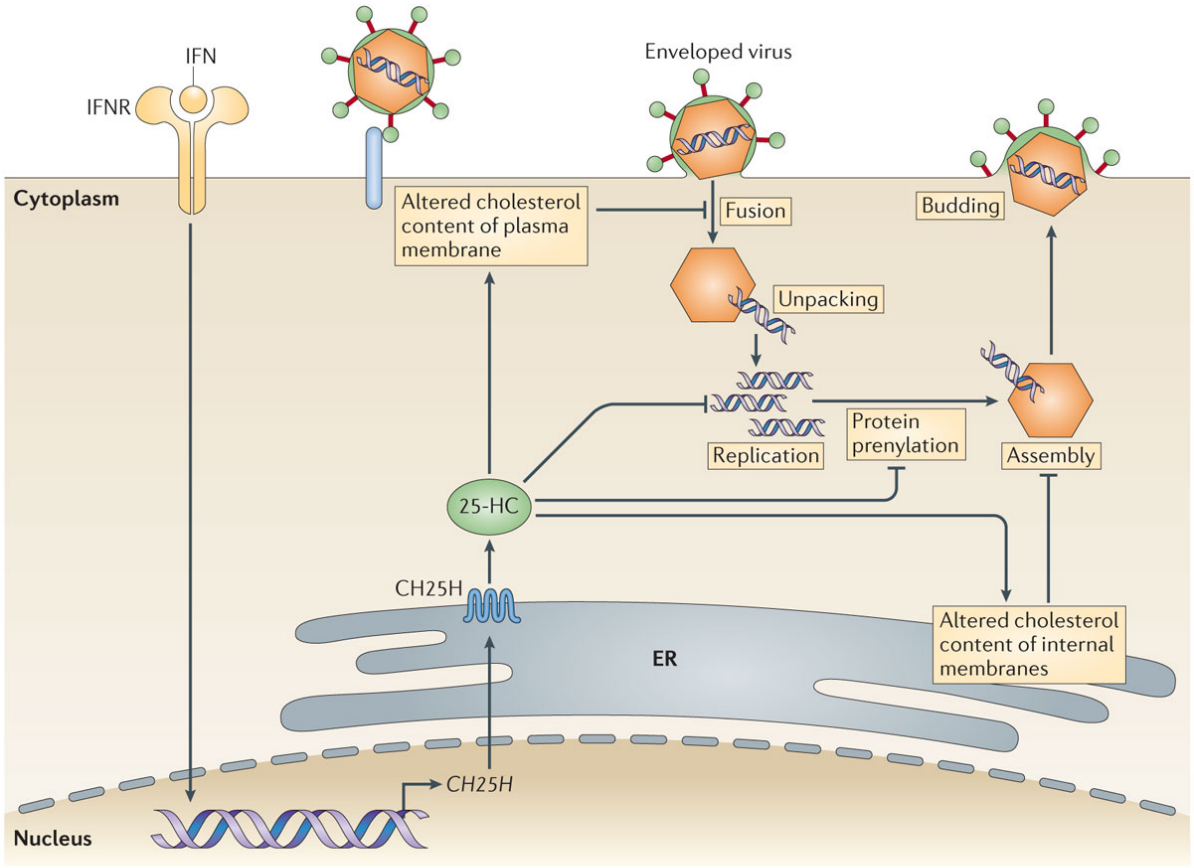

Figure 4. Summary of the anti-viral activities of 25-HC.
Interferon receptor (IFNR) signaling induces the expression of CH25H and promotes increased production of 25-HC from cholesterol. Various studies have suggested the 25-HC can have the following anti-viral effects: alter plasma membrane lipids (in particular cholesterol content) to antagonize viral fusion and entry; antagonize viral replication; antagonize viral and endogenous protein prenylation that can be involved in viral replication and assembly; and alter the cholesterol distribution in internal membranes to antagonize formation of membrane-associated 'factories' involved in viral assembly and packaging.

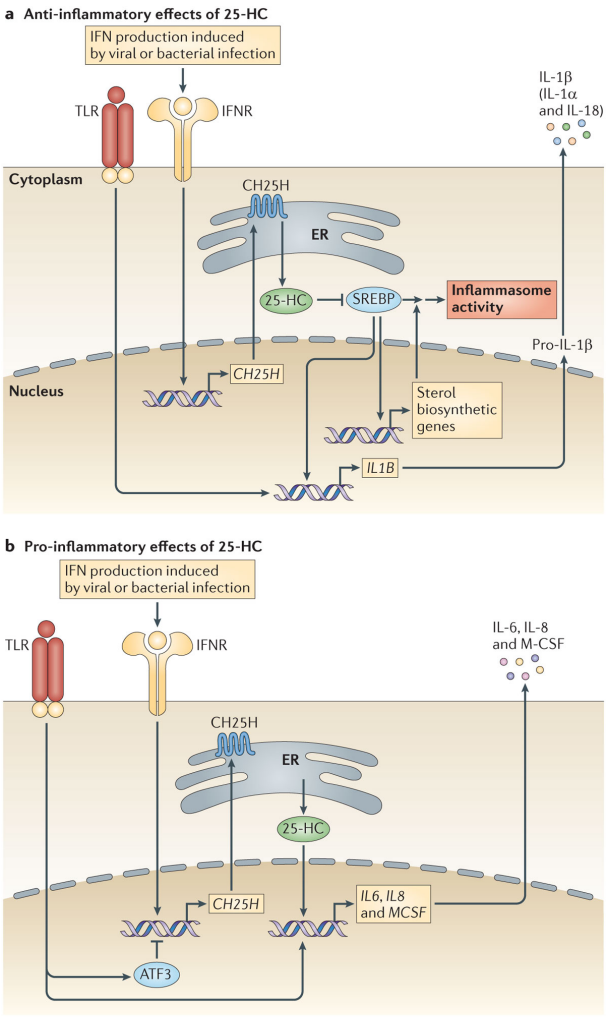

Figure 5. Inflammation-regulatory activities of 25-HC.
IFNα/β and IFNγ induced by viruses and bacteria promote CH25H expression and the generation of 25-HC.
(A) 25-HC-mediated inhibition of SREBP processing diminishes *Il1b* expression and inflammasome activity, acting in a negative feedback pathway to counteract IL-1β production, as well as IL-1α and IL-18 release. The mechanism by which SREBP promotes *Il1b* expression and inflammasome activity is not defined and may be both downstream of and independent from sterol biosynthesis. No direct interaction between SREBPs and the *Il1b* promoter has been reported, which indicates that the effect is probably indirect.
(B) 25-HC amplifies the expression of some inflammatory genes such as those encoding IL-6, IL-8 and MCSF by a pathway that is not defined. The transcription factor ATF3 antagonizes CH25H expression. Inflammasome components are also induced by TLR signaling.

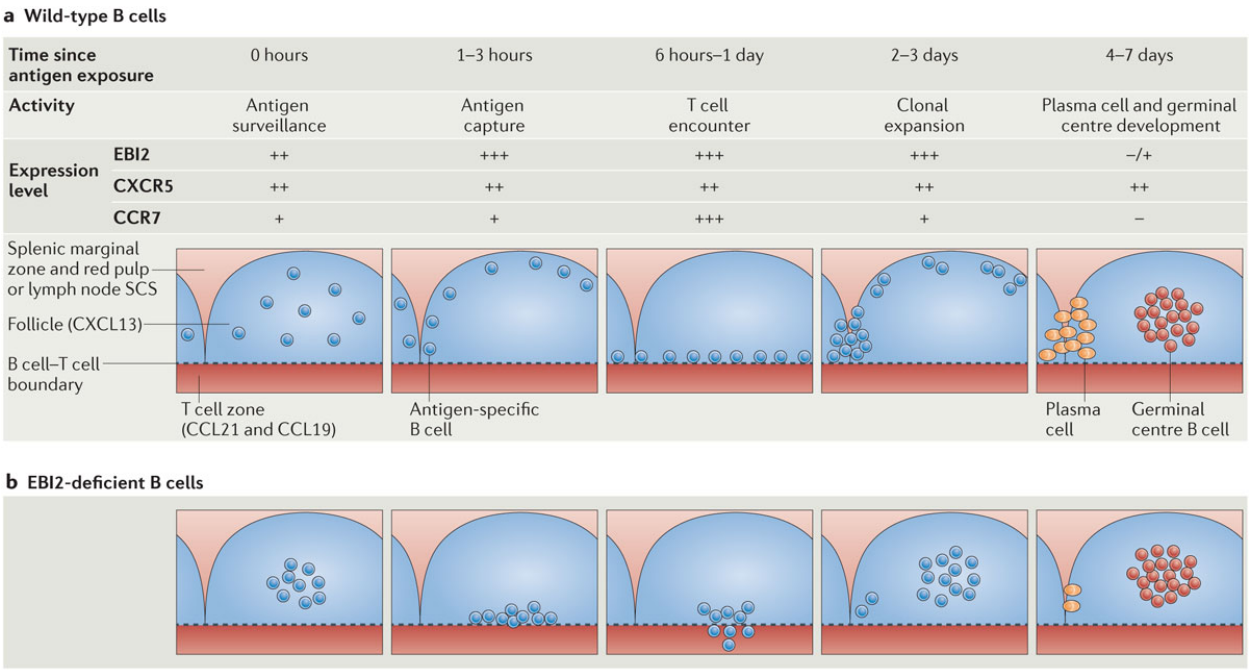

Figure 6. EBI2 guides naïve and activated B cell positioning.
(A) Relative expression levels of EBI2, CXCR5 and CCR7 on wild-type antigen-specific B cells before and during the response to antigen are summarized. CXCL13, the ligand for CXCR5, is abundant throughout the follicle (dark blue shading); CCL21 and CCL19, ligands for CCR7, are abundant in the T-cell zone (light blue shading). The EBI2 ligand, 7α,25-HC, is thought to be most abundant in inter- and outer-follicular regions. Within a few hours of antigen encounter, EBI2 promotes B cell positioning in the outer follicles of lymphoid tissue, close to sites where antigen enters these structures. After 6 hours to 1 day of antigen encounter, EBI2 functions together with the chemokine receptor CCR7 to distribute activated B cells along the interface between the B cell follicle and T cell zone, a location that facilitates encounters between B cells and cognate T helper (TH) cells. CD40 signals derived from TH cells sustain EBI2 expression on activated B cells while promoting CCR7 downregulation, which leads to EBI2-dependent B cell positioning again in the outer follicle but with a preference for interfollicular regions. During differentiation into GC B cells, EBI2 down-regulation is important for precursor cell movement to the follicle centre.
(B) The altered distribution and reduced plasma cell response of EBI2-deficient B cells.

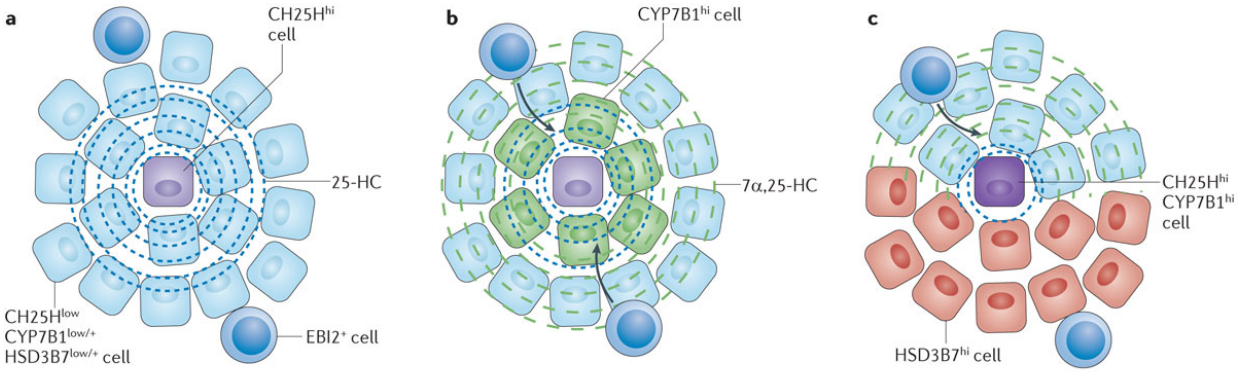

Figure 7. Models to account for how 25-HC and 7α,25-HC distribution in tissues may be regulated and influence the migration of EBI2-expressing cells.
(A) A CH25H^{hi} cell generates large amounts of 25-HC that travels several cell diameters through the surrounding tissue and has possible anti-viral and inflammation-regulatory effects (not shown) over those distances. The minimal expression level of CYP7B1 in the surrounding cells leads to little 7α,25-HC production but also limits the extent of degradation of 25-HC.
(B) A CH25H^{hi} cell is surrounded by cells that express CYP7B1 and this gives rise to overlapping gradients of 25-HC and 7α,25-HC, with the latter chemoattracting EBI2^{+} cells toward the CH25H^{+} cells and promoting their exposure to 25-HC.
(C) A CH25H and CYP7B1 co-expressing cell generates large amounts of 7α,25-HC and small amounts of 25-HC and attracts EBI2^{+} cells across a long distance; the presence of HSD3B7^{hi} cells in a tissue compartment adjacent to the CH25H^{hi} CYP7B1^{hi} cell sharply limits the spread of 7α,25-HC in that direction.

References:

1. Ikonen, E. Cellular cholesterol trafficking and compartmentalization. *Nat. Rev. Mol. Cell Biol.* **9**, 125-138 (2008).
2. Simons, K. & Gerl, M.J. Revitalizing membrane rafts: new tools and insights. *Nat. Rev. Mol. Cell Biol.* **11**, 688-699 (2010).
3. Heaton, N.S. & Randall, G. Multifaceted roles for lipids in viral infection. *Trends Microbiol.* **19**, 368-375 (2011).
4. Chukkapalli, V., Heaton, N.S. & Randall, G. Lipids at the interface of virus-host interactions. *Curr. Opin. Microbiol.* **15**, 512-518 (2012).
5. Goldstein, J.L., DeBose-Boyd, R.A. & Brown, M.S. Protein sensors for membrane sterols. *Cell* **124**, 35-46 (2006).

Concise review on the pioneering work that defined the molecular mechanism of cholesterol- and 25-HC-mediated feedback regulation of the sterol biosynthetic pathway.

6. Russell, D.W. Oxysterol biosynthetic enzymes. *Biochim. Biophys. Acta* **1529**, 126-135 (2000).
7. Russell, D.W. The enzymes, regulation, and genetics of bile acid synthesis. *Annu. Rev. Biochem.* **72**, 137-174 (2003).

Founding review on the enzyme requirements for synthesis of bile acids and oxysterols in the liver and other tissues.

8. Brown, M.S. & Goldstein, J.L. Suppression of 3-hydroxy-3-methylglutaryl coenzyme A reductase activity and inhibition of growth of human fibroblasts by 7-ketocholesterol. *J. Biol. Chem.* **249**, 7306-7314 (1974).

9. Kandutsch, A.A. & Chen, H.W. Inhibition of sterol synthesis in cultured mouse cells by cholesterol derivatives oxygenated in the side chain. *J. Biol. Chem.* **249**, 6057-6061 (1974).

10. Bjorkhem, I. Are side-chain oxidized oxysterols regulators also in vivo? *J. Lipid Res.* **50 Suppl**, S213-218 (2009).

11. Diczfalusy, U. On the formation and possible biological role of 25-hydroxycholesterol. *Biochimie* **95**, 455-460 (2013).

12. Diczfalusy, U. et al. Marked upregulation of cholesterol 25-hydroxylase expression by lipopolysaccharide. *J. Lipid Res.* **50**, 2258-2264 (2009).

13. Bauman, D.R. et al. 25-Hydroxycholesterol secreted by macrophages in response to Toll-like receptor activation suppresses immunoglobulin A production. *Proc. Natl. Acad. Sci. U. S. A.* **106**, 16764-16769 (2009).

Early demonstration that 25-HC can affect the adaptive immune system with the discovery of increased IgA levels in *Ch25h*-deficient mice and decreased IgA levels in *Cyp7b1*-deficient mice.

14. Park, K. & Scott, A.L. Cholesterol 25-hydroxylase production by dendritic cells and macrophages is regulated by type I interferons. *J. Leukoc. Biol.* **88**, 1081-1087 (2010).

15. Zou, T., Garifulin, O., Berland, R. & Boyartchuk, V.L. Listeria monocytogenes infection induces prosurvival metabolic signaling in macrophages. *Infect. Immun.* **79**, 1526-1535 (2011).

Listeria monocytogenes **infection and type I IFN treatment of macrophages is shown to upregulate *Ch25h* and this leads to repression of caspase-1 activation.**

16. Blanc, M. et al. The transcription factor STAT-1 couples macrophage synthesis of 25-hydroxycholesterol to the interferon antiviral response. *Immunity* **38**, 106-118 (2013).

Shows that 25-HC is strongly induced following viral infection and by IFN and has a broad ability *in vitro* to antagonize the replication of enveloped viruses.

17. Liu, S.Y. et al. Interferon-inducible cholesterol-25-hydroxylase broadly inhibits viral entry by production of 25-hydroxycholesterol. *Immunity* **38**, 92-105 (2013).

Complementary to reference 16, this study shows that CH25H and 25-HC inhibit the replication of a wide range of enveloped viruses *in vitro* and shows the *in vivo* effects of 25-HC and *Ch25h*-deficiency on viral replication.

18. Gatto, D., Paus, D., Basten, A., Mackay, C.R. & Brink, R. Guidance of B cells by the orphan G protein-coupled receptor EBI2 shapes humoral immune responses. *Immunity* **31**, 259-269 (2009).

19. Pereira, J.P., Kelly, L.M., Xu, Y. & Cyster, J.G. EBI2 mediates B cell segregation between the outer and centre follicle. *Nature* **460**, 1122-1126 (2009).

References 18 and 19 show, using independently generated *Gpr183*-deficient mice, an *in vivo* function for EBI2 in guiding immune cell migration.

20. Hannedouche, S. et al. Oxysterols direct immune cell migration via EBI2. *Nature* **475**, 524-527 (2011).

21. Liu, C. et al. Oxysterols direct B-cell migration through EBI2. *Nature* **475**, 519-523 (2011).

References 20 and 21 both used classical biochemical methods to de-orphanize EBI2 and identify 7a,25-HC as the most potent ligand.

22. Gold, E.S. et al. ATF3 protects against atherosclerosis by suppressing 25-hydroxycholesterol-induced lipid body formation. *J. Exp. Med.* **209**, 807-817 (2012).

***CH25H* is shown to be a major target gene repressed by ATF3 and increased levels of 25-HC in the absence of ATF3 are associated with macrophage foam cell formation.**

23. Gold, E.S. et al. 25-Hydroxycholesterol acts as an amplifier of inflammatory signaling. *Proc. Natl. Acad. Sci. U. S. A.* **111**, 10666-10671 (2014).

Shows that 25-HC can augment expression of some inflammatory genes in macrophages and correlates these findings with reduced inflammation-mediated pathology following influenza infection of *Ch25h*$^{-/-}$ mice.

24. Koarai, A. et al. 25-Hydroxycholesterol enhances cytokine release and Toll-like receptor 3 response in airway epithelial cells. *Respir. Res.* **13**, 63 (2012).

25. Reboldi, A. et al. Inflammation. 25-Hydroxycholesterol suppresses interleukin-1-driven inflammation downstream of type I interferon. *Science* **345**, 679-684 (2014).

Shows that CH25H deficiency leads to increased production of IL-1-family cytokines following inflammatory insults *in vivo* and demonstrates that 25-

HC represses *Il1b* expression and inflammasome activation in activated macrophages.

26. Gatto, D. et al. The chemotactic receptor EBI2 regulates the homeostasis, localization and immunological function of splenic dendritic cells. *Nat. Immunol.* **14**, 446-453 (2013).

27. Yi, T. & Cyster, J.G. EBI2-mediated bridging channel positioning supports splenic dendritic cell homeostasis and particulate antigen capture. *Elife* **2**, e00757 (2013).

References 26 and 27 establish that $CD4^+$ DCs in the spleen require EBI2 and 7a,25-HC for positioning in marginal zone bridging channels and this positioning is important for maintaining their homeostasis and for mounting T cell-dependent antibody responses against certain blood-borne antigens.

28. Lund, E.G., Kerr, T.A., Sakai, J., Li, W.P. & Russell, D.W. cDNA cloning of mouse and human cholesterol 25-hydroxylases, polytopic membrane proteins that synthesize a potent oxysterol regulator of lipid metabolism. *J. Biol. Chem.* **273**, 34316-34327 (1998).

29. Stiles, A.R., McDonald, J.G., Bauman, D.R. & Russell, D.W. CYP7B1: one cytochrome P450, two human genetic diseases, and multiple physiological functions. *J. Biol. Chem.* **284**, 28485-28489 (2009).

30. Schwarz, M. et al. The bile acid synthetic gene 3beta-hydroxy-Delta(5)-C(27)-steroid oxidoreductase is mutated in progressive intrahepatic cholestasis. *J. Clin. Invest.* **106**, 1175-1184 (2000).

31. Yi, T. et al. Oxysterol gradient generation by lymphoid stromal cells guides activated B cell movement during humoral responses. *Immunity* **37**, 535-548 (2012).

Demonstrates that CH25H and CYP7B1 are abundant in interfollicular stromal cells and low in the central region of follicles, while also showing that HSD3B7 is needed to inactivate 7a,25-HC as an EBI2 ligand and thereby establish 7a,25-HC 'gradients' that guide cell movement.

32. Brown, M.S. & Goldstein, J.L. Cholesterol feedback: from Schoenheimer's bottle to Scap's MELADL. *J. Lipid Res.* **50 Suppl**, S15-27 (2009).

33. Spann, N.J. & Glass, C.K. Sterols and oxysterols in immune cell function. *Nat. Immunol.* **14**, 893-900 (2013).

34. Sever, N., Yang, T., Brown, M.S., Goldstein, J.L. & DeBose-Boyd, R.A. Accelerated degradation of HMG CoA reductase mediated by binding of insig-1 to its sterol-sensing domain. *Mol. Cell* **11**, 25-33 (2003).

35. Mackenzie, J.M., Khromykh, A.A. & Parton, R.G. Cholesterol manipulation by West Nile virus perturbs the cellular immune response. *Cell host & microbe* **2**, 229-239 (2007).

36. Rothwell, C. et al. Cholesterol biosynthesis modulation regulates dengue viral replication. *Virology* **389**, 8-19 (2009).

37. Robinzon, S. et al. Impaired cholesterol biosynthesis in a neuronal cell line persistently infected with measles virus. *J. Virol.* **83**, 5495-5504 (2009).

38. Petersen, J. et al. The major cellular sterol regulatory pathway is required for Andes virus infection. *PLoS Pathog.* **10**, e1003911 (2014).

39. Lu, Y.E., Cassese, T. & Kielian, M. The cholesterol requirement for sindbis virus entry and exit and characterization of a spike protein region involved in cholesterol dependence. *J. Virol.* **73**, 4272-4278 (1999).

40. Danthi, P. & Chow, M. Cholesterol removal by methyl-beta-cyclodextrin inhibits poliovirus entry. *J. Virol.* **78**, 33-41 (2004).

41. Daya, M., Cervin, M. & Anderson, R. Cholesterol enhances mouse hepatitis virus-mediated cell fusion. *Virology* **163**, 276-283 (1988).

42. Phalen, T. & Kielian, M. Cholesterol is required for infection by Semliki Forest virus. *J. Cell Biol.* **112**, 615-623 (1991).

43. Blanc, M. et al. Host defense against viral infection involves interferon mediated down-regulation of sterol biosynthesis. *PLoS Biol.* **9**, e1000598 (2011).

Demonstrates that several viral infections and type I IFN repress SREBP2 cleavage and sterol biosynthesis in macrophages and fibroblasts.

44. Shibata, N. et al. 25-Hydroxycholesterol activates the integrated stress response to reprogram transcription and translation in macrophages. *J. Biol. Chem.* **288**, 35812-35823 (2013).

45. Liu, S.Y., Sanchez, D.J., Aliyari, R., Lu, S. & Cheng, G. Systematic identification of type I and type II interferon-induced antiviral factors. *Proc. Natl. Acad. Sci. U. S. A.* **109**, 4239-4244 (2012).

Identifies CH25H as a major IFN-stimulated gene that has anti-viral activity.

46. Moog, C., Aubertin, A.M., Kirn, A. & Luu, B. Oxysterols, but not cholesterol, inhibit human immunodeficiency virus replication in vitro. *Antivir. Chem. Chemother.* **9**, 491-496 (1998).

47. Su, A.I. et al. Genomic analysis of the host response to hepatitis C virus infection. *Proc. Natl. Acad. Sci. U. S. A.* **99**, 15669-15674 (2002).

48. Arita, M. et al. Oxysterol-binding protein family I is the target of minor enviroxime-like compounds. *J. Virol.* **87**, 4252-4260 (2013).

49. Gale, S.E. et al. Side chain oxygenated cholesterol regulates cellular cholesterol homeostasis through direct sterol-membrane interactions. *J. Biol. Chem.* **284**, 1755-1764 (2009).

50. Olsen, B.N., Schlesinger, P.H., Ory, D.S. & Baker, N.A. 25-Hydroxycholesterol increases the availability of cholesterol in phospholipid membranes. *Biophys. J.* **100**, 948-956 (2011).

51. Chang, T.Y., Chang, C.C., Ohgami, N. & Yamauchi, Y. Cholesterol sensing, trafficking, and esterification. *Annu. Rev. Cell Dev. Biol.* **22**, 129-157 (2006).

52. Arita, M. Phosphatidylinositol-4 kinase III beta and oxysterol-binding protein accumulate unesterified cholesterol on poliovirus-induced membrane structure. *Microbiol. Immunol.* **58**, 239-256 (2014).

53. Mesmin, B. et al. A four-step cycle driven by PI(4)P hydrolysis directs sterol/PI(4)P exchange by the ER-Golgi tether OSBP. *Cell* **155**, 830-843 (2013).

54. Amini-Bavil-Olyaee, S. et al. The antiviral effector IFITM3 disrupts intracellular cholesterol homeostasis to block viral entry. *Cell host & microbe* **13**, 452-464 (2013).

55. Trinchieri, G. Type I interferon: friend or foe? *J. Exp. Med.* **207**, 2053-2063 (2010).

56. Gonzalez-Navajas, J.M., Lee, J., David, M. & Raz, E. Immunomodulatory functions of type I interferons. *Nat. Rev. Immunol.* **12**, 125-135 (2012).

57. Ludigs, K., Parfenov, V., Du Pasquier, R.A. & Guarda, G. Type I IFN-mediated regulation of IL-1 production in inflammatory disorders. *Cell. Mol. Life Sci.* **69**, 3395-3418 (2012).

58. Inoue, M. & Shinohara, M.L. The role of interferon-beta in the treatment of multiple sclerosis and experimental autoimmune encephalomyelitis - in the perspective of inflammasomes. *Immunology* **139**, 11-18 (2013).

59. Guarda, G. et al. Type I interferon inhibits interleukin-1 production and inflammasome activation. *Immunity* **34**, 213-223 (2011).

Elegant study demonstrating that type I IFN suppresses inflammasome activation by an undefined mechanism.

60. Schroder, K. & Tschopp, J. The inflammasomes. *Cell* **140**, 821-832 (2010).

61. Franchi, L., Munoz-Planillo, R. & Nunez, G. Sensing and reacting to microbes through the inflammasomes. *Nat. Immunol.* **13**, 325-332 (2012).

62. Kuijk, L.M. et al. HMG-CoA reductase inhibition induces IL-1beta release through Rac1/PI3K/PKB-dependent caspase-1 activation. *Blood* **112**, 3563-3573 (2008).

63. Liao, Y.H. et al. HMG-CoA reductase inhibitors activate caspase-1 in human monocytes depending on ATP release and P2X7 activation. *J. Leukoc. Biol.* **93**, 289-299 (2013).

64. Mayer-Barber, K.D. et al. Host-directed therapy of tuberculosis based on interleukin-1 and type I interferon crosstalk. *Nature* **511**, 99-103 (2014).

65. Berry, M.P. et al. An interferon-inducible neutrophil-driven blood transcriptional signature in human tuberculosis. *Nature* **466**, 973-977 (2010).

66. Masters, S.L., Simon, A., Aksentijevich, I. & Kastner, D.L. Horror autoinflammaticus: the molecular pathophysiology of autoinflammatory disease (*). *Annu. Rev. Immunol.* **27**, 621-668 (2009).

67. Mandey, S.H., Kuijk, L.M., Frenkel, J. & Waterham, H.R. A role for geranylgeranylation in interleukin-1beta secretion. *Arthritis Rheum.* **54**, 3690-3695 (2006).

68. Pontillo, A., Paoluzzi, E. & Crovella, S. The inhibition of mevalonate pathway induces upregulation of NALP3 expression: new insight in the pathogenesis of mevalonate kinase deficiency. *Eur. J. Hum. Genet.* **18**, 844-847 (2010).

69. Kim, J. et al. Sufficient production of geranylgeraniol is required to maintain endotoxin tolerance in macrophages. *J. Lipid Res.* **54**, 3430-3437 (2013).

70. Gibson, K.M. et al. 3-Hydroxy-3-methylglutaryl coenzyme A reductase activity in cultured fibroblasts from patients with mevalonate kinase deficiency: differential response to lipid supplied by fetal bovine serum in tissue culture medium. *J. Lipid Res.* **31**, 515-521 (1990).

71. Umetani, M. et al. The Cholesterol Metabolite 27-Hydroxycholesterol Promotes Atherosclerosis via Proinflammatory Processes Mediated by Estrogen Receptor Alpha. *Cell Metab.* **20**, 172-182 (2014).

72. Umetani, M. et al. 27-Hydroxycholesterol is an endogenous SERM that inhibits the cardiovascular effects of estrogen. *Nat. Med.* **13**, 1185-1192 (2007).

73. Lundberg, B. Chemical composition and physical state of lipid deposits in atherosclerosis. *Atherosclerosis* **56**, 93-110 (1985).

74. Brown, A.J. & Jessup, W. Oxysterols and atherosclerosis. *Atherosclerosis* **142**, 1-28 (1999).

75. Brown, M.S., Dana, S.E. & Goldstein, J.L. Cholesterol ester formation in cultured human fibroblasts. Stimulation by oxygenated sterols. *J. Biol. Chem.* **250**, 4025-4027 (1975).

76. Miller, S.C. & Melnykovych, G. Regulation of cholesterol biosynthesis and esterification by 25-hydroxycholesterol in a macrophage-like cell line: uncoupling by progesterone. *J. Lipid Res.* **25**, 991-999 (1984).

77. Cheng, D., Chang, C.C., Qu, X. & Chang, T.Y. Activation of acyl-coenzyme A:cholesterol acyltransferase by cholesterol or by oxysterol in a cell-free system. *J. Biol. Chem.* **270**, 685-695 (1995).

78. Li-Hawkins, J., Lund, E.G., Turley, S.D. & Russell, D.W. Disruption of the oxysterol 7alpha-hydroxylase gene in mice. *J. Biol. Chem.* **275**, 16536-16542 (2000).

79. Gilchrist, M. et al. Systems biology approaches identify ATF3 as a negative regulator of Toll-like receptor 4. *Nature* **441**, 173-178 (2006).

80. McDonald, J.G. & Russell, D.W. 25-Hydroxycholesterol: a new life in immunology. *J. Leukoc. Biol.* **88**, 1071-1072 (2010).

81. Birkenbach, M., Josefsen, K., Yalmanchili, R., Lenoir, G. & Kieff, E. Epstein-Barr virus induced genes: first lymphocyte-specific G-protein coupled peptide receptors. *J. Virol.* **67**, 2209-2220 (1993).

82. Rosenkilde, M.M. et al. Molecular pharmacological phenotyping of EBI2. An orphan seven-transmembrane receptor with constitutive activity. *J. Biol. Chem.* **281**, 13199-13208 (2006).

83. Benned-Jensen, T. et al. Ligand modulation of the Epstein-Barr virus-induced seven-transmembrane receptor EBI2: identification of a potent and efficacious inverse agonist. *J. Biol. Chem.* **286**, 29292-29302 (2011).

84. Benned-Jensen, T. et al. Small molecule antagonism of oxysterol-induced Epstein-Barr virus induced gene 2 (EBI2) activation. *FEBS open bio* **3**, 156-160 (2013).

85. Benned-Jensen, T. & Rosenkilde, M.M. Structural motifs of importance for the constitutive activity of the orphan 7TM receptor EBI2: analysis of receptor activation in the absence of an agonist. *Molecular pharmacology* **74**, 1008-1021 (2008).

86. Benned-Jensen, T. et al. Molecular characterization of oxysterol binding to the Epstein-Barr virus-induced gene 2 (GPR183). *The Journal of biological chemistry* **287**, 35470-35483 (2012).

87. Zhang, L. et al. Identification of structural motifs critical for epstein-barr virus-induced molecule 2 function and homology modeling of the ligand docking site. *Molecular pharmacology* **82**, 1094-1103 (2012).

88. Hanson, M.A. et al. Crystal structure of a lipid G protein-coupled receptor. *Science* **335**, 851-855 (2012).

89. Gessier, F. et al. Identification and characterization of small molecule modulators of the Epstein-Barr virus-induced gene 2 (EBI2) receptor. *J. Med. Chem.* **57**, 3358-3368 (2014).

90. Gatto, D. & Brink, R. B cell localization: regulation by EBI2 and its oxysterol ligand. *Trends Immunol.* **34**, 336-341 (2013).

Excellent review of EBI2 biology in B cells.

91. Kelly, L.M., Pereira, J.P., Yi, T., Xu, Y. & Cyster, J.G. EBI2 guides serial movements of activated B cells and ligand activity is detectable in lymphoid and nonlymphoid tissues. *J. Immunol.* **187**, 3026-3032 (2011).

Establishes the time course of EBI2 influence on B cell behavior *in vivo* and uses a sensitive bioassay to show that EBI2 ligand is widely distributed in tissues.

92. Gatto, D., Wood, K. & Brink, R. EBI2 operates independently of but in cooperation with CXCR5 and CCR7 to direct B cell migration and organization in follicles and the germinal center. *J. Immunol.* **187**, 4621-4628 (2011).

By removing the influence of two major chemokines, this report reveals additional influences of EBI2 in B cell positioning in the spleen.

93. Chan, T.D. et al. Antigen affinity controls rapid T-dependent antibody production by driving the expansion rather than the differentiation or extrafollicular migration of early plasmablasts. *J. Immunol.* **183**, 3139-3149 (2009).

94. MacLennan, I. & Vinuesa, C. Dendritic cells, BAFF, and APRIL: innate players in adaptive antibody responses. *Immunity* **17**, 235-238 (2002).

95. Xu, W. & Banchereau, J. The antigen presenting cells instruct plasma cell differentiation. *Front Immunol* **4**, 504 (2014).

96. Mueller, S.N. & Germain, R.N. Stromal cell contributions to the homeostasis and functionality of the immune system. *Nat. Rev. Immunol.* **9**, 618-629 (2009).

97. Coffey, F., Alabyev, B. & Manser, T. Initial clonal expansion of germinal center B cells takes place at the perimeter of follicles. *Immunity* **30**, 599-609 (2009).

98. Cyster, J.G. B cell follicles and antigen encounters of the third kind. *Nat. Immunol.* **11**, 989-996 (2010).

99. Shaffer, A.L. et al. BCL-6 represses genes that function in lymphocyte differentiation, inflammation, and cell cycle control. *Immunity* **13**, 199-212 (2000).

100. Turqueti-Neves, A. et al. B-cell-intrinsic STAT6 signaling controls germinal center formation. *Eur. J. Immunol.* **44**, 2130-2138 (2014).

101. Kawamoto, S. et al. Foxp3 T Cells Regulate Immunoglobulin A Selection and Facilitate Diversification of Bacterial Species Responsible for Immune Homeostasis. *Immunity* **41**, 152-165 (2014).

102. Coelho, F.M. et al. Naive B-cell trafficking is shaped by local chemokine availability and LFA-1-independent stromal interactions. *Blood* **121**, 4101-4109 (2013).

103. Barroso, R. et al. EBI2 regulates CXCL13-mediated responses by heterodimerization with CXCR5. *FASEB J.* **26**, 4841-4854 (2012).

104. Lund, R., Aittokallio, T., Nevalainen, O. & Lahesmaa, R. Identification of novel genes regulated by IL-12, IL-4, or TGF-beta during the early polarization of CD4+ lymphocytes. *J. Immunol.* **171**, 5328-5336 (2003).

105. Kroenke, M.A. et al. Bcl6 and Maf cooperate to instruct human follicular helper CD4 T cell differentiation. *J. Immunol.* **188**, 3734-3744 (2012).

106. Kraal, G. & Mebius, R. New insights into the cell biology of the marginal zone of the spleen. *Int. Rev. Cytol.* **250**, 175-215 (2006).

107. Kabashima, K. et al. Intrinsic Lymphotoxin-beta Receptor Requirement for Homeostasis of Lymphoid Tissue Dendritic Cells. *Immunity* **22**, 439-450 (2005).

108. Heinig, M. et al. A trans-acting locus regulates an anti-viral expression network and type 1 diabetes risk. *Nature* **467**, 460-464 (2010).

109. Wallace, C. et al. Statistical colocalization of monocyte gene expression and genetic risk variants for type 1 diabetes. *Hum. Mol. Genet.* **21**, 2815-2824 (2012).

110. Jostins, L. et al. Host-microbe interactions have shaped the genetic architecture of inflammatory bowel disease. *Nature* **491**, 119-124 (2012).

111. Chiang, E.Y., Johnston, R.J. & Grogan, J. EBI2 is a negative regulator of type I interferons in plasmacytoid and myeloid dendritic cells. *PLoS One* **8**, e83457 (2013).

112. Nau, G.J. et al. Human macrophage activation programs induced by bacterial pathogens. *Proc. Natl. Acad. Sci. U. S. A.* **99**, 1503-1508 (2002).

113. Preuss, I. et al. Transcriptional regulation and functional characterization of the oxysterol/EBI2 system in primary human macrophages. *Biochem. Biophys. Res. Commun.* **446**, 663-668 (2014).

114. Cantor, R.M. et al. Systemic lupus erythematosus genome scan: support for linkage at 1q23, 2q33, 16q12-13, and 17q21-23 and novel evidence at 3p24, 10q23-24, 13q32, and 18q22-23. *Arthritis and rheumatism* **50**, 3203-3210 (2004).

115. Moser, K.L. et al. Genome scan of human systemic lupus erythematosus: evidence for linkage on chromosome 1q in African-American pedigrees. *Proceedings of the National Academy of Sciences of the United States of America* **95**, 14869-14874 (1998).

116. Ye, S. et al. Protein interaction for an interferon-inducible systemic lupus associated gene, IFIT1. *Rheumatology* **42**, 1155-1163 (2003).

117. Pascual, V., Chaussabel, D. & Banchereau, J. A genomic approach to human autoimmune diseases. *Annu. Rev. Immunol.* **28**, 535-571 (2010).

118. Wilson, L.E., Widman, D., Dikman, S.H. & Gorevic, P.D. Autoimmune disease complicating antiviral therapy for hepatitis C virus infection. *Semin. Arthritis Rheum.* **32**, 163-173 (2002).

119. Niedobitek, G. et al. Patterns of Epstein-Barr virus infection in non-neoplastic lymphoid tissue. *Blood* **79**, 2520-2526 (1992).

120. Kurth, J. et al. EBV-infected B cells in infectious mononucleosis: viral strategies for spreading in the B cell compartment and establishing latency. *Immunity* **13**, 485-495 (2000).

121. Hanlon, P., Avenell, A., Aucott, L. & Vickers, M.A. Systematic review and meta-analysis of the sero-epidemiological association between Epstein-Barr virus and systemic lupus erythematosus. *Arthritis Res. Ther.* **16**, R3 (2014).

122. Lin, C.Y. & Morel, D.W. Esterification of oxysterols in human serum: effects on distribution and cellular uptake. *J. Lipid Res.* **37**, 168-178 (1996).

123. Frederico, B., Chao, B., May, J.S., Belz, G.T. & Stevenson, P.G. A murid gamma-herpesviruses exploits normal splenic immune communication routes for systemic spread. *Cell host & microbe* **15**, 457-470 (2014).

124. Janowski, B.A., Willy, P.J., Devi, T.R., Falck, J.R. & Mangelsdorf, D.J. An oxysterol signalling pathway mediated by the nuclear receptor LXR alpha. *Nature* **383**, 728-731 (1996).

125. Bensinger, S.J. & Tontonoz, P. Integration of metabolism and inflammation by lipid-activated nuclear receptors. *Nature* **454**, 470-477 (2008).

126. Jin, L. et al. Structural basis for hydroxycholesterols as natural ligands of orphan nuclear receptor RORgamma. *Mol. Endocrinol.* **24**, 923-929 (2010).

127. Soroosh, P. et al. Oxysterols are agonist ligands of RORgt and drive Th1 cell differentiation. *Proc. Natl. Acad. Sci. USA* **111**, 12163-12168 (2014).

128. Huh, J.R. et al. Digoxin and its derivatives suppress TH17 cell differentiation by antagonizing RORgammat activity. *Nature* **472**, 486-490 (2011).

129. Kidani, Y. et al. Sterol regulatory element-binding proteins are essential for the metabolic programming of effector T cells and adaptive immunity. *Nat. Immunol.* **14**, 489-499 (2013).

Chapter 3

Oxysterol restraint of cholesterol synthesis prevents AIM2 inflammasome activation

Summary

Type I interferon restrains interleukin-1β (IL-1β)-driven inflammation in macrophages by upregulating cholesterol-25-hydroxylase (Ch25h) and repressing SREBP transcription factors. However, the molecular links between lipid metabolism and IL-1β production remain obscure. Here we demonstrate that production of 25-hydroxycholesterol (25-HC) by macrophages is required to prevent inflammasome activation by the DNA sensor protein absent in melanoma 2 (AIM2). We find that in response to bacterial infection or lipopolysaccharide (LPS) stimulation, macrophages upregulate Ch25h to maintain repression of SREBP2 activation and cholesterol synthesis. Increasing macrophage cholesterol content is sufficient to trigger IL-1β release in a crystal-independent but AIM2-dependent manner. Ch25h-deficiency results in cholesterol-dependent reduced mitochondrial respiratory capacity and release of mitochondrial DNA into the cytosol. Ch25h/Aim2 double-deficiency rescues the increased inflammasome activity observed in Ch25h single knockouts. Therefore, activated macrophages utilize 25-HC in an anti-inflammatory circuit that maintains mitochondrial integrity and prevents spurious AIM2 inflammasome activation.

Introduction

Cholesterol is a crucial structural component of mammalian cell membranes. However, unlike fatty acids, cholesterol cannot be catabolized as an energy source, necessitating feedback mechanisms to control cellular cholesterol content. The molecular basis for cholesterol feedback inhibition involves the Sterol Regulatory Element Binding Protein 2 (SREBP2) pathway, whereby increased endoplasmic reticulum (ER) cholesterol content causes the chaperone protein SCAP to bind more tightly to INSIG, which results in SREBP2 sequestration in the ER (Goldstein et al., 2006). In states of low ER cholesterol, SCAP dissociates from INSIG, allowing for translocation of the SCAP-SREBP2 complex to the Golgi apparatus where SREBP2 is cleaved (Goldstein et al., 2006). This releases the transcription factor domain of SREBP2, which translocates to the nucleus and activates the transcription of genes involved in cholesterol biosynthesis and uptake.

While cholesterol can inhibit sterol biosynthesis, the oxysterol 25-hydroxycholesterol (25-HC) is even more potent than cholesterol in its capacity to inhibit SREBP2 in biochemical studies (Goldstein et al., 2006). Whereas cholesterol is sensed by SCAP, 25-HC binds directly to INSIG causing increased association with SCAP-SREBP2. However, it has been unclear whether endogenously produced 25-HC contributes to cholesterol regulation in mammalian cells. Mice deficient in the enzyme cholesterol 25-hydroxylase (Ch25h), which produces 25-HC from cholesterol, do not show defects in baseline cholesterol homeostasis, raising the question of whether this metabolite has a physiologic function (McDonald and Russell, 2010).

It has recently been appreciated that Ch25h is an interferon (IFN)-inducible gene in macrophages. Stimulation of mouse bone marrow-derived macrophages (BMDMs) with lipopolysaccharide (LPS) or polyI:C results in IFNAR1-dependent upregulation of *Ch25h* mRNA and 25-HC synthesis (Cyster et al., 2014). Consistent with the key role of type I interferon (IFN) in responses to viruses, 25-HC has antiviral activity (Blanc et al., 2013; Cyster et al., 2014; Liu et al., 2013). Type I IFN additionally acts to inhibit IL-1β production in a program that helps prevent unrestrained inflammatory responses (Cyster et al., 2014). This occurs by repression of *Il1b* transcription and inflammasome-dependent IL-1β processing (Guarda et al., 2011). Recent work suggests that the inhibitory action of type I IFN on IL-1β requires induction of Ch25h/25-HC (Reboldi et al., 2014).

Inflammasomes are multi-protein complexes that form within the cytosol following exposure to a wide variety of pathogen-derived stimuli (Rathinam and Fitzgerald, 2016). Inflammasome activation requires recognition of ligand by a sensor protein such as NLRP3 or AIM2 followed by recruitment of the adaptor protein ASC (Rathinam and Fitzgerald, 2016). This results in ASC oligomerization and the recruitment and activation of caspase-1, a protease that processes pro-IL-1β into mature IL-1β. How 25-HC represses inflammasome activation has been unclear. The effects of Ch25h-deficiency on pro-IL-1β processing could be rescued by overexpression of INSIG1 or deletion of SCAP, suggesting a contribution by the SREBP pathway, but the nature of this contribution has not been defined (Reboldi et al., 2014).

Here, we describe a metabolic circuit that links regulation of cellular cholesterol content to the prevention of inflammasome activation by endogenous ligands. We find

LPS-activated macrophages shut down cholesterol biosynthesis and decrease their cholesterol content in a Ch25h-dependent manner. Enforcement of increased macrophage cholesterol content after LPS stimulation is sufficient to drive inflammasome-dependent IL-1β production. Cholesterol-dependent inflammasome activation unexpectedly requires the cytosolic DNA sensor Absent in Melanoma 2 (AIM2). Metabolic studies reveal that *Ch25h*$^{-/-}$ and cholesterol-loaded macrophages have impaired mitochondrial respiration and increased sensitivity to mitochondrial damage. This results in increased cytosolic mitochondrial DNA (mtDNA) content and depletion of mtDNA reduces cholesterol-dependent IL-1β release. Finally, we find that Ch25h/Aim2 double-deficiency reverses inflammasome activation caused by Ch25h-deficiency. These findings suggest that macrophage upregulation of 25-HC after recognition of pathogens prevents cholesterol-dependent mitochondrial dysfunction and spurious crosstalk between mtDNA and the inflammasome.

Results

Ch25h controls IL-1β release and intracellular bacterial growth through ASC-dependent inflammasomes

Previous work demonstrated that *Ch25h*$^{-/-}$ BMDMs overproduced IL-1β in response to *Listeria monocytogenes* infection and had increased control of intracellular bacterial growth (Reboldi et al., 2014). To determine whether these responses were due to increased inflammasome activity, we generated *Ch25h*$^{-/-}$*Asc*$^{-/-}$ mice. BMDMs from these mice and their matched controls were treated with either carrier (ethanol) or 25-HC (1uM), and infected with *L. monocytogenes* for 24 hours. *Ch25h*$^{-/-}$*Asc*$^{+/+}$ BMDMs had increased production of IL-1β, which could be inhibited by addition of 25-HC as expected (Fig. 1A) (Reboldi et al., 2014). However, in the setting of ASC-deficiency, *Ch25h*$^{-/-}$ BMDMs showed no elevation in levels of extracellular IL-1β and 25-HC addition to these cultures did not reduce IL-1β levels (Fig. 1B). We also observed decreased *L. monocytogenes* colony forming units (CFUs) in *Ch25h*$^{-/-}$*Asc*$^{+/+}$ BMDMs, which could be rescued by the addition of 25-HC to the cellular medium (Fig. 1C). *Asc*$^{-/-}$ BMDMs showed an overall increase in *L. monocytogenes* CFUs, and the difference between *Ch25h*$^{+/-}$ and *Ch25h*$^{-/-}$ BMDMs was lost in the absence of *Asc* (Fig. 1D).

In previous work we demonstrated that *Ch25h*$^{-/-}$ BMDMs overproduced IL-1β following exposure to LPS and the NLRP3 inflammasome activator ATP (Reboldi et al., 2014). Consistent with these observations, LPS+ATP treated *Ch25h*$^{-/-}$ cells produced increased IL-1β compared to heterozygous controls (Fig. 1E). However, in the setting of *Asc*$^{-/-}$, neither Ch25h genotype produced detectable IL-1β, ruling out the possibility that

the increased cytokine production by *Ch25h*$^{-/-}$ cells was due to passive loss of membrane integrity (Fig. 1E). These data support a model in which IL-1β overproduction and decreased bacterial replication in *Ch25h*$^{-/-}$ BMDMs are due to increased activity of ASC-dependent inflammasomes. These observations led us to more deeply explore how Ch25h and 25-HC act to restrain inflammasome activity.

Ch25h and 25-HC enforce repression of the SREBP2 pathway and cholesterol synthesis in LPS-activated macrophages

Type I IFN has been described to repress the SREBP2 pathway in macrophages (Reboldi et al., 2014; York et al., 2015), but it is not clear to what extent this process depends on 25-HC. We therefore performed time-course analyses of cholesterol biosynthetic enzyme mRNA expression in control and *Ch25h*$^{-/-}$ BMDMs after stimulation with LPS. As expected, *Ch25h* transcript levels peaked at approximately 4 hours post-LPS stimulation and subsequently declined (Fig. 2A) (Cyster et al., 2014). Similar *Ch25h* induction kinetics were observed following *L. monocytogenes* infection (Fig. S1A). The sterol biosynthetic enzymes *Hmgcs1*, *Lss*, *Dhcr24* and *Sqle* were initially repressed 2 hours post-LPS, regardless of the genetic status of Ch25h (Fig. 2A). However, by 8 hours after LPS stimulation, *Ch25h*$^{-/-}$ BMDMs showed increased expression of sterol biosynthetic enzyme mRNAs (Fig. 2A). Overexpression of cholesterol biosynthesis mRNAs in the absence of Ch25h was also observed after 8 hours of intracellular *L. monocytogenes* infection (Fig. S1B). The early repression of the SREBP2 pathway in the context of LPS stimulation was IFNAR1-dependent (data not shown) consistent with previous studies (York et al., 2015). These data suggest that

Ch25h is induced in macrophages by bacterial sensing, and acts to repress sterol biosynthetic enzyme expression. However, Ch25h is not required for initial shutdown of the cholesterol biosynthesis pathway, but instead is necessary for enforcing sustained repression.

As a second approach to determine whether Ch25h represses cholesterol biosynthesis in activated macrophages, we performed liquid chromatography-mass spectrometry (LC-MS) for cholesterol biosynthetic intermediates in control and *Ch25h*$^{-/-}$ BMDMs after 8 hours of LPS treatment. *Ch25h*$^{-/-}$ BMDMs showed an expected reduction in 25-HC levels (Fig. 2B). Consistent with our hypothesis, these cells also showed increased levels of desmosterol, lanosterol, and 7-dehydrocholesterol, suggesting that *Ch25h*$^{-/-}$ increased cholesterol biosynthesis pathway activity (Fig. 2B).

We next tested whether cholesterol content itself was altered in *Ch25h*$^{-/-}$ macrophages. Using a cholesterol fluorescence assay, we found that *Ch25h*$^{-/-}$ BMDMs showed an initial increase in total cholesterol content compared to wild-type cells (Fig. 2C). LPS stimulation resulted in decreased cholesterol content in both genotypes by 4 hours, whereas only *Ch25h*$^{-/-}$ cells showed an increase in total cholesterol by 8 hours, which is consistent with the sterol enzyme mRNA analysis (Fig. 2C). Similarly, staining with filipin, a fluorescent cholesterol-binding antibiotic, showed higher fluorescence intensity in 8-hour LPS-activated *Ch25h*$^{-/-}$ macrophages (Fig. 2D). We additionally quantified cholesterol levels using LC-MS at the 8-hour LPS time point, which confirmed that *Ch25h*$^{-/-}$ resulted in increased cholesterol content (Fig. 2E). To determine whether *Ch25h*$^{-/-}$ macrophages increase their cholesterol content in vivo, we injected mice I.P. with LPS and sorted peritoneal macrophages after 8 hours. LPS stimulation caused

Ch25h$^{-/-}$ peritoneal macrophages to increase their cholesterol content, whereas cholesterol levels in controls remained constant (Fig. S1C).

The increased expression of SREBP2-responsive genes between 4 and 8 hours of LPS exposure in the Ch25h-deficient setting suggested that there is a latent positive drive for cholesterol synthesis that is kept in check by 25-HC. mTORC1 signaling has been shown to drive SREBP1 and SREBP2 activation, and is activated by TLR stimulation (Düvel et al., 2010; Porstmann et al., 2008; Wang et al., 2011). We therefore tested whether this pathway was active in LPS stimulated BMDMs. Phospho-flow cytometry for total S6K1, pS6K1 (Thr389) and pS6 (Ser240/244) showed that LPS stimulation resulted in a time-dependent increase in mTORC1 activity (Fig. 2F). We confirmed that S6 phosphorylation during LPS stimulation was mTORC1-dependent since it was prevented by rapamycin treatment (Fig. S1D). Consistent with mTORC1 activity driving SREBP2 activation, the augmented expression of *Hmgcs1* mRNA in *Ch25h*$^{-/-}$ cells was largely prevented by rapamycin (Fig. 2G). Moreover, in accord with a connection between SREBP pathway activity and IL-1β production (Reboldi et al., 2014), rapamycin reversed the overproduction of IL-1β in response to ATP in LPS stimulated *Ch25h*$^{-/-}$ macrophages, while having minimal effect on IL-1β production by *Ch25h*$^{+/-}$ BMDMs (Fig. 2H). Taken together, these data indicate that Ch25h/25-HC are required in 8-hour LPS activated macrophages to antagonize mTORC1-induced SREBP2 pathway activity and prevent cholesterol over-accumulation in the cell.

Non-crystalline cholesterol is sufficient to promote inflammasome activation

To determine whether increased cholesterol biosynthesis can be functionally linked to inflammasome activation, we used a murine MSCV retrovirus system to transduce cDNAs expressing HMG-CoA reductase (Hmgcr) and dehydrocholesterol 24-reductase (Dhcr24), enzymes in the cholesterol biosynthetic pathway, into BMDMs. Using a fluorescent FLICA peptide that acts as a reporter for caspase-1 activity, we found that over-expression of either of these two cDNAs resulted in increased inflammasome activity after 8 hours of LPS stimulation (Fig. 3A). Inflammasome activation in mouse macrophages typically requires addition of a 'second signal' (such as ATP) to engage an inflammasome sensor protein (Rathinam and Fitzgerald, 2016). However, the effect of increased expression of Hmgcr and Dhcr24 mRNAs on caspase-1 was observed in the absence of an exogenous second signal. Attempts to measure IL-1β in the LPS-stimulated macrophage supernatant by ELISA were unsuccessful, consistent with a low amount of inflammasome activity. We therefore used an IL-17A-based IL-1β bioassay (Reboldi et al., 2014) to test whether cholesterol synthesis could drive inflammasome activation. We found that supernatants from BMDMs transduced with either Hmgcr or Dhcr24 had augmented capacity to stimulate IL-17A production from T cells, whereas this capacity was lost in the setting of ASC-deficiency (Fig. 3B).

To determine whether cholesterol itself was involved in driving inflammasome activity, we treated BMDMs with LPS and cholesterol that had been solubilized by forming complexes with the carrier methyl-β-cyclodextrin (MCD) at a 25:1 ratio of MCD:cholesterol (MCD-chol). Strikingly, treatment of LPS activated macrophages with 100ug/ml MCD-chol, a concentration typical of other studies (Robinson et al., 2014; York et al., 2015), was sufficient to promote IL-1β production as measured by ELISA

(Fig. 3C). A 10-fold lower dose of MCD-chol also triggered IL-1β production as detected using the IL-1β bioassay (Fig. 3D).

Previous work has suggested that the NLRP3 inflammasome is activated by cholesterol crystals in macrophages associated with atherosclerotic plaques (Franklin et al., 2016). To determine whether our observed IL-1β release in response to MCD-chol challenge was due to crystal formation, we took advantage of the fact that crystalline inflammasome activators depend on phagocytic uptake (Hornung et al., 2008). We treated LPS-activated BMDMs with cytochalasin D to inhibit actin polymerization and challenged them with MCD-chol, ATP, or alum. Whereas IL-1β release by the crystalline activator alum was blocked by cytochalasin D treatment, IL-1β release in response to MCD-chol or ATP was unaffected, providing evidence that MCD-chol is acting in a soluble fashion (Fig. 3E).

To determine whether 25-HC can prevent cholesterol-dependent IL-1β release, we reconstituted *Ch25h*$^{-/-}$ BMDMs with either wild-type Ch25h, a mutant Ch25h that cannot synthesize 25-HC (Reboldi et al., 2014), or empty vector using retroviruses. Overexpression of wild-type Ch25h could repress mRNA expression of the sterol biosynthesis enzyme *Sqle*, whereas vector and Ch25hmut had no effect on this expression, confirming the functional status of these constructs (Fig. S2A). We found that while overexpression of Ch25h had a small capacity to diminish IL-1β release in response to ATP, it more substantially reduced the capacity of MCD-cholesterol to stimulate IL-1β release, whereas the mutant enzyme had no effect (Fig. 3F). In addition to its ability to inhibit SREBP2 activation, 25-HC could possibly protect cells from cholesterol overloading by acting as an LXR agonist. Reconstitution of LXRα/β double

knockout BMDMs with wild type versus mutant Ch25h showed the same repressive effect on MCD-cholesterol-dependent IL-1β release, suggesting that this phenomenon does not involve ligand action of 25-HC on LXRs (Fig. S2B). These observations provide further evidence that a key function of Ch25h/25-HC induction in activated macrophages is to prevent cholesterol-dependent IL-1β production.

Cholesterol-dependent IL-1β release requires the AIM2 inflammasome

Mitochondrial reactive oxygen species (mtROS) have been implicated as activators of the NLRP3 inflammasome in response to a diverse range of stimuli (Zhou et al., 2011). Additionally, diseases associated with cholesterol dysregulation have been shown to induce mtROS (Kennedy et al., 2014). Therefore, we tested whether mtROS induction could be responsible for cholesterol-dependent IL-1β production. We treated *Ch25h*$^{+/-}$ and *Ch25h*$^{-/-}$ BMDMs with either LPS alone or LPS plus ATP and measured mtROS by staining with MitoSOX. LPS plus ATP treatment induced an increase in mtROS as expected (Yu et al., 2014; Zhou et al., 2011). We observed that *Ch25h*$^{-/-}$ BMDMs had heightened mtROS production after LPS plus ATP treatment compared to control BMDMs (Fig. 4A). Retroviral reconstitution of *Ch25h*$^{-/-}$ BMDMs with Ch25h reduced MitoSOX staining, whereas Ch25hmut showed no effect (Fig. 4B). Treatment of *Ch25h*$^{+/-}$ and *Ch25h*$^{-/-}$ BMDMs with the mtROS scavenger MitoTEMPO inhibited IL-1β in both genotypes (Fig. S3A). Furthermore, treatment of uninfected BMDMs with LPS plus MCD-chol resulted in increased mtROS compared to LPS alone, consistent with data suggesting that elevated cholesterol content can cause mitochondrial dysfunction (Fig. 4C). Moreover, using a 293T NLRP3 inflammasome reconstitution system we

found that the increased cholesterol biosynthesis induced by SREBP2 over-expression was capable of promoting IL-1β cleavage and release (Fig. S3B, S3C, S3D). Combined, these observations suggested that IL-1β release by macrophages following cholesterol accumulation would occur via NLPR3-inflammasome activation. Surprisingly, however, BMDMs lacking NLRP3 had no defect in IL-1β production in response to LPS plus MCD-chol treatment, whereas these cells failed to respond to LPS plus ATP (Fig. 4D).

To test whether the observed IL-1β release in MCD-chol challenged BMDMs was an inflammasome-dependent process, as opposed to occurring by passive increases in permeability, we challenged *Asc*$^{-/-}$ and *Casp-1/11*$^{-/-}$ BMDMs with LPS and MCD-chol. *Asc*$^{-/-}$ (Fig. 4E) and *Casp-1/11*$^{-/-}$ (Fig. 4F) BMDMs showed complete abrogation of IL-1β production in response to cholesterol, establishing that this process was indeed inflammasome-dependent.

To identify the relevant sensor protein required for cholesterol-dependent IL-1β production, we challenged *Nlrc4*$^{-/-}$, *Casp11*$^{-/-}$, and *Aim2*$^{-/-}$ BMDMs with LPS and MCD-Chol. *Nlrc4*$^{-/-}$ (Fig. 4G) and *Casp11*$^{-/-}$ (Fig. 4H) BMDMs showed no difference in IL-1β production in response to cholesterol challenge. On the other hand, *Aim2*$^{-/-}$ BMDMs showed a striking reduction in IL-1β release under these conditions (Fig. 4I). Given that different inflammasomes can cooperate in some contexts, we tested whether the low amount of remaining inflammasome activity in *Aim2*$^{-/-}$ BMDMs involved NLRP3. Consistent with a partially redundant contribution of NLRP3 to cholesterol-induced IL-1β release, *Aim2*$^{-/-}$*Nlrp3*$^{-/-}$ double-deficient BMDMs showed a near complete loss of secreted IL-1β when compared with *Casp1/11*$^{-/-}$ BMDMs (Fig. 4J).

Neutrophilic peritonitis is a well-described model system for in vivo assessment of inflammasome activation. To determine whether cholesterol loading could drive inflammasome activation in vivo, we intraperitoneally injected LPS, LPS and MCD-chol, or LPS and Alum. Strikingly, MCD-chol was as efficacious as alum in causing neutrophil accumulation in the peritoneal lavage fluid (Fig. 5A and 5B). To determine whether the AIM2-dependent inflammasome activation caused by cholesterol *in vitro* was also required for neutrophilic peritonitis, we used lethally irradiated mice reconstituted with wild-type or *Aim2*$^{-/-}$ BM. We found that lack of AIM2 in the hematopoietic compartment resulted in a reduction in MCD-chol induced neutrophil recruitment (Fig. 5C and 5D). We also generated irradiated chimeras using *Nlrp3*$^{-/-}$, or *Casp1/11*$^{-/-}$ BM; consistent with our observations in BMDMs, we found that lack of NLRP3 had no effect on neutrophil recruitment following MCD-chol challenge, whereas deletion of caspase-1 resulted in the expected strong reduction (Fig. 5E).

Ch25h-deficiency results in impaired mitochondrial metabolism

The requirement for AIM2, a DNA sensor, in cholesterol-dependent inflammasome activation led us to consider the possibility that dysregulation of cellular cholesterol homeostasis results in release of host DNA into the cytosol. Mitochondria contain multiple copies of mtDNA that encodes for components of the oxidative metabolism machinery. A number of recent studies have demonstrated that mitochondrial dysfunction can lead to mtDNA release into the cytosol (Rongvaux et al., 2014; West et al., 2015; White et al., 2014). Additionally, baseline mitochondrial cholesterol levels are low, and increased mitochondrial cholesterol accumulation is

associated with impaired mitochondrial function (Kennedy et al., 2014). Due to these observations and our findings that Ch25h-deficiency and cholesterol accumulation cause mtROS production, we asked whether the altered cholesterol homeostasis caused by Ch25h-deficiency resulted in impaired mitochondrial function in macrophages. For this analysis we first assessed mitochondrial respiration and abundance using Mitotracker Deep Red and Mitotracker Green dyes, respectively, by flow cytometry. We found that *Ch25h*$^{-/-}$ BMDMs showed diminished Mitotracker Deep Red staining compared to control macrophages after 8 hours of LPS stimulation (Fig. 6A). Additionally, Mitotracker Deep Red staining could be genetically rescued by retrovirally reconstituting *Ch25h*$^{-/-}$ BMDMs with wild-type Ch25h enzyme, but not Ch25hmut (Fig. 6B). Mitotracker Green staining also showed a small but statistically significant decrease in 8 hour LPS-stimulated *Ch25h*$^{-/-}$ BMDMs compared to control macrophages (Fig. 6C). This defect could also be rescued by wild-type but not mutant Ch25h (Fig. 6D). We additionally found that *Ch25h*$^{-/-}$ macrophages showed diminished Mitotracker Deep Red and Mitotracker Green staining in response to 8 hours of *L. monocytogenes* infection (Fig. S4A and S4B).

To determine whether increased cholesterol content was sufficient to explain the Mitotracker staining effects in *Ch25h*$^{-/-}$ BMDMs, we treated *Asc*$^{+/+}$ and *Asc*$^{-/-}$ BMDMs with LPS and MCD-chol (10ug/ml) and measured Mitotracker staining by flow cytometry. Both Mitotracker Deep Red and Mitotracker Green staining were diminished by increasing cellular cholesterol content (Fig. S4C and S4D). Importantly, *Asc*$^{-/-}$ BMDMs also showed decreased Mitotracker staining, demonstrating that this effect was not secondary to increased inflammasome activation (Yu et al., 2014). As a second test

of whether increased cholesterol content was sufficient to affect Mitotracker staining, we again transduced BMDMs with Hmgcr, or Dhcr24 and stimulated these macrophages with LPS. Both Mitotracker Deep Red and Mitotracker Green staining were diminished by enzyme overexpression (Fig. S4E and S4F). To determine whether cholesterol efflux could rescue Mitotracker staining, we treated macrophages with HDL or the LXR agonist GW3965 along with LPS. We found that the diminished Mitotracker Deep Red staining in *Ch25h*$^{-/-}$ cells was rescued by both HDL and GW3965, further supporting a role for cholesterol in this outcome (Fig. S4G).

Mitochondrial dysfunction is often associated with alterations in the ion potential of the inner membrane (Shimida et al., 2012). We therefore tested whether Ch25h-deficiency affected mitochondrial membrane potential using tetramethylrhodamine methyl ester (TMRM), a cationic dye that becomes sequestered in the mitochondrial matrix in amounts directly proportional to the membrane potential. LPS stimulation resulted in diminished TMRM staining in *Ch25h*$^{-/-}$ macrophages compared to controls (Fig. 6E). TMRM staining could be rescued by retroviral transduction of *Ch25h*$^{-/-}$ macrophages with active but not mutant Ch25h enzyme (Fig. 6F). Diminished TMRM staining was also observed in *Ch25h*$^{-/-}$ macrophages after *L. monocytogenes* infection (Fig. S4H)

As another approach to assess mitochondrial function in *Ch25h*$^{-/-}$ macrophages, we utilized the Seahorse assay to measure oxygen consumption by BMDMs after 8 hours of LPS stimulation. *Ch25h*$^{-/-}$ macrophages showed a decreased basal oxygen consumption rate (OCR) compared to wild-type cells (Fig. 6G and 6H). More strikingly, BMDMs lacking Ch25h showed impaired spare respiratory capacity (SRC) after FCCP

treatment, suggesting that maximal mitochondrial respiration is impaired in settings of altered cholesterol homeostasis (Fig. 6G). The decrease in basal oxygen consumption rate in *Ch25h*$^{-/-}$ macrophages was also coupled to an increased extracellular acidification rate (ECAR), suggesting that these cells were metabolically reprogrammed towards aerobic glycolysis (Fig. 6H). To determine whether impaired mitochondrial respiration in the absence of Ch25h could be explained by increased cholesterol content, we treated BMDMs with MCD-chol and again performed Seahorse analysis. Consistent with our hypothesis, cholesterol loaded macrophages also showed impaired basal OCR as well as diminished SRC (Fig. S4I).

To test whether *Ch25h*$^{-/-}$ macrophages showed signs of mitochondrial dysfunction in vivo, we intraperitoneally injected control and *Ch25h*$^{-/-}$ mice with saline or LPS for 8 hours and assessed Mitotracker staining on peritoneal macrophages by flow cytometry. While saline treated mice showed no difference between genotypes, we observed diminished Mitotracker Deep Red and Mitotracker Green staining in peritoneal macrophages derived from *Ch25h*$^{-/-}$ mice after LPS treatment (Fig. 6I, 6J, and S4J).

Increased mitochondrial cholesterol content results in cytosolic mtDNA accumulation and inflammasome activation

Given our observation that *Ch25h*$^{-/-}$ macrophages showed increased cellular cholesterol and mitochondrial dysfunction, we asked whether these cells had increased mitochondrial cholesterol content. We used a MACS-based immunoprecipitation system with anti-Tomm22 coupled beads to isolate mitochondria and mitochondrial-associated membrane (MAM) from either control or 8 hour LPS-stimulated *Ch25h*$^{+/-}$ or *Ch25h*$^{-/-}$

BMDMs. Immunoblots of these fractions showed an expected enrichment in the outer mitochondrial membrane protein Tomm20, depletion of the cytosolic protein β-tubulin, and partial depletion of the ER/MAM protein calreticulin compared to whole cell extracts (Fig. S5A). The incomplete depletion of calreticulin was most likely due to MAM contamination (Hayashi et al., 2007). We saw that while *Ch25h*$^{+/-}$ macrophages showed no change after stimulation, *Ch25h*$^{-/-}$ BMDMs show increased mitochondrial/MAM cholesterol content after LPS stimulation (Fig. 7A). Additionally, we found that retroviral reconstitution of *Ch25h*$^{-/-}$ macrophages with wild type but not mutant Ch25h enzyme could decrease mitochondrial/MAM cholesterol levels(Fig 7B). Mitochondrial/MAM cholesterol content was also increased in BMDMs treated with LPS and MCD-Chol (Fig. S5B). These findings together with the evidence of mitochondrial damage and the requirement for AIM2 in cholesterol-dependent inflammasome activation led us to test whether Ch25h-deficiency and cholesterol loading increased cytosolic mtDNA. We stimulated control and KO BMDMs with either vehicle or LPS for 8 hours and then extracted cytosolic DNA. qPCR analysis for mtDNA and nuclear DNA (nucDNA) showed that *Ch25h*$^{-/-}$ BMDMs increased their cytosolic mtDNA, but not nucDNA, after LPS stimulation (Fig. 7C). Additionally, cholesterol treatment of BMDMs was sufficient to drive increased mtDNA but not nucDNA accumulation in the cytosol (Fig. S5C). Consistent with our observation that rapamycin blocks the SREBP2 pathway in *Ch25h*$^{-/-}$ macrophages, we found that rapamycin could also decrease mitochondrial cholesterol accumulation and cytosolic mtDNA in LPS-treated *Ch25h*$^{-/-}$ BMDMs (Fig. S5D, S5E). A number of recent studies have demonstrated that cytosolic release of mtDNA can activate the cGAS/STING DNA sensing pathway that triggers the production of type I

IFNs (Rongvaux et al., 2014; West et al., 2015; White et al., 2014; Aguirre et al, 2017; Sun et al., 2017). Therefore we asked whether cholesterol treatment of BMDMs would show evidence of type I IFN induction. However, under the LPS stimulation conditions required for our inflammasome studies there is a large amount of TLR4-mediated IFN production and induction of interferon-stimulated genes (ISGs) (Fig. S5F), and we were unable to detect increased ISG expression with LPS plus MCD-chol stimulation (Supp. Fig. S5F).

The release of mtDNA into the cytosol of *Ch25h*$^{-/-}$ macrophages would theoretically require an increase in mitochondrial membrane permeability. To test this more directly, we assessed whether *Ch25h*$^{-/-}$ macrophages had increased cytochrome C (cyt C), a protein normally sequestered between the mitochondrial inner and outer membrane, in the cytosol (Campos et al., 2006). Intracellular staining for cyt C in non-digitonin treated cells detected both cytosolic and mitochondrial cyt C. This signal was then compared to that for cells that were digitonin-treated, causing cytosolic cyt C to leak out, prior to intracellular staining. We found that LPS treated, *Ch25h*$^{-/-}$ cells showed a preferential loss of cyt C after digitonin treatment compared to *Ch25h*$^{+/-}$ cells (Fig. 7D).

To functionally link increased cytosolic mtDNA accumulation with inflammasome activation, we used two approaches to deplete mtDNA from BMDMs. Ethidium bromide (EtBr) is a DNA intercalating agent that has been used in a number of studies to deplete mtDNA (Rongvaux et al., 2014; Shimada et al., 2012; Zhong et al., 2016). 2'-3'-dideoxycytidiine (ddC) is an antiviral nucleoside analogue that has selectivity for the mtDNA polymerase (Chen and Cheng, 1989; Rongvaux et al., 2014). We cultured

mature BMDMs for 7 days in the presence of either EtBr or ddC; both conditions resulted in an approximately 66% loss of cellular mtDNA (Fig. 7E). Strikingly, after stimulating these cells with LPS alone, LPS plus MCD-chol, or LPS plus ATP we found that mtDNA depletion selectively reduced IL-1β release in response to cholesterol but not ATP treatment (Fig. 7F). These results suggest that dysregulated cholesterol metabolism results in mitochondrial damage, leading to mtDNA-dependent AIM2 inflammasome activation.

To directly test whether Ch25h-deficiency leads to AIM2-dependent inflammasome activation, we generated *Ch25h*$^{-/-}$*Aim2*$^{-/-}$ mice. BMDMs from these mice and their matched controls were stimulated with LPS and supernatants tested for IL-17A induction in the IL-1β bioassay. *Ch25h*$^{-/-}$ cells showed increased IL-1β bioactivity as expected (Fig. 7G). However, deletion of AIM2 in the setting of Ch25h-deficiency reduced the IL-1β bioactivity back to Ch25h-sufficient levels (Fig. 7G).

As a second test of whether increased inflammasome activity in *Ch25h*$^{-/-}$ macrophages required AIM2, we stimulated BMDMs with LPS+ATP, a classic NLRP3 activator, and measured IL-1β by ELISA. We again observed increased IL-1β production in *Ch25h*$^{-/-}$ macrophages compared to *Ch25h*$^{+/-}$ cells (Fig. 7H). Importantly, deletion of AIM2 in the setting of Ch25h-deficiency resulted in diminished IL-1β production whereas AIM2-deficiency did not alter the response of Ch25h-sufficient cells (Fig. 7H). These results suggest that Ch25h deficiency creates a partial switch in the inflammasome sensor requirement for responses to ATP. We additionally tested the inflammasome response of these cells to FlaTOX, an NLRC4 activator, and poly(dA:dT), an AIM2-activator. With FlaTOX treatment, Ch25h/AIM2 double-deficiency again rescued the

overproduction of IL-1β observed in *Ch25h*$^{-/-}$ macrophages (Fig. S5G), whereas the response to poly(dA:dT) was abrogated in the setting of AIM2-deficiency regardless of the genetic status of Ch25h, as was expected (Fig. S5H).

We next tested whether the enhanced protection from *Listeria* infection observed in *Ch25h*$^{-/-}$ macrophages (Fig. 1C) required AIM2. *Listeria* engages multiple inflammasome pathways (NLPR3, AIM2, NLRC4) (Wu et al., 2010) and in accord with this knowledge, AIM2 deficiency led to increased *Listeria* growth (Fig. 7I). Importantly, however, in contrast to the protective effect of Ch25h loss from *Aim2*$^{+/+}$ macrophages, Ch25h-deficiency did not lead to a significant protection of *Aim2*$^{-/-}$ macrophages (Fig. 7I). These findings provide evidence in the context of a bacterial infection that Ch25h restricts AIM2-inflammasome activation.

Caspase-1 activation has been suggested to cause mitochondrial damage under some conditions (Yu et al., 2014). To test whether caspase-1 activity was required for AIM2 inflammasome activation in the setting of Ch25h-deficiency we stimulated BMDMs with LPS and treated with FLICA to irreversibly inhibit caspase-1. By binding to the caspase-1 active site, FLICA also allows detection of inflammasome specks. Consistent with our observations that IL-1β production in response to LPS without 'signal 2' is below the limit of detection of ELISA, speck formation was rare in this condition. However, speck formation was increased in *Ch25h*$^{-/-}$ BMDMs, and this effect was rescued by AIM2 double-deficiency (Fig. S5I). These data suggest that caspase-1 activity is not required for AIM2 inflammasome formation in the setting of Ch25h-deficiency.

Finally, to determine whether AIM2 is required for the overproduction of IL-1β from Ch25h-deficient hematopoietic cells in vivo, lethally irradiated wild-type mice were reconstituted with *Ch25h*$^{+/-}$, *Ch25h*$^{-/-}$, *Ch25h*$^{+/-}$*Aim2*$^{-/-}$, or *Ch25h*$^{-/-}$*Aim2*$^{-/-}$ BM. Following reconstitution the mice were injected intravenously with saline or LPS for 8 hours and then serum was harvested for cytokine analysis. Consistent with our previous results, we saw increased serum IL-1β in LPS-challenged *Ch25h*$^{-/-}$ BM chimeras (Reboldi et al, 2014) (Fig. 7I). In keeping with our in vitro observations, we found that *Ch25h*$^{-/-}$*Aim2*$^{-/-}$ BM chimeras had diminished serum IL-1β levels that were similar to Ch25h-sufficient levels (Fig. 7I). Collectively, these data suggest that Ch25h deficiency results in altered nucleic acid compartmentalization that triggers inflammation via AIM2.

Discussion

In this study, we identify a metabolic circuit that is crucial for limiting inflammasome activity in activated macrophages. We show that induction of Ch25h by type I IFN plays a key role in maintaining suppression of the SREBP2 pathway and cholesterol biosynthesis in the context of bacterial infection and LPS exposure. These observations are consistent with a number of recent studies that have demonstrated the ability of type I IFNs to repress cholesterol metabolism (Robertson et al., 2016)(York et al, 2015). However, our study suggests that Ch25h is not required to initiate suppression of sterol biosynthesis, but is instead required to maintain this effect over time. Consistent with work suggesting that mTORC1 signaling can drive SREBP2 activation (Düvel et al., 2010; Porstmann et al., 2008; Wang et al., 2011), we find that the overexpression of cholesterol biosynthesis enzymes in Ch25h-deficient cells is rapamycin-sensitive. Both TCR-activated T cells and LPS-activated macrophages switch to aerobic glycolysis and engage mTORC1 signaling due to the mutual requirement of both cell types to massively increase protein synthesis capacity (Powell et al., 2012). However, activated T cells undergo many rounds of proliferation and thus are constantly using cholesterol to synthesize new cellular membranes, whereas macrophages are largely quiescent and therefore susceptible to mTORC1-driven cholesterol over-accumulation. We speculate that the acute induction of Ch25h in macrophages allows them to selectively utilize the protein synthesis arm of mTORC1 signaling to produce cytokines and other important anti-microbial factors, while preventing cholesterol buildup and cellular pathology.

Inflammasome sensor proteins are positioned in the cytosol and this allows them to distinguish highly pathogenic bacteria from commensals due to the propensity of pathogens to break out of the phagosome. Because mitochondria are derived from endosymbiotic bacteria, they contain a number of potential danger-associated molecular patterns (DAMPs) that could be released into the cytosol to trigger inflammation. Cholesterol levels in mitochondria are about 40-fold lower than in the plasma membrane and these organelles are highly sensitive to cellular cholesterol alterations (Bosch et al., 2011; Marí et al., 2006; Martin et al., 2016). We rationalize that Ch25h upregulation upon extracellular TLR-based bacterial sensing helps prevent cholesterol-dependent mitochondrial damage and release of endogenous DAMPS into the cytosol. In the absence of this pathway, cholesterol-mediated membrane damage can lead to increases in cytosolic DNA, resulting in engagement of the AIM2 inflammasome and exaggerated IL-1β production.

It is notable that Ch25h-deficiency augments the response to multiple types of inflammasome activators. This could in principle be due to a general antagonistic effect of 25-HC on inflammasome assembly. However, we find that this augmented inflammasome activity is reversed in the setting of AIM2 deletion, suggesting that the broad overproduction of IL-1β is due to ectopic AIM2 activation. This may indicate that the altered metabolic state occurring in the absence of Ch25h makes cells poised to engage AIM2 inflammasomes. With further mitochondrial stress resulting from infection or potentially dietary lipid overload, sufficient mtDNA may become released to engage the AIM2 inflammasome. While our data establish a temporal requirement for Ch25h to restrain IL-1β production by TLR-activated macrophages, Ch25h expression is not

preventing IL-1β production. Rather, we suggest that by maintaining the metabolic health of the cell, Ch25h and 25-HC are helping to ensure that macrophages make a beneficial and not pathological amount of IL-1β while also being able to perform other functions. While we have mostly tested this circuit in the context of TLR agonists or bacterial infection, Ch25h may also be important in controlling IL-1β production during metabolic inflammation, where it would be critical to keep cytokine concentrations below a pathologic threshold.

Beyond repressing cholesterol biosynthesis through SREBP2, our data suggest that 25-HC can counter mitotoxic effects of cholesterol accumulation, based on the capacity of Ch25h overexpression to block IL-1β release in response to exogenous cholesterol. The LXR family members were intriguing candidates for this effect, since they promote cholesterol efflux through upregulation of ABCA1 and ABCG1, and tentative evidence suggests that 25-HC does have some ligand activity for these nuclear hormone receptors (Cyster et al., 2014). However, Ch25h retained its capacity to blunt cholesterol-dependent effects when expressed in LXRα/β double knockout macrophages. We speculate that this activity of Ch25h may instead be related to the capacity of 25-HC to act as an allosteric activator of ACAT1, an enzyme that esterifies cholesterol to allow storage in lipid droplets (Metherall et al., 1991). However, there is at present no genetic evidence that ACAT1 activity is affected by endogenously produced 25-HC. Future work will be needed to examine effects of 25-HC on cholesterol esterification in activated macrophages. Alternatively, it is possible that 25-HC itself has intrinsic mitochondrial protective functions that counter cholesterol. It will be of interest

in future studies to determine whether 25-HC accumulates in mitochondrial membranes during conditions of bacterial sensing.

AIM2 is a well-described sensor of cytosolic DNA that can trigger inflammasome activation (Rathinam and Fitzgerald, 2016). Activation of this sensing pathway is usually described in the context of pathogen-derived nucleic acids that enter the host cell cytosol (Rathinam and Fitzgerald, 2016). However, the AIM2 HIN-200 domain is not sequence-specific, and therefore host DNA represents a potential pool of ligand if the nucleic acid is de-compartmentalized. Cytosolic release of mtDNA can trigger the cGAS-dependent DNA sensing pathway in the context of caspase-3/7- and TFAM-deficiency (Rongvaux et al., 2014; West et al., 2015; White et al., 2014) and in dengue virus infected cells (Aguirre et al, 2017; Sun et al., 2017), but there are few examples of AIM2 activation by mtDNA. A number of studies have suggested that oxidized mtDNA can act as a ligand for NLRP3 (Nakahira et al., 2011; Shimada et al., 2012), which is consistent with our findings that NLRP3 redundantly contributes to cholesterol-dependent IL-1β production. Interestingly, the cited studies had to use AIM2-deficient macrophages to reveal NLRP3-dependent effects in response to transfected mtDNA; but to our knowledge there are no prior examples of endogenous mtDNA release triggering AIM2. It remains an open question as to how exactly cholesterol buildup leads to cytosolic mtDNA release in macrophages. It would be of interest to determine whether this process involves Bax/Bak-mediated membrane permeabilization, as there is conflicting evidence on whether cholesterol promotes or antagonizes Bax oligomerization and pore formation (Christenson et al., 2008; Montero et al., 2010). Cholesterol-induced reduced membrane fluidity and increased oxidative stress might

also lead to other forms of mitochondrial membrane damage (Kennedy et al., 2014; Martin et al., 2016). Given the complexities associated with determining the exact nucleic acid sources that trigger cytosolic DNA sensor proteins, and the large size of the nuclear genome, our studies do not exclude the possibility that increased cholesterol content of intracellular membranes causes cytosolic accumulation of nuclear DNA as an additional AIM2 ligand.

Finally, while we believe Ch25h upregulation by type I IFN represents a physiological circuit that prevents mtDNA from engaging AIM2, these observations raise additional questions about the role of cholesterol in driving inflammation in chronic diseases like obesity and metabolic syndrome. A number of studies have implicated inflammatory cytokines like TNF and IL-1β in promoting insulin resistance in high-fat diet (HFD) conditions (de Luca and Olefsky, 2008). Additionally, inflammasomes have been suggested to play a causal role in metabolic inflammation (Stienstra et al., 2011; Vandanmagsar et al., 2011). However, the exact mechanisms underlying lipid-driven inflammation are still unclear. Ceramide accumulation has been argued to engage the NLRP3 inflammasome during HFD (Vandanmagsar et al., 2011), but little is known about the role of cholesterol-driven inflammation in obesity, despite the fact that LDL and HDL levels have been used as risk factors for atherosclerosis for decades. A limited number of reports have noted a connection between cholesterol-dependent mitochondrial dysfunction under high fat conditions and development of metabolic diseases (Martin et al., 2016). While it is recognized that cholesterol levels in cells are tightly controlled and not readily altered by changes in dietary cholesterol, it will be of interest to determine whether Ch25h-deficient mice have exacerbated mitochondrial

dysfunction and inflammation in response to HFD, and whether AIM2 deficiency blunts the inflammatory effects of HFD.

In conclusion, the studies described herein provide mechanistic insight into how regulation of macrophage cholesterol homeostasis during pathogen sensing integrates with inflammasome regulation, and they advance our understanding of how cellular cholesterol can act as an inflammatory driver.

Experimental procedures

Mice

CD45.1 congenic C57BL/6 (B6) male and female mice, 6-12 weeks old were from National Cancer Institute. *Ch25h*$^{-/-}$ mice were backcrossed onto C57BL/6J for 10 generations. *Nr1h2*$^{-/-}$, *Nr1h3*$^{-/-}$, *Nlrc4*$^{-/-}$, *Aim2*$^{-/-}$, *Casp11*$^{-/-}$, *Casp1/11*$^{-/-}$, *Asc*$^{-/-}$ and *Ifnar1*$^{-/-}$ mice have all been previously described. Animals were housed in a specific pathogen-free environment in the Laboratory Animal Research Center at UCSF and all experiments conformed to the ethical principles and guidelines approved by the UCSF Institutional and Animal Care and Use Committee.

Cells

Bone marrow cells were grown in DMEM with 10% FBS and 10% M-CSF media in bacterial petri dishes for 6 days, then plated at $1x10^6$ cells/ml and left to adhere overnight. BMDMs were stimulated with 100ng/ml LPS (*E. coli* 0111:B4; Sigma) for the indicated times. For ELISA detection of IL-1β in response to MCD-Chol (Sigma), BMDMs were primed with 100ng/ml LPS for 4 hours, and then MCD-Chol (100ug/ml unless indicated) was added for the final 4 hours of culture. For other inflammasome activation experiments, ATP (Sigma) was added for the final 45 minutes of culture at a concentration of 5mM, alum (400mg/ml; Pierce) and poly(dA:dT) (1ug/ml; Invivogen) was added for the final 4 hours of culture, and FlaTox (1:100 dilution) was added for the final 45 minutes of culture. For two sets of experiments, rapamycin (20nM) or cytochalasin D (2uM; Sigma) was also added for the final 4 hours of culture.

Bone marrow chimeras

CD45.1 congenic mice were lethally irradiated with 1,100 rad in split doses 3 hours apart, and reconstituted with 1-3 x 10^6 BM cells per mouse from wild type, *Aim2*$^{-/-}$, *Nlrp3*$^{-/-}$, or *Casp1/11*$^{-/-}$, *Ch25h*$^{+/-}$, *Ch25h*$^{-/-}$, *Ch25h*$^{+/-}$*Aim2*$^{-/-}$, or *Ch25h*$^{-/-}$*Aim2*$^{-/-}$ mice. Mice were analyzed 8-10 weeks later.

BMDM transduction

BM cells were cultured in DMEM with 10% FBS and 10% M-CSF conditioned medium for 2 days, then spinfected for 2 hours on days 2 and 3 with retroviruses expressing Ch25h, Ch25hmut, Hmgcr, Dhcr24, or control and an IRES-thy1.1 cassette as a reporter. Cells were then plated at 1x10^6 cells/ml and left to adhere overnight on day 6. Cells were always cultured in 10% M-CSF conditioned medium.

***Listeria monocytogenes* infection of BMDMs**

L. monocytogenes single colonies were incubated in brain heart infusion (BHI) broth overnight at 30^{o}C without shaking. Cultures were then diluted 1:10 in BHI broth and incubated at 37^{o}C with shaking. When cultures were in log-phase growth, bacteria were added to BMDMs seeded on TC-treated plates at a multiplicity of infection (MOI) of 10 to 1. After 30 minutes infected cells were washed, and media containing gentamicin (50ug/ml) was added. For CFU determination, cells were lysed in cold ddH_2O and lysates were streaked onto BHI agar plates.

Flow cytometry

Cells were stained with Abs to CD4 (RM4-5), TCRβ (H57-597), IL-17A (17B7), CD11b (M1/70), or Ly6G (1A8). For mitochondrial studies, cells were treated as indicated and then stained with 30 minutes with Mitotracker Deep Red (100nM), Mitotracker Green (100nM), TMRM (100nM) or MitoSOX (2.5 uM) at 37^{o}C. All mitochondrial staining reagents were from Life Technologies. For intracellular cytochrome C staining, cells were stimulated as indicated and then treated on ice with either control or digitonin (25 ug/ml) for 10 minutes. Cells were then treated with BM Cytofix Buffer and Perm/Wash reagent (BD Biosciences), and stained with anti-cytochrome C (6H2.B4). Antibodies were purchased from BD Biosciences or eBiosciences.

IL-1β T cell bioassay

Peripheral lymph nodes (LNs) and spleens from wild type mice were harvested and mashed through a 70 micron strainer. CD4+ T cells were enriched by positive selection using CD4+ MACS beads (Miltenyi). T cells (5 x 10^5) were then cultured for 4 days in 24-well plates with plate-bound anti-CD3 (2 ug/mL), soluble anti-CD28 (1 ug/mL), and recombinant TGF-β (2 ng/mL) and the indicated BMDM supernatants. On day 4, T cells were stimulated with PMA/iononmycin and brefeldin A (BD Biosciences) for 4 hrs. Cells were stained with fixable viability dye (eFluor780; eBiosciences) to exclude dead cells, surface stained with Abs to CD4 (RM4-5) and TCRβ (H57-597), treated with BM Cytofix Buffer and Perm/Wash reagent (BD Biosciences), and stained with anti-IL-17A (17B7). Antibodies were purchased from BD Biosciences or eBiosciences.

Cytokine enzyme-linked immunosorbent assays

Supernatants from cultured BMDMs and serum from LPS-injected mice were collected from the indicated conditions and times points. Unconjugated anti-IL-1β (B122; Biolegend) (2ug/ml) was coated onto 96-well high binding plates and then plates were washed and blocked for 1 hour with PBS containing 5% FBS. Supernatants were added to the plates O/N at 4^{o}C. Plates were washed again and biotinylated anti-IL-1β (polyclonal; eBiosciences) (1ug/ml) was added for 1-2 hours at RT. Biotinylated detection antibodies were then labeled by streptavidin-conjugated horseradish peroxidase (HRP) and visualized by addition of Substrate Reagent Pack (R&D). Color development was stopped by addition of 2N H_2SO_4. Recombinant IL-1β (eBiosciences) was used as a standard. Absorbance at 450 nm was measured on a tunable microplate reader (VersaMax, Molecular Devices). Cytokine supernatant concentrations were calculated by extrapolating absorbance values from standard curves where known concentrations were plotted against absorbance using SoftMax Pro 5 software.

In vivo peritonitis

For neutrophil recruitment into the peritoneum, mice were injected I.P. with saline containing either LPS (10ug), LPS(10ug)+MCD-Chol(100ug), or LPS+Alum(400ug). 8-10 hours after injection, mice were sacrificed, peritoneal cavities were lavaged using 5 ml of PBS with 1% FBS and 1mM HEPES, and peritoneal cells were analyzed using FACS. For mitochondrial cholesterol measurements and Mitotracker staining on peritoneal macrophages, mice were injected I.P. with saline or LPS (2mg/kg) for 8 hours.

Quantification of sterols

BMDMs were treated as indicated, sterols were extracted with organic solvents, and quantitated using a SCIEX API 5000 mass spectrometer coupled to a Shimadzu LC-20XR high performance liquid chromatograph as previously described(McDonald et al., 2012).

RNA isolation and Real-time RT-PCR

Total RNA was isolated from $5x10^5$ BMDMs treated as indicated with the Trizol reagent (Life Technology) following the manufacturer's protocol. Real-time PCR was performed using SYBR Green PCR Mix (Roche) and an ABI Prism 7300 sequence detection system (Applied Biosystems, Foster City, CA). *Hprt* levels were used as internal controls. Primer sequences are available upon request.

Seahorse analysis of mitochondrial respiration

For real-time analysis of oxygen consumption rate (OCR) and extracellular acidification rate (ECAR), BMDMs were analyzed with an XF-24 Extracellular Flux Analyzer (Seahorse Bioscience). $2x10^5$ BMDMs were plated in Seahorse 24-well plates and the Seahorse XF Cell Mitochondria Stress assay was performed per manufacturer's instructions. Oligomycin was added at 1uM, FCCP at 1uM, and Rotenone/Antimycin A at 0.5uM each (Seahorse Biosciences).

293T inflammasome reconstitution

$1.5x10^5$ 293T cells were seeded in 24-well plates O/N in DMEM with 10% FBS and antibiotics. The next day, cells were switched to antibiotic-free DMEM with 10% FBS and transfected using Lipofectamine 2000 (Life Technologies) with the indicated plasmids (all 50ng). 24 hours later, cells were stimulated with nigericin (15uM; Sigma) for 45 minutes. Supernatants were then collected, and cells were lysed in RIPA buffer (25mM Tris-HCl pH 7.5, 150mM NaCl, 0.1% SDS, 0.5% sodium deoxycholate, 1% Triton X-100). Western blots were performed with rabbit polyconal anti-caspase-1 p10 (M-20, Santa Cruz), mouse monoclonal anti-NLRP3 (Cryo-2, Adipogen), rabbit polyclonal anti-ASC (AL177, Adipogen), and goat anti-IL-1β (polyclonal; R&D).

Cytosolic and total DNA extraction

$2x10^6$ BMDMs per well seeded in 6-well plates were stimulated as indicated, washed with ice cold PBS, and scraped off the plates. Cells were then pelleted in a table top centrifuge by spinning at 800g for 5 minutes at 4^oC. Cell pellets were resuspended in 500ul of cytosolic extraction buffer (150mM NaCl, 50mM HEPES pH 7.4, 25 ug/ml digitonin) and rotated for 10 minutes at 4^oC. Cells were then centrifuged at 800g for 3 minutes. Supernatants were collected and centrifuged at 800g for 3 minutes twice more, followed by a 5 minute centrifugation at 10,000g. DNA was then extracted from the cell pellets and cytosolic fraction using a QIAamp DNA Micro Kit (Qiagen). DNA was quantified using qPCR with mtDNA (*D loop)* and nucDNA (*Tert)* primers; cytosolic DNA signals were normalized to cell pellet DNA signals. Primer sequence are available upon request.

Mitochondrial DNA depletion

BMDMs were grown as described above. On day 6, media was replaced with DMEM containing 10% FBS and 10% M-CSF conditioned media containing either ethidium bromide (100ng/ml) or 2',3'-dideoxycytidine (40ug/ml). After 5-7 days, BMDMs were detached and mitochondrial DNA depletion was assessed by total DNA extraction followed by qPCR for mtDNA and nucDNA as described above.

Amplex Red Cholesterol Quantification

For total cholesterol content, BMDMs were seeded in 6-well plates at $2x10^6$ cells per well and stimulated as described. Peritoneal macrophages were sorted using a FACS Aria II (BD Biosciences). Cells were then lysed in 500 ul RIPA buffer. Cholesterol quantification was then performed using the Amplex Red Cholesterol Assay (Life Technologies) per manufacturer's instructions and readout on a Qubit 3.0 Fluorometer (Life Technologies). For mitochondrial cholesterol content, BMDMs were seeded in 10cm dishes at $1x10^7$ cells per dish and treated as indicated. Mitochondria were then isolated using anti-TOM22 MACS beads with the Mouse Mitochondria Isolation Kit (Miltenyi Biotec) per manufacturer's instructions. Isolated mitochondria were then lysed in 200ul RIPA buffer. Amplex Red fluorescent concentrations were normalized based on total protein content using the BCA Protein Assay Kit (Pierce).

Confocal microscopy

BMDMs ($1x10^5$) were seeded on round glass coverslips in 24-well plates overnight and then stimulated with LPS for 8 hours along with 150X FLICA reagent (ImmunoChemistry

Technologies). Cells were then fixed with 1% PFA for 20min at 37^{o}C and washed 3x with 1X PBS and stained with DAPI. Images were then taken on a Leica SP5 laser-scanning confocal microscope using a 63X oil immersion lense.

Acknowledgements

We thank Jinping An and Ying Xu for expert technical assistance, Averil Ma for *Casp1/11*$^{-/-}$*, Asc*$^{-/-}$*, and Nlrp3*$^{-/-}$ bone marrow, Tony DeFranco for *Nlrc4*$^{-/-}$ bone marrow, Kate Fitzgerald for *Nlrp3*$^{-/-}$*Aim2*$^{-/-}$ bone marrow, Russell Vance for FlaTox, Christophe Paillart for help with Seahorse setup, and Jeffrey Cox, Richard Locksley, Andrea Reboldi and Jiaxi Wu for helpful discussions. EVD is supported by NIH F30 grant F30AI120527 and the UCSF Medical Scientist Training Program (MSTP) and JGC is an Investigator of the Howard Hughes Medical Institute. This work was supported in part by NIH grant AI040098 (to JGC) and grant HL20948 (to JGM and DWR).

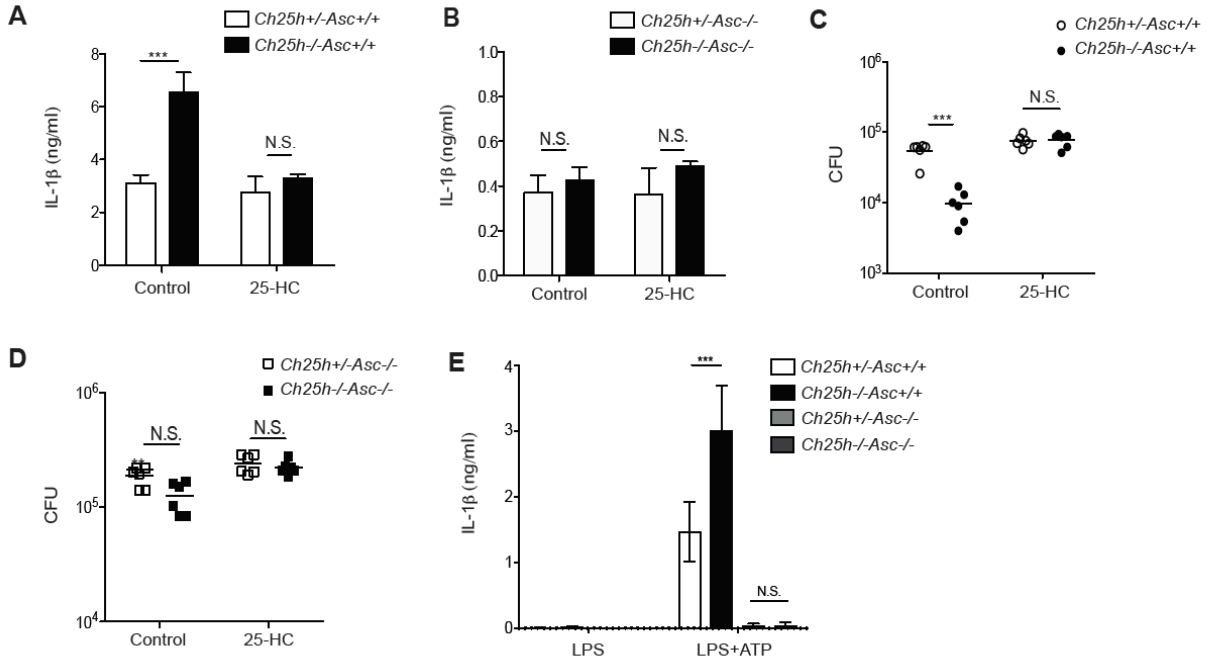

Figure 1. Increased IL-1β production and control of *L. monocytogenes* intracellular growth in *Ch25h*$^{-/-}$ macrophages involves ASC-dependent inflammasome activation.

IL-1β enzyme-linked immunosorbent assay (ELISA) from supernatants (A, B) and bacterial colony forming units (CFU) from cell lysates (C, D) of control (EtOH) or 25-HC (1uM) treated *Ch25h*$^{+/-}$*Asc*$^{+/+}$ and *Ch25h*$^{-/-}$*Asc*$^{+/+}$ (A, C) or *Ch25h*$^{+/-}$*Asc*$^{-/-}$ and *Ch25h*$^{-/-}$ *Asc*$^{-/-}$ (B, D) BMDMs after 24 hours of *L. monocytogenes* infection (M.O.I. 10:1). (E) IL-1β ELISA from supernatants of LPS and LPS+ATP stimulated BMDMs of the indicated genotypes. (n = 3 per genotype, means +/- SD). *P<0.05, **P<0.01, ***P < 0.005 (unpaired Students *t* test). See also related Supplementary Figure 1.

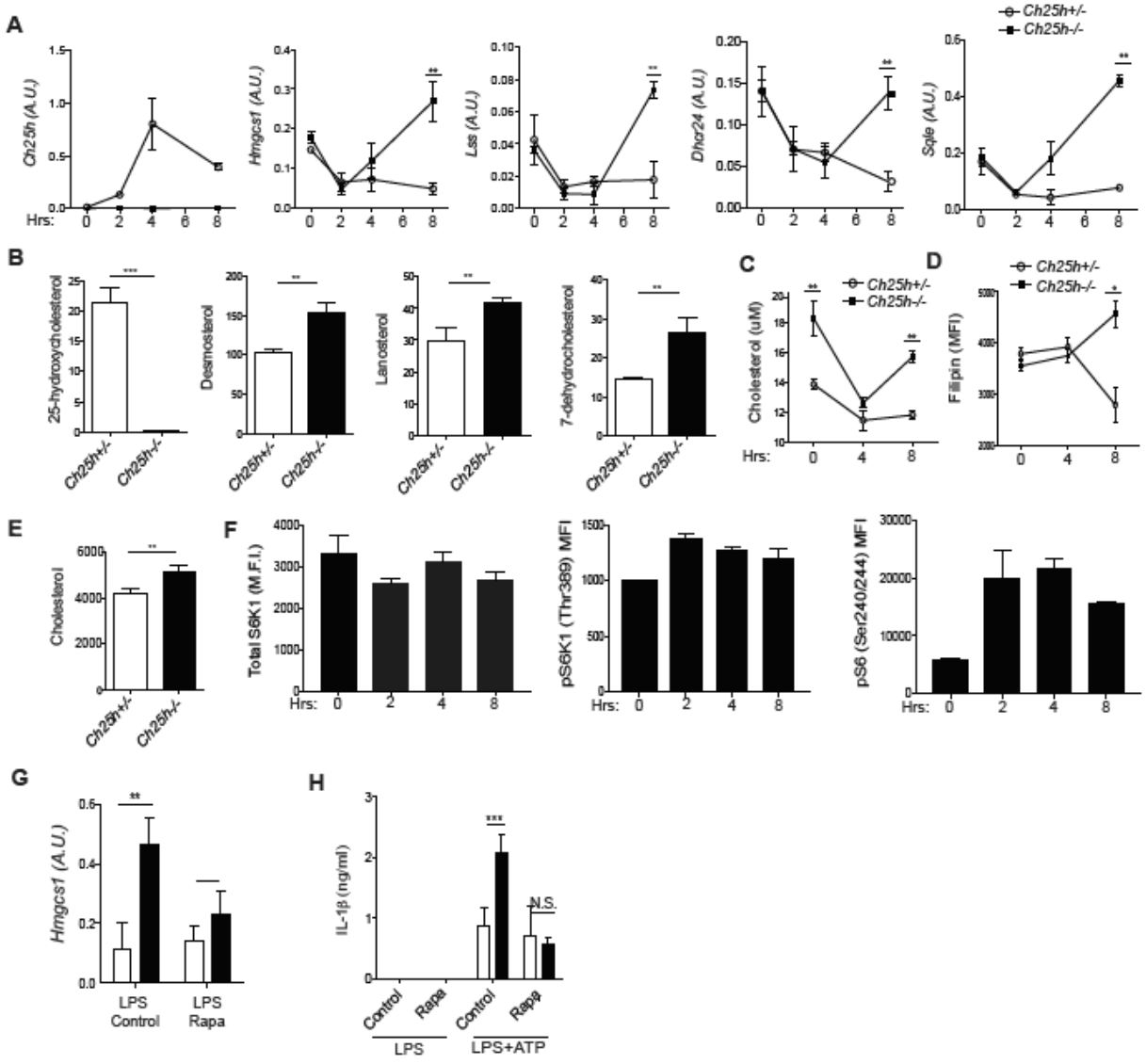

Figure 2. Ch25h induction prevents cholesterol buildup in macrophages by enforcing repression of mTORC1-dependent SREBP activity.

(A) RT-qPCR analysis of *Ch25h*, *Hmgcs1*, *Lss*, *Dhcr24*, and *Sqle* in *Ch25h*$^{+/-}$ *and* *Ch25h*$^{-/-}$ BMDMs stimulated with LPS. Data are standardized by comparison to *Hprt*, and A.U. indicates arbitrary unit (means +/- SD from 4 independent experiments).

(B) LC-MS quantification of 25-HC, desmosterol, lanosterol, and 7-dehydrocholestrol in *Ch25h*$^{+/-}$ *and Ch25h*$^{-/-}$ BMDMs stimulated with LPS for 8 hrs. Data from two independent experiments (mean +/- SD).

(C) Quantification of cholesterol content by Amplex Red fluorescence in *Ch25h*$^{+/-}$ *and* *Ch25h*$^{-/-}$ BMDMs stimulated with LPS. Data from 4 independent experiments (mean +/- SD).

(D) FACS-based readout of cholesterol content by Filipin staining. Representative of three independent experiments (mean +/- SD).

(E) GC-MS quantification of cholesterol content in *Ch25h*$^{+/-}$ *and Ch25h*$^{-/-}$ BMDMs stimulated with LPS for 8 hrs (n = 3, mean +/- SD).

(F) Flow cytometry for pS6K1 (Thr389) and pS6 (S240/244) from BMDMs stimulated with LPS.
(G) RT-qPCR analysis of *Hmgcs1* expression in *Ch25h*$^{+/-}$ *and Ch25h*$^{-/-}$ BMDMs treated with LPS and DMSO or rapamycin. Data from three independent experiments (mean +/- SD).
(H) IL-1β ELISA from supernatants of *Ch25h*$^{+/-}$ *and Ch25h*$^{-/-}$ BMDMs treated with LPS and DMSO or rapamycin, and then with ATP. Data from two independent experiments (mean +/- SD). *P<0.05, **P<0.01, ***P < 0.005 (unpaired Students *t* test). See also related Supplementary Figure 1.

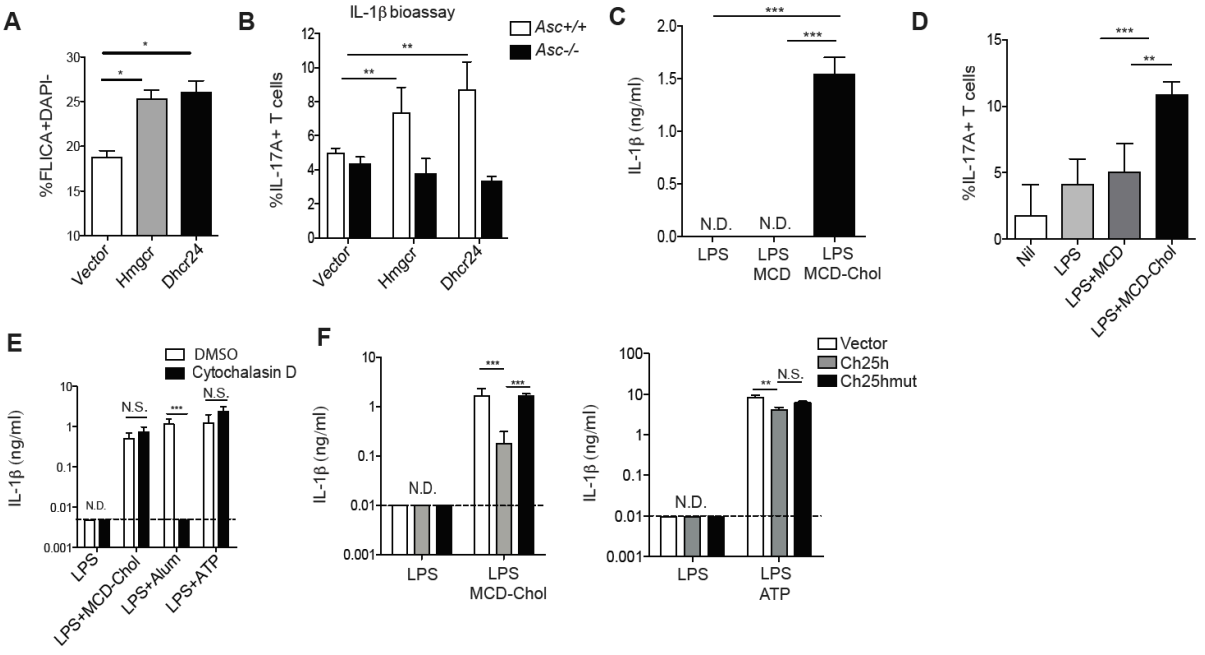

Figure 3. Increased macrophage cholesterol content promotes crystal-independent inflammasome activation.

(A) FACS analysis of FLICA staining on BMDMs transduced with either MSCV-vector, -Hmgcr, or -Dhcr24 retrovirus and stimulated with LPS for 8 hrs. Data from 3 independent experiments (mean +/- SD).

(B) IL-1β bioactivity detected as percentage of $CD4^+$ T cells producing IL-17A after culture for 4 days in supernatants from *Asc*$^{+/+}$ or *Asc*$^{-/-}$ BMDMs transduced and stimulated as in A. Graph is representative of 3 independent experiments (mean +/- SD).

(C) IL-1β ELISA of supernatants from BMDMs treated with 4 hrs with LPS+MCD-Chol. Data from 6 independent experiments (mean +/-SD).

(D) IL-1β bioactivity detected as in (B) with supernatants from BMDMs stimulated for 8 hrs with either nil, LPS, LPS+MCD (10ug/ml), or LPS+MCD-Chol (10ug/ml). Data from three independent experiments (mean+/- SD).

(E) IL-1β ELISA from supernatants of BMDMs treated with LPS, LPS+MCD-Chol, LPS+Alum or LPS+ATP and with DMSO or cytochalasin D. Data from 3 independent experiments (mean +/- SD).

(F) IL-1β ELISA of supernatants from *Ch25h*$^{-/-}$ BMDMs transduced with MSCV-vector, -Ch25h, or -Ch25hmut and stimulated with either LPS, LPS+MCD-Chol, or LPS+ATP. Data from four independent experiments (mean +/- SD).

*P<0.05, **P<0.01, ***P < 0.005 (unpaired Students *t* test or one way ANOVA with bonferroni test). See also related Supplementary Figure 2.

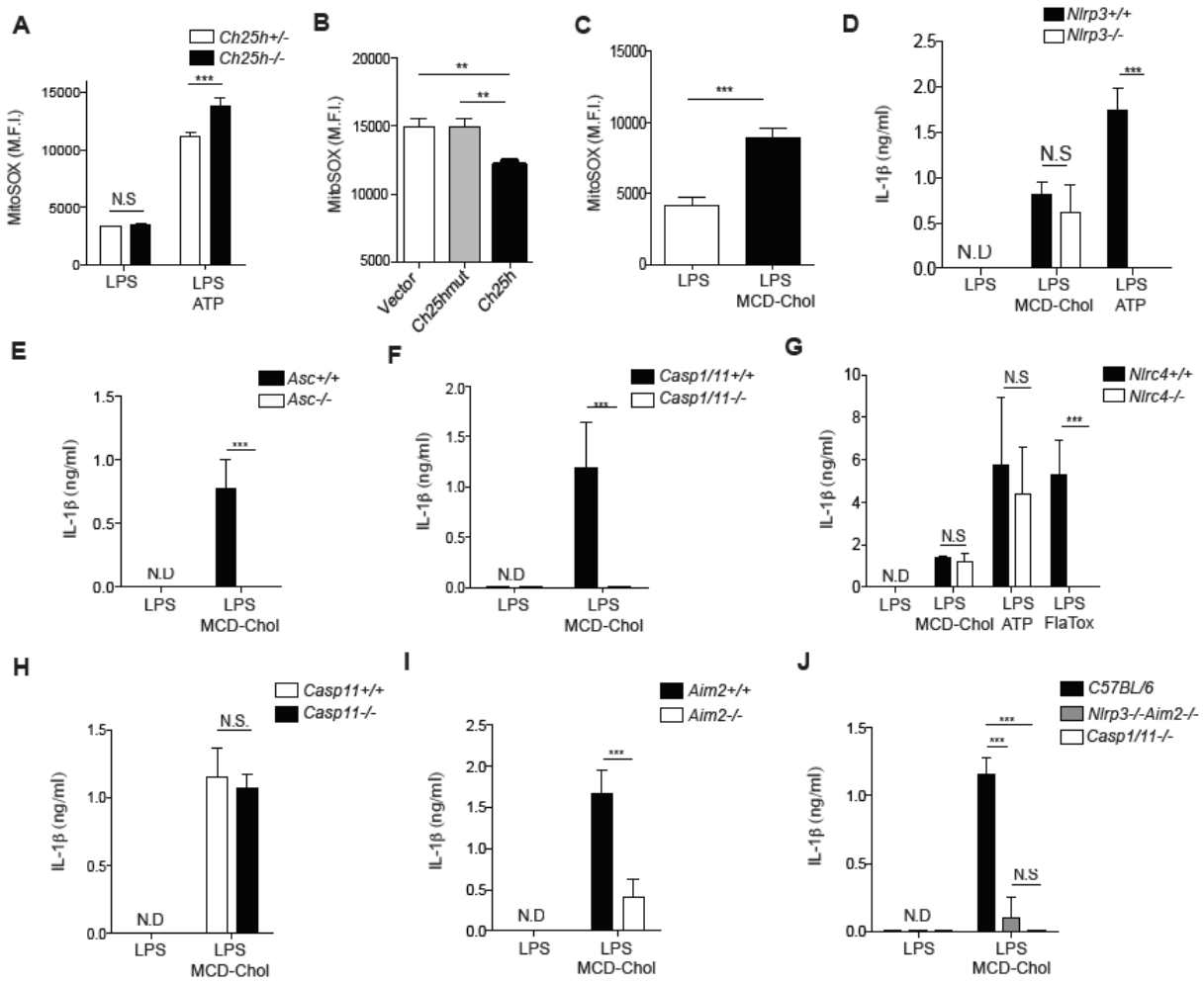

Figure 4. Cholesterol-dependent inflammasome activation requires AIM2 and redundantly involves NLRP3.

(A) Mitochondrial superoxide levels determined by MitoSOX staining of *Ch25h*$^{+/-}$ and *Ch25h*$^{-/-}$ BMDMs stimulated for 8 hrs with LPS, or LPS+ATP treatment. Data are representative of 6 independent experiments (mean +/- SD).
(B) MitoSOX staining of *Ch25h*$^{-/-}$ BMDMs transduced with MSCV-vector, -Ch25h, or -Ch25hmut and stimulated as in A. Data from 2 independent experiments (mean +/- SD).
(C) MitoSOX staining from BMDMs stimulated for with LPS or LPS+MCD-Chol. Data are representative of 3 independent experiments (mean +/- SD). (D-J) IL-1β ELISA of supernatants from *Nlrp3*$^{+/+}$ and *Nlrp3*$^{-/-}$
(D), *Asc*$^{+/+}$ and *Asc*$^{-/-}$ (E), *Casp1/11*$^{+/+}$ and *Casp1/11*$^{-/-}$ (F), *Nlrc4*$^{+/+}$ and *Nlrc4*$^{-/-}$ (G), *Casp11*$^{+/+}$ and *Casp11*$^{-/-}$ (H), *Aim2*$^{+/+}$ and *Aim2*$^{-/-}$ (I), or *Nlrp3*$^{+/+}$*Aim2*$^{+/+}$ and *Nlrp3*$^{-/-}$*Aim2*$^{-/-}$ BMDMs treated as indicated. Data from 2 to 4 experiments (mean +/- SD). *P<0.05, **P<0.01, ***P < 0.005 (unpaired Students *t* test or one way ANOVA with bonferroni test). See also related Supplementary Figure 3.

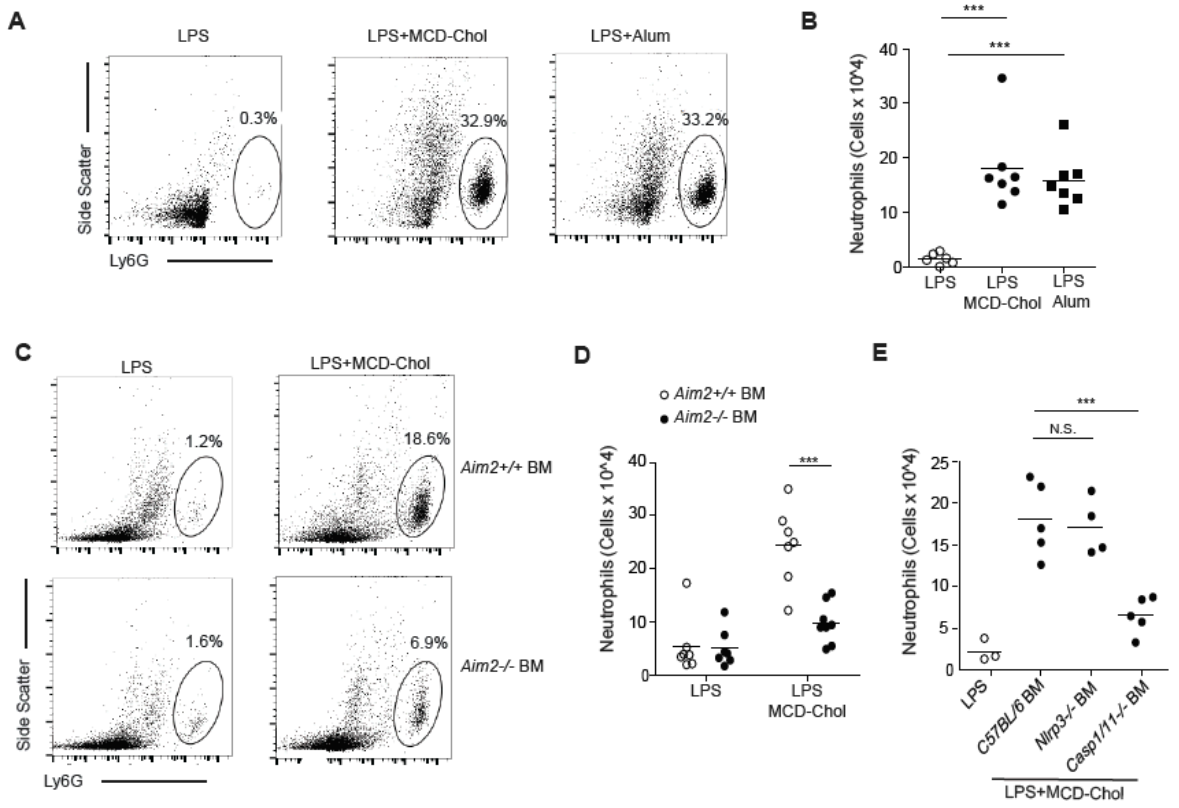

Figure 5. AIM2 is required for cholesterol-dependent neutrophilic peritonitis.
(A) Representative FACS plots of peritoneal Ly6G+ cells from mice injected I.P. 8 hrs earlier with the indicated treatments displaying percentage of Ly6G+ cells.
(B) Number of peritoneal neutrophils from mice as treated in A.
(C) Representative FACS plots of peritoneal Ly6G+ cells from LPS or LPS+MCD-Chol treated wild type *or Aim2*$^{-/-}$ BM chimeras.
(D) Number of peritoneal neutrophils from mice of the type in C treated with LPS or LPS+MCD-chol for 8 hrs.
(E) Number of peritoneal neutrophils from wild type mice irradiated and transplanted with either wild type, *Nlrp3*$^{-/-}$, or *Casp1/11*$^{-/-}$ BM, and treated as in D. Each dot represents an individual mouse and data are pooled from 3 independent experiments (mean +/- SD). *P<0.05, **P<0.01, ***P < 0.005 (unpaired Students *t* test or one way ANOVA with bonferroni test).

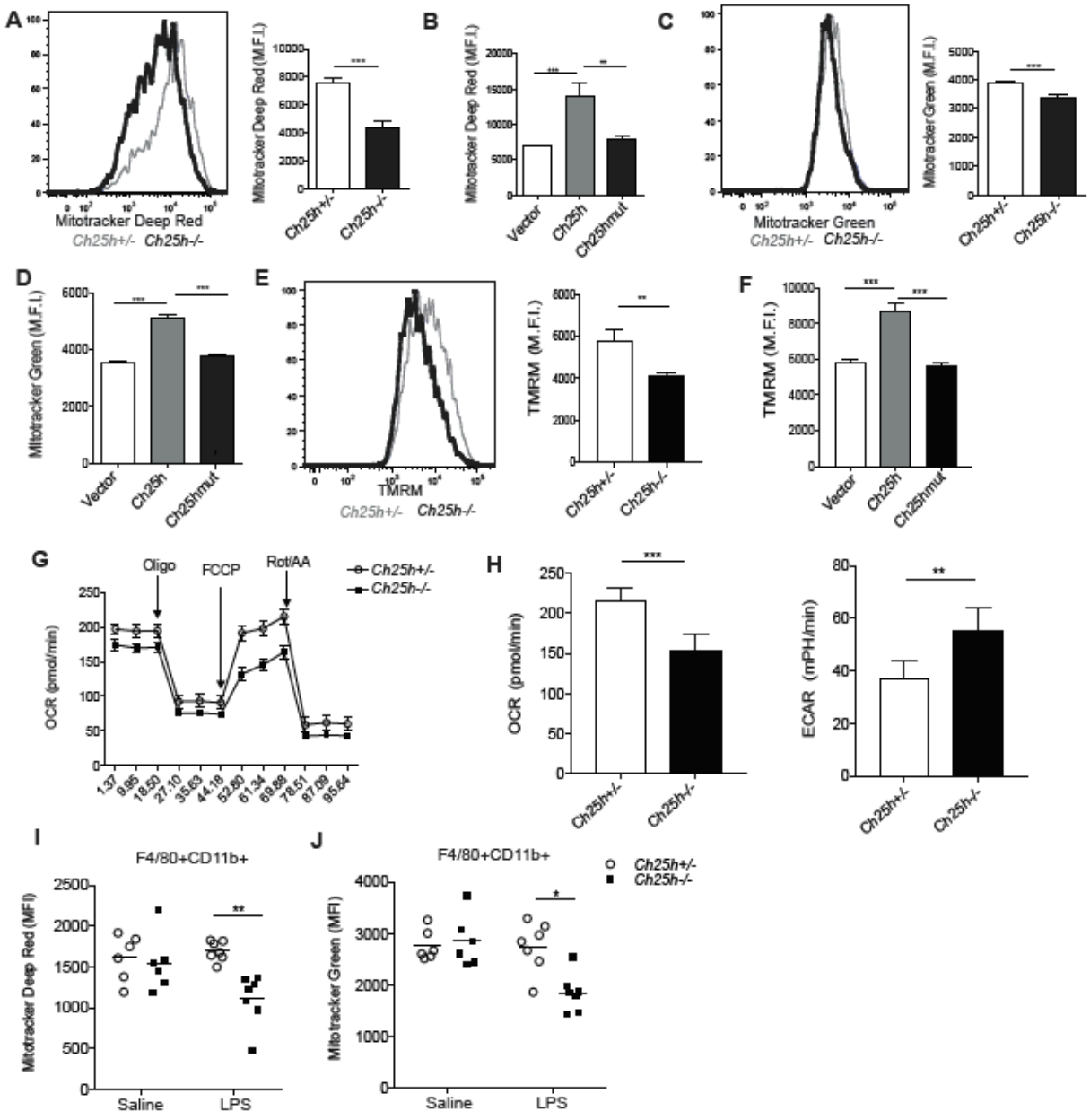

Figure 6. Ch25h-deficient and cholesterol loaded macrophages have impaired mitochondrial metabolism.

(A) (Left) Representative histogram of Mitotracker Deep Red staining on *Ch25h*$^{+/-}$ and *Ch25h*$^{-/-}$ BMDMs stimulated with LPS for 8 hrs. (Right) Summary mean fluorescence intensity (MFI) data from 3 experiments (mean +/- SD). Representative of 8-10 independent experiments.

(B) MFI of Mitotracker Deep Red staining on *Ch25h*$^{-/-}$ BMDMs transduced with MSCV-vector, -Ch25h, or -Ch25hmut. Data from 4 independent experiments (mean +/- SD).

(C) (Left) Representative histogram of Mitotracker Green staining on *Ch25h*$^{+/-}$ and *Ch25h*$^{-/-}$ BMDMs stimulated as above. (Right) Summary MFI data from 3 experiments (mean +/- SD). Representative of 8-10 independent experiments (mean +/- SD).

(D) MFI of Mitotracker Green staining on *Ch25h*$^{-/-}$ BMDMs transduced with MSCV-vector, -Ch25h, or -Ch25hmut. Data from 4 independent experiments (mean +/- SD).
(E) Representative histogram of TMRM staining on *Ch25h*$^{+/-}$ and *Ch25h*$^{-/-}$ BMDMs stimulated with LPS for 8 hrs. Graph shows summary MFI data from 3 experiments (mean +/- SD).
(F) MFI of TMRM staining on *Ch25h*$^{-/-}$ BMDMs transduced with MSCV-vector, -Ch25h, or -Ch25hmut. Data from 2 independent experiments (mean +/- SD).
(G) Seahorse analysis of oxygen consumption rate (OCR) over time from BMDMs pretreated for 8 hrs with LPS and after the indicated additional treatments. Data are representative of 3 independent experiments (mean +/- SD).
(H) Seahorse analysis of basal OCR and extracellular acidification rate (ECAR) of *Ch25h*$^{+/-}$ and *Ch25h*$^{-/-}$ BMDMs stimulated with LPS for 8 hrs. Data from 3 independent experiments (mean +/- SD).
(I, J) Mitotracker Deep Red (I) and Mitotracker Green (J) staining of *Ch25h*$^{+/-}$ and *Ch25h*$^{-/-}$ peritoneal macrophages 8 hours after I.P. saline or LPS injection. Data from 3 independent (n = 6-7 mice per group). See also related Supplementary Figure 4.

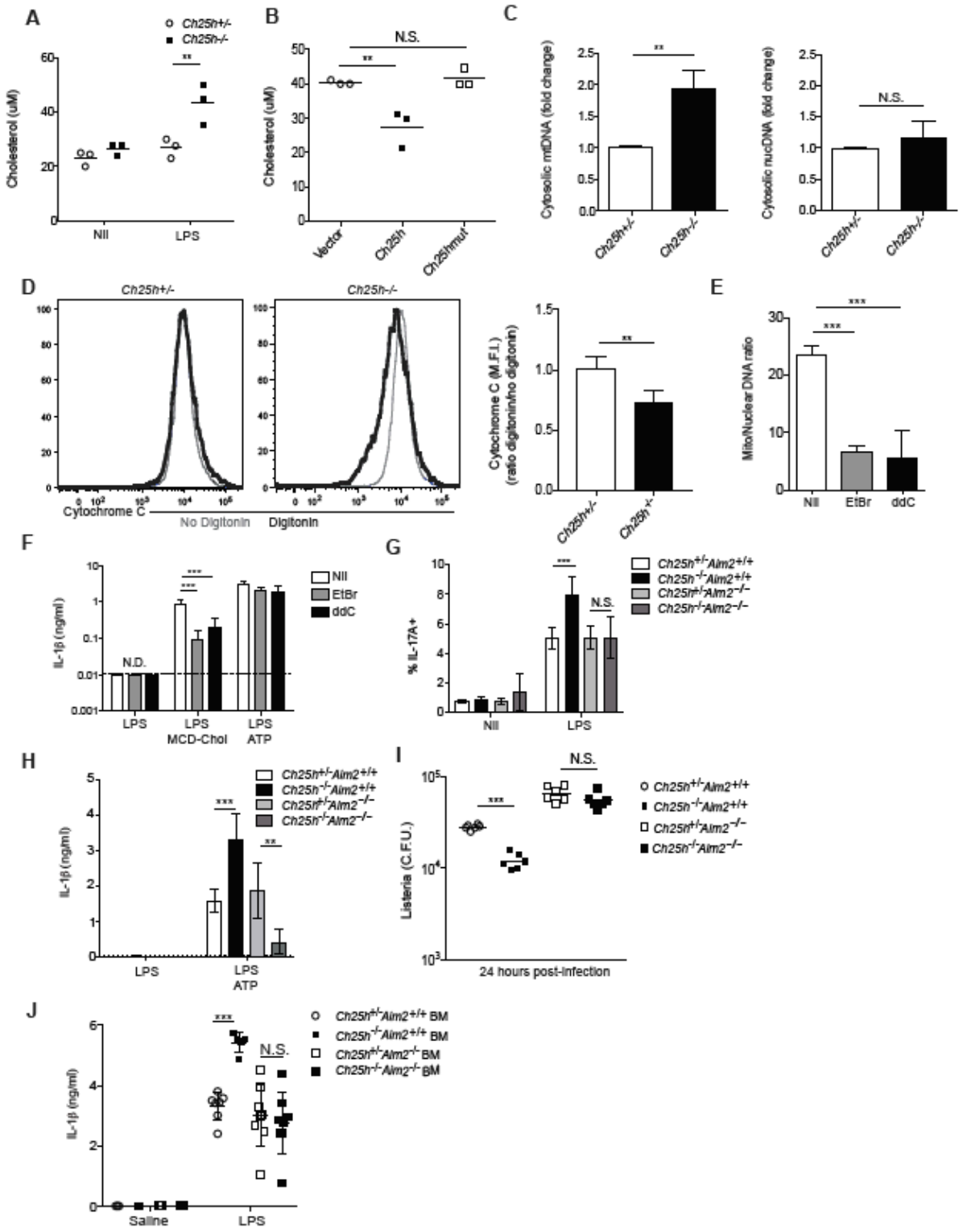

Figure 7. Cholesterol buildup in mitochondrial causes cytosolic release of mtDNA.

(A) Quantification of cholesterol in isolated mitochondria from *Ch25h*$^{+/-}$ and *Ch25h*$^{-/-}$ BMDMs either untreated or stimulated with LPS for 8 hrs. Data from 3 independent experiments (mean +/- SD).
(B) Quantification of cholesterol in *Ch25h*$^{-/-}$ BMDMs transduced with MSCV-vector, -Ch25h, or -Ch25hmut and treated for 8 hours with LPS. Data from three independent experiments (mean +/- SD).
(C) mtDNA (Left) or nucDNA (Right) RT-qPCR from cytosolic extracts derived from *Ch25h*$^{+/-}$ and *Ch25h*$^{-/-}$ BMDMs treated as above. Data from 4 independent experiments (mean +/- SD).
(D) Representation histograms (left) and summary graph (right) of intracellular cyt C staining in *Ch25h*$^{+/-}$ and *Ch25h*$^{-/-}$ BMDMs stimulated for 8 hours with LPS and either permeabilized with digitonin or not. Data from two independent experiments (mean +/- SD).
(E) mtDNA RT-qPCR of total DNA extractions from BMDMs treated for 7 days with either nil, ethidium bromide (EtBr), or ddC. Data from 3 independent experiments (mean +/- SD).
(F) IL-1β ELISA from supernatants of BMDMs depleted of mtDNA as described above, and stimulated with either LPS alone, LPS+MCD-Chol, or LPS+ATP. Data from 3 independent experiments (mean +/- SD).
(G) IL-1β bioactivity detected as in Fig. 3 using supernatants from LPS-stimulated BMDMs of the indicated genotypes. Data from three independent experiments (mean +/- SD).
(H) IL-1β ELISA of supernatants from BMDMs of the indicated genotypes stimulated with LPS or LPS+ATP. Data from three independent experiments (mean +/- SD).
(I) *L. monocytogenes* CFU from BMDMs of the indicated genotypes infected for 24hrs. Data from three independent experiments (mean +/- SD).
(J) IL-1β ELISA of serum from mice of the indicated genotypes injected with LPS (20mg/kg) I.V. for 8 hours. Data from three independent experiments (n = 5 to 8 mice per group, mean +/- SD). *P<0.05, **P<0.01, ***P < 0.005 (unpaired Students *t* test or one way ANOVA with bonferroni test). See also related Supplementary Figure 5.

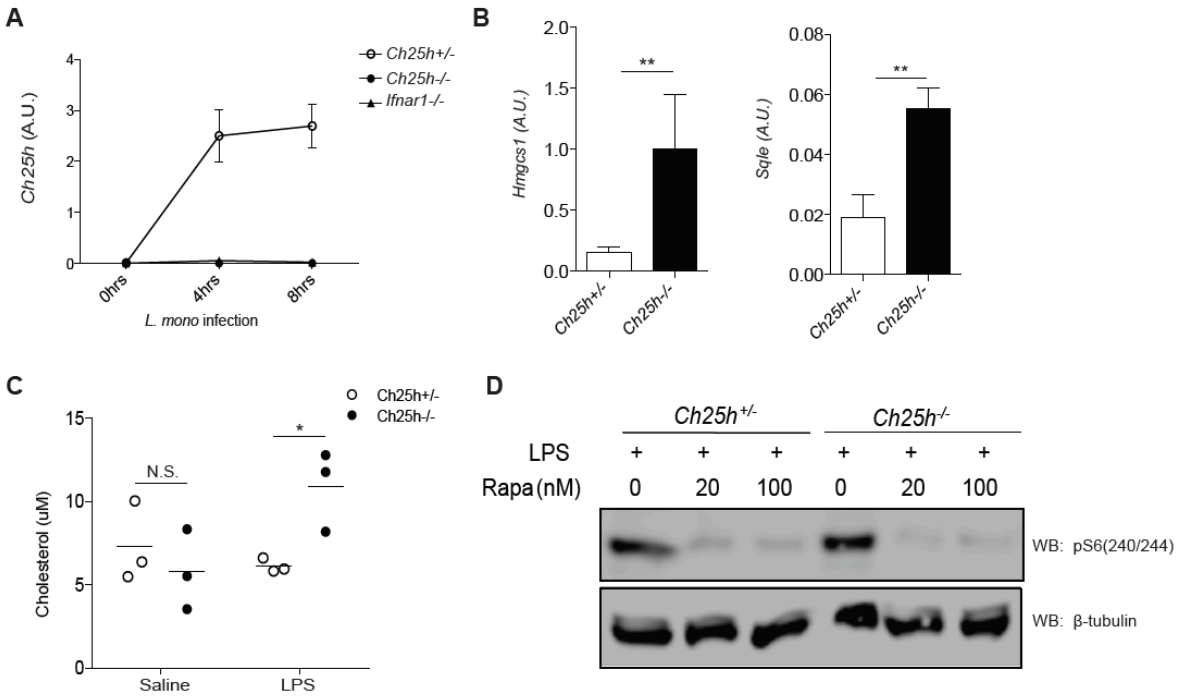

Supplementary Figure 1. Listeria infection and in vivo LPS injection cause dysregulated cholesterol synthesis in Ch25h-/- BMDM and mTORC1 dependence of LPS-induced S6 phosphorylation in BMDMs, related to Figures 1 and 2.
(A) RT-qPCR analysis of *Ch25h* mRNA in *Ch25h*$^{+/-}$, *Ch25h*$^{-/-}$, or *Ifnar1*$^{-/-}$ BMDMs infected with *L. monocytogenes* (MOI = 10:1) for 0, 4, or 8 hrs. Data are pooled from 3 independent experiments (mean +/- SD).
(B) RT-qPCR analysis of *Hmgcs1* and *Sqle* mRNA in *Ch25h*$^{+/-}$ and *Ch25h*$^{-/-}$ BMDMs infected with *L. monocytogenes* for 8 hrs. Data are pooled from 3 independent experiments (mean +/- SD).
(C) Quantification of cholesterol by Amplex Red fluorescence in sorted peritoneal macrophages from mice injected intraperitoneally with saline or LPS for 8 hrs (n = 3 mice per group, mean +/- SD).
(D) Immunoblotting for pS6 (S240/244) and β-tubulin in *Ch25h*$^{+/-}$ and *Ch25h*$^{-/-}$ BMDMs treated for 4 hrs with LPS followed by 4 hrs of LPS alone, LPS+Rapa (20nM), or LPS+Rapa (100nM). *P<0.05, **P<0.01, ***P < 0.005 (unpaired Students *t* test).

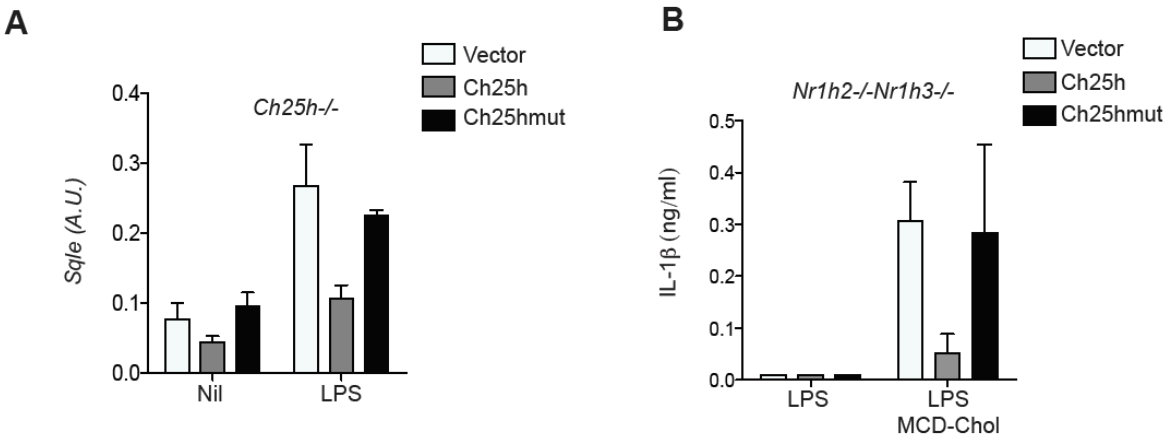

Supplementary Figure 2. Regulation of SREBP2 target gene expression by Ch25h and LXR-independent inhibition of cholesterol-dependent inflammasome activation by Ch25h, related to Figure 3.
(A) RT-qPCR analysis of *Sqle* mRNA in *Ch25h*$^{-/-}$ BMDMs transduced with MSCV-vector, MSCV-Ch25h, or MSCV-Ch25hmut (mean +/- SD).
(B) IL-1β ELISA from supernatants LXRα/β double-deficient BMDMs transduced with MSCV-vector, -Ch25h, or -Ch25hmut (mean +/- SD).

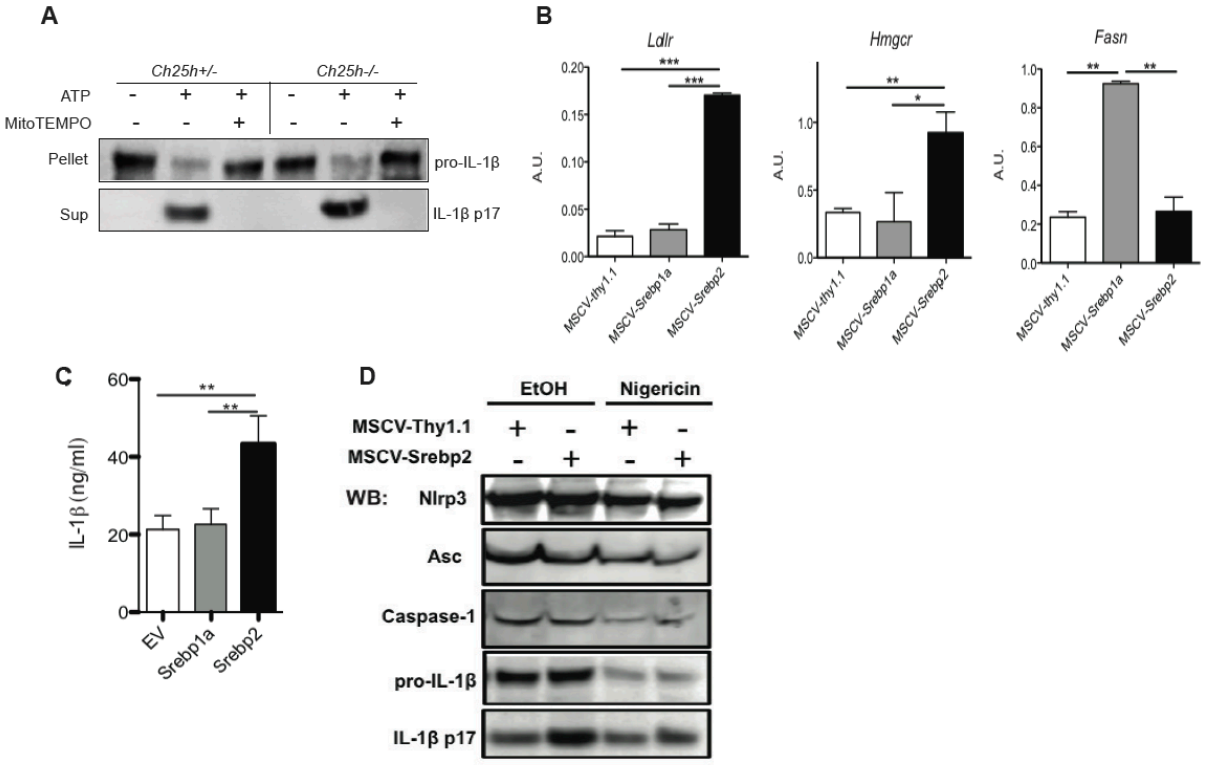

Supplementary Figure 3. MitoTemp represses ATP-induced IL-1b processing in BMDM and SREBP2 drives NLRP3 activation in a 293T inflammasome reconstitution system, related to Figure 4.

(A) Immunoblot for IL-1β on cell pellets and trichloroacetic acid (TCA)-precipitated supernatants from *Ch25h*$^{+/-}$ and *Ch25h*$^{-/-}$ BMDMs treated with LPS alone, LPS+ATP, or LPS+ATP+MitoTEMPO. Data are representative of two independent experiments.

(B) RT-qPCR analysis of *Ldlr* (Left), *Hmgcr* (Middle), or *Fasn* (Right) from 293T cells transfected with either MSCV-thy1.1, MSCV-Srebp1a, or MSCV-Srebp2 (mean +/- SD).

(C) IL-1β ELISA of supernatants from 293T cells co-transfected with NLRP3, ASC, Caspase-1, pro-IL-1β, and either vector, SREBP1a, or SREBP2 (all 50ng) and 24 hrs later treated with 15uM nigercin for 45 min. Data are pooled from 3 independent experiments (mean +/- SD).

(D) Immunoblotting for NLRP3, ASC, Caspase-1, pro-IL-1β, and IL-1β p17 on cell lysates from 293T cells prepared and treated as in C.

*P<0.05, **P<0.01, ***P < 0.005 (one way ANOVA with bonferroni test).

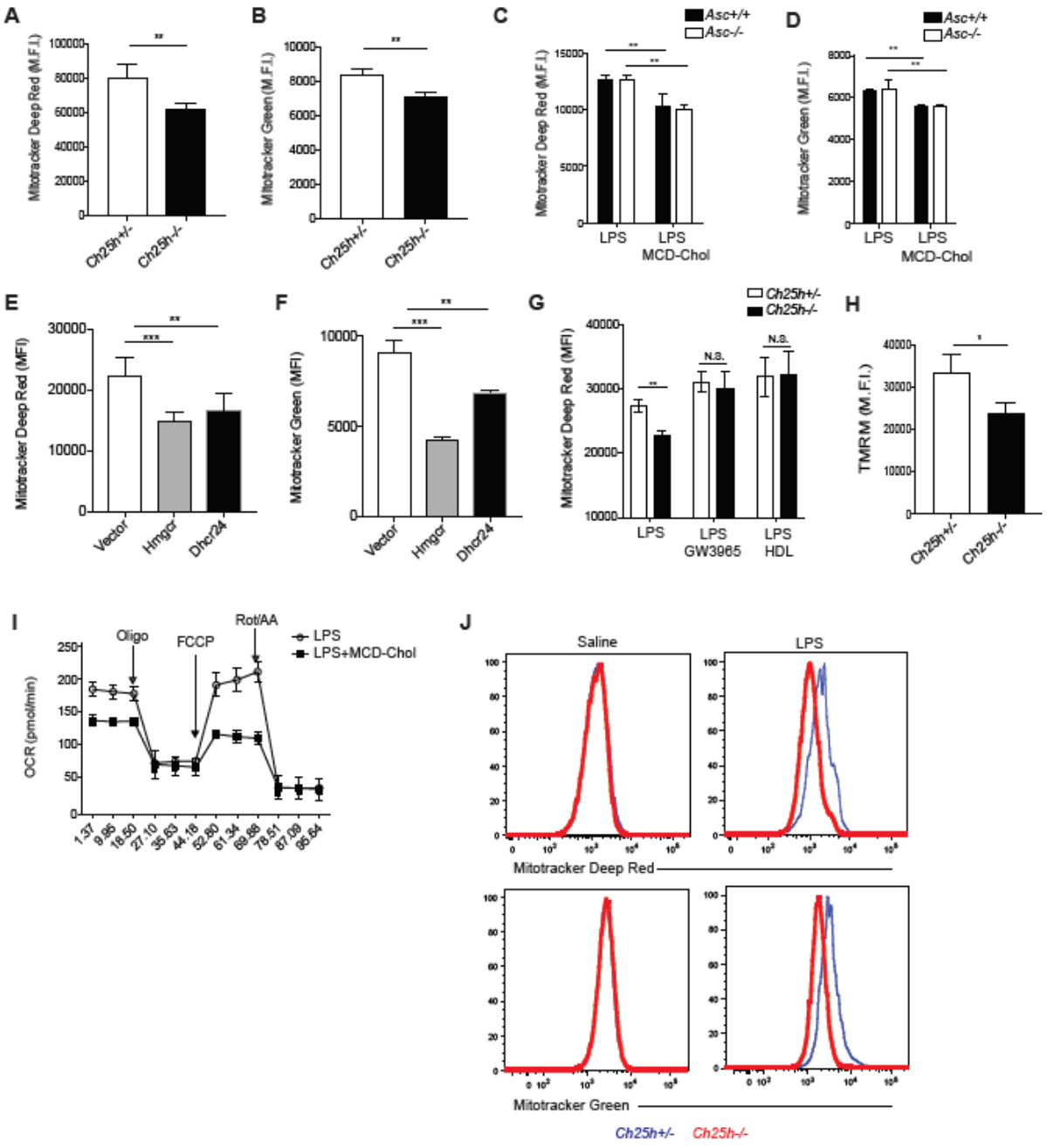

Supplementary Figure 4. Cholesterol accumulation causes mitochondrial damage in macrophages, related to Figure 6.

(A, B) MFI of Mitotracker Deep Red (A) and Mitotracker Green (B) staining on *Ch25h*$^{+/-}$ and *Ch25h*$^{-/-}$ BMDMs infected with *L. monocytogenes* for 8 hrs.

(C, D) MFI of Mitotracker Deep Red (C) and Mitotracker Green (D) staining on *Asc*$^{+/+}$ or *Asc*$^{-/-}$ BMDMs treated for 4 hrs with LPS, followed by 4 hrs of MCD-Chol (10ug/ml). Data are pooled from 3 independent experiments (mean +/- SD).

(E, F) MFI of Mitotracker Deep Red (E) or Mitotracker Green (F) staining on BMDMs transduced with MSCV-vector, -Hmgcr, or -Dhcr24 and stimulated with LPS for 8 hrs. Data are pooled from two independent experiments (mean +/- SD).
(G) MFI of Mitotracker Deep Red staining on *Ch25h*$^{+/-}$ and *Ch25h*$^{-/-}$ BMDMs stimulated for 8 hrs with LPS, LPS+HDL (100ug/ml), or LPS+GW3965 (2.5uM). Data are pooled from two independent experiments (mean +/- SD).
(H) MFI of TMRM staining on *Ch25h*$^{+/-}$ and *Ch25h*$^{-/-}$ BMDMs infected with *L. monocytogenes* for 8 hrs.
(I) Seahorse analysis of oxygen consumption rate (OCR) from BMDMs treated for 4 hrs with LPS followed by 4 hours of MCD-Chol. Data are representative of 3 independent experiments (mean +/- SD).
(J) Representative histograms of Mitotracker Deep Red (Top) and Mitotracker Green (Bottom) staining of *Ch25h*$^{+/-}$ and *Ch25h*$^{-/-}$ peritoneal macrophages 8 hrs after intraperitoneal saline or LPS injection. Data are representative of three independent experiments.

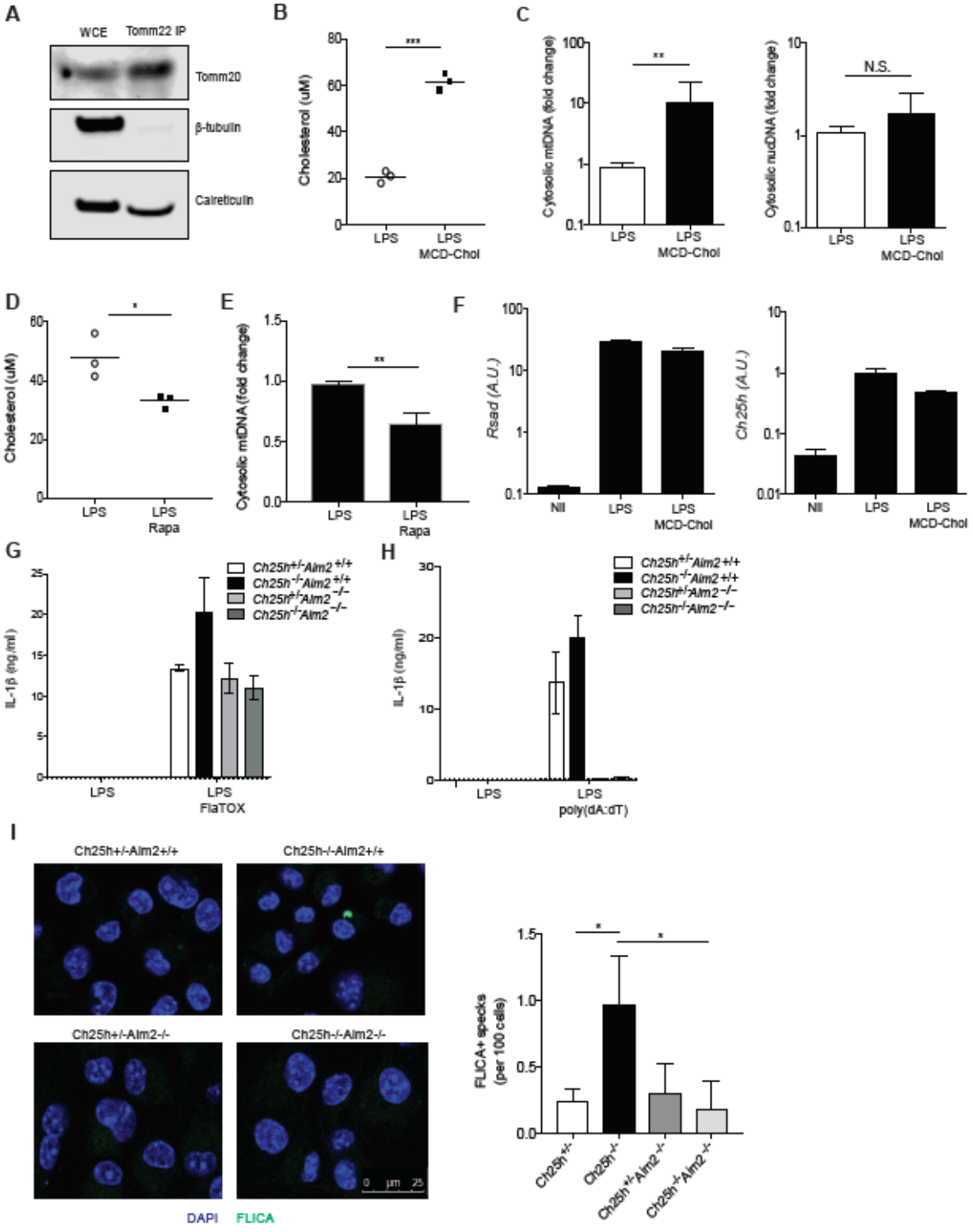

Supplementary Figure 5. Cholesterol drives mtDNA release and AIM2 inflammasome activation in macrophages, related to Figure 7.

(A) Immunoblot for Tomm20 (top), β-tubulin (middle), and calreticulin (bottom) on whole cell extracts (WCE) or mitochondria immunoprecipitated using anti-Tomm22 MACS beads.
(B) Quantification of cholesterol by Amplex Red fluorescence in mitochondria isolated with anti-Tomm22 MACS beads from wild type BMDMs stimulated with LPS alone or 4 hrs of LPS followed by 4hrs of MCD-Chol.
(C) mtDNA (left) or nucDNA (right) RT-qPCR of total DNA from cytosolic extracts derived from BMDMs treated with either LPS alone, or 4 hrs of LPS followed by 4 hrs of MCD-Chol. Data are pooled from 4 independent experiments (mean +/- SD).
(D) Quantification of cholesterol by Amplex Red fluorescence in mitochondria isolated with anti-Tomm22 MACS beads from *Ch25h*$^{-/-}$ BMDMs stimulated with LPS alone or 4 hrs of LPS followed by 4 hrs of rapamycin (20nM).
(E) mtDNA RT-qPCR of total DNA from cytosolic extracts derived from BMDMs treated with either LPS alone, or 4 hrs of LPS followed by 4 hrs of rapamycin (20nM).
(F) RT-qPCR analysis of *Rsad* (Left) and *Ch25h* (Right) transcripts in BMDMs treated for 4 hrs with either nil, LPS, MCD-Chol or LPS+MCD-Chol (mean +/- SD).
(G, H) IL-1β ELISA from supernatants of BMDMs of the indicated genotypes stimulated with either LPS alone, LPS+FlaTOX (G) or LPS+poly(dA:dT)
(H). Data are pooled from three independent experiments (mean +/- SD).
(I) Representative images (left) and quantification (right) of confocal microscopy on BMDMs of the indicated genotypes incubated for 8hrs with LPS and FLICA and subsequently stained with DAPI. Data are pooled from 4 technical replicates of two independent experiments (mean +/- SD). At least 600 cells were counted for each replicate. *P<0.05, **P<0.01, ***P < 0.005 (unpaired Students *t* test or one way ANOVA with bonferroni test).

REFERENCES

Aguirre, S., Luthra, P., Sanchez-Aparicio, M.T., Maestre, A.M., Patel, J., Lamothe, F., Fredericks, A.C., Tripathi, S., Zhu, T., Pintado-Silva, J., et al. (2017). Dengue virus NS2B protein targets cGAS for degradation and prevents mitochondrial DNA sensing during infection. Nature Microbiology *2*, 17037.

Blanc, M., Hsieh, W.Y., Robertson, K.A., Kropp, K.A., Forster, T., Shui, G., Lacaze, P., Watterson, S., Griffiths, S.J., Spann, N.J., et al. (2013). The Transcription Factor STAT-1 Couples Macrophage Synthesis of 25-Hydroxycholesterol to the Interferon Antiviral Response. Immunity *38*, 106–118.

Bosch, M., Marí, M., Herms, A., Fernández, A., Fajardo, A., Kassan, A., Giralt, A., Colell, A., Balgoma, D., Barbero, E., et al. (2011). Caveolin-1 deficiency causes cholesterol-dependent mitochondrial dysfunction and apoptotic susceptibility. Curr. Biol. *21*, 681–686.

Campos, C.B.L., Paim, B.A., Cosso, R.G., Castilho, R.F., Rottenberg, H., Vercesi, A.E. (2006). Method for monitoring of mitochondrial cytochrome C release during cell death: Immunodetection of Cytochrome C by flow cytometry after selective permeabilization of the plasma membrane. Cytometry *69*, 515-523.

Chen, C.H., and Cheng, Y.C. (1989). Delayed cytotoxicity and selective loss of mitochondrial DNA in cells treated with the anti-human immunodeficiency virus compound 2“,3-”dideoxycytidine. J. Biol. Chem. *264*, 11934–11937.

Cyster, J.G., Dang, E.V., Reboldi, A., and Yi, T. (2014). 25-Hydroxycholesterols in

innate and adaptive immunity. Nature Reviews Immunology *14*, 731–743.

de Luca, C., and Olefsky, J.M. (2008). Inflammation and insulin resistance. FEBS Letters *582*, 97–105.

Düvel, K., Yecies, J.L., Menon, S., Raman, P., Lipovsky, A.I., Souza, A.L., Triantafellow, E., Ma, Q., Gorski, R., Cleaver, S., et al. (2010). Activation of a metabolic gene regulatory network downstream of mTOR complex 1. Mol. Cell *39*, 171–183.

Franklin B.S., Mangan M.S., and Latz, E. (2016). Crystal Formation in Inflammation. Ann. Rev. Immuno. *34*, 173-202.

Goldstein, J.L., DeBose-Boyd, R.A., and Brown, M.S. (2006). Protein sensors for membrane sterols. Cell *124*, 35–46.

Guarda, G., Braun, M., Staehli, F., Tardivel, A., Mattmann, C., Förster, I., Farlik, M., Decker, T., Pasquier, Du, R.A., Romero, P., et al. (2011). Type I interferon inhibits interleukin-1 production and inflammasome activation. Immunity *34*, 213–223.

Hayashi, T., Su, T.P. Sigma-1 Receptor Chaperones at the ER-Mitochondrion Interface Regulate Ca^{2+} Signaling and Cell Survival. Cell *131*, 596-610.

Hornung, V., Bauernfeind, F., Halle, A., Samstad, E.O., Kono, H., Rock, K.L., Fitzgerald, K.A., and Latz, E. (2008). Silica crystals and aluminum salts activate the NALP3 inflammasome through phagosomal destabilization. Nature Immunology *9*, 847–856.

Kennedy, B.E., Madreiter, C.T., Vishnu, N., Malli, R., Graier, W.F., and Karten, B. (2014). Adaptations of energy metabolism associated with increased levels of

mitochondrial cholesterol in Niemann-Pick type C1-deficient cells. J. Biol. Chem. *289*, 16278–16289.

Liu, S.-Y., Aliyari, R., Chikere, K., Li, G., Marsden, M.D., Smith, J.K., Pernet, O., Guo, H., Nusbaum, R., Zack, J.A., et al. (2013). Interferon-Inducible Cholesterol-25-Hydroxylase Broadly Inhibits Viral Entry by Production of 25-Hydroxycholesterol. Immunity *38*, 92–105.

Marí, M., Caballero, F., Colell, A., Morales, A., Caballeria, J., Fernandez, A., Enrich, C., Fernandez-Checa, J.C., and García-Ruiz, C. (2006). Mitochondrial free cholesterol loading sensitizes to TNF- and Fas-mediated steatohepatitis. Cell Metab. *4*, 185–198.

Martin, L.A., Kennedy, B.E., and Karten, B. (2016). Mitochondrial cholesterol: mechanisms of import and effects on mitochondrial function. J. Bioenerg. Biomembr. *48*, 137–151.

McDonald, J.G., and Russell, D.W. (2010). Editorial: 25-Hydroxycholesterol: a new life in immunology. Journal of Leukocyte Biology *88*, 1071–1072.

Metherall, J.E., Ridgway, N.D., Dawson, P.A., Goldstein, J.L., and Brown, M.S. (1991). A 25-hydroxycholesterol-resistant cell line deficient in acyl-CoA: cholesterol acyltransferase. J. Biol. Chem. *266*, 12734–12740.

Montero, J., Marí, M., Colell, A., Morales, A., Basañez, G., García-Ruiz, C., and Fernandez-Checa, J.C. (2010). Cholesterol and peroxidized cardiolipin in mitochondrial membrane properties, permeabilization and cell death. Biochim. Biophys. Acta *1797*, 1217–1224.

Nakahira, K., Haspel, J.A., Rathinam, V.A.K., Lee, S.-J., Dolinay, T., Lam, H.C., Englert, J.A., Rabinovitch, M., Cernadas, M., Kim, H.P., et al. (2011). Autophagy proteins regulate innate immune responses by inhibiting the release of mitochondrial DNA mediated by the NALP3 inflammasome. Nature Immunology *12*, 222–230.

Porstmann, T., Santos, C.R., Griffiths, B., Cully, M., Wu, M., Leevers, S., Griffiths, J.R., Chung, Y.-L., and Schulze, A. (2008). SREBP activity is regulated by mTORC1 and contributes to Akt-dependent cell growth. Cell Metab. *8*, 224–236.

Powell, J.D., Pollizzi, K.N., Heikamp, E.B., and Horton, M.R. (2012). Regulation of immune responses by mTOR. Annu. Rev. Immunol. *30*, 39–68.

Rathinam, V.A.K., and Fitzgerald, K.A. (2016). Inflammasome Complexes: Emerging Mechanisms and Effector Functions. Cell *165*, 792–800.

Reboldi, A., Dang, E.V., McDonald, J.G., Liang, G., Russell, D.W., and Cyster, J.G. (2014). 25-Hydroxycholesterol suppresses interleukin-1–driven inflammation downstream of type I interferon. Science *345*, 679–684.

Robertson, K.A., Hsieh, W.Y., Forster, T., Blanc, M., Lu, H., Crick, P.J., Yutuc, E., Watterson, S., Martin, K., Griffiths, S.J., et al. (2016). An Interferon Regulated MicroRNA Provides Broad Cell-Intrinsic Antiviral Immunity through Multihit Host-Directed Targeting of the Sterol Pathway. PLOS Biology *14*, e1002364.

Robinson, L.E., Shridar, M., Smith, P., and Murrell-Lagnado, R.D. (2014). Plasma membrane cholesterol as a regulator of human and rodent P2X7 receptor activation and sensitization. J. Biol. Chem. *289*, 31983–31994.

Rongvaux, A., Jackson, R., Harman, C.C.D., Li, T., West, A.P., de Zoete, M.R., Wu, Y., Yordy, B., Lakhani, S.A., Kuan, C.-Y., et al. (2014). Apoptotic caspases prevent the induction of type I interferons by mitochondrial DNA. Cell *159*, 1563–1577.

Shimada, K., Crother, T.R., Karlin, J., Dagvadorj, J., Chiba, N., Chen, S., Ramanujan, V.K., Wolf, A.J., Vergnes, L., Ojcius, D.M., et al. (2012). Oxidized mitochondrial DNA activates the NLRP3 inflammasome during apoptosis. Immunity *36*, 401–414.

Stienstra, R., van Diepen, J.A., Tack, C.J., Zaki, M.H., van de Veerdonk, F.L., Perera, D., Neale, G.A., Hooiveld, G.J., Hijmans, A., Vroegrijk, I., et al. (2011). Inflammasome is a central player in the induction of obesity and insulin resistance. Proc. Natl. Acad. Sci. U.S.a. *108*, 15324–15329.

Sun, B., Sundstrom, K.B., Chew, J.J., Bist, P., Gan, E.S., Tan, H.C., Goh, K.C., Chawla, T., Tang, C.K., Ooi, E.E. (2017). Dengue virus activates cGAS through release of mitochondrial DNA. Scientific Reports *7*, 3594.

Vandanmagsar, B., Youm, Y.-H., Ravussin, A., Galgani, J.E., Stadler, K., Mynatt, R.L., Ravussin, E., Stephens, J.M., and Dixit, V.D. (2011). The NLRP3 inflammasome instigates obesity-induced inflammation and insulin resistance. Nat. Med. *17*, 179–188.

West, A.P., Khoury-Hanold, W., Staron, M., Tal, M.C., Pineda, C.M., Lang, S.M., Bestwick, M., Duguay, B.A., Raimundo, N., MacDuff, D.A., et al. (2015). Mitochondrial DNA stress primes the antiviral innate immune response. Nature *520*, 553–557.

White, M.J., McArthur, K., Metcalf, D., Lane, R.M., Cambier, J.C., Herold, M.J., van Delft, M.F., Bedoui, S., Lessene, G., Ritchie, M.E., et al. (2014). Apoptotic Caspases

Suppress mtDNA-Induced STING-Mediated Type I IFN Production. Cell *159*, 1549–1562.

Wu, J., Fernandes-Alnemri, T., Alnemri, E.S. (2010). Involvement of the AIM2, NLRC4, and NLRP3 inflammasomes in caspase-1 activation by Listeria monocytogenes. J. Clin. Immunology *5*, 693-702.

York, A.G., Williams, K.J., Argus, J.P., Zhou, Q.D., Brar, G., Vergnes, L., Gray, E.E., Zhen, A., Wu, N.C., Yamada, D.H., et al. (2015). Limiting Cholesterol Biosynthetic Flux Spontaneously Engages Type I IFN Signaling. Cell *163*, 1716–1729.

Yu, J., Nagasu, H., Murakami, T., Hoang, H., Broderick, L., Hoffman, H.M., and Horng, T. (2014). Inflammasome activation leads to Caspase-1-dependent mitochondrial damage and block of mitophagy. Proc. Natl. Acad. Sci. U.S.a. *111*, 15514–15519.

Zhong, Z., Umemura, A., Sanchez-Lopez, E., Liang, S., Shalapour, S., Wong, J., He, F., Boassa, D., Perkins, G., Ali, S.R., et al. (2016). NF-κB Restricts Inflammasome Activation via Elimination of Damaged Mitochondria. Cell *164*, 896–910.

Zhou, R., Yazdi, A.S., Menu, P., and Tschopp, J. (2011). A role for mitochondria in NLRP3 inflammasome activation. Nature *475*, 122–122.

Publishing Agreement

It is the policy of the University to encourage the distribution of all theses, dissertations, and manuscripts. Copies of all UCSF theses, dissertations, and manuscripts will be routed to the library via the Graduate Division. The library will make all theses, dissertations, and manuscripts accessible to the public and will preserve these to the best of their abilities, in perpetuity.

Please sign the following statement:

I hereby grant permission to the Graduate Division of the University of California, San Francisco to release copies of my thesis, dissertation, or manuscript to the Campus Library to provide access and preservation, in whole or in part, in perpetuity.

Author Signature

3/27/18

Date